

REPORT NO.
UCB/EERC-85/09
JANUARY 1986

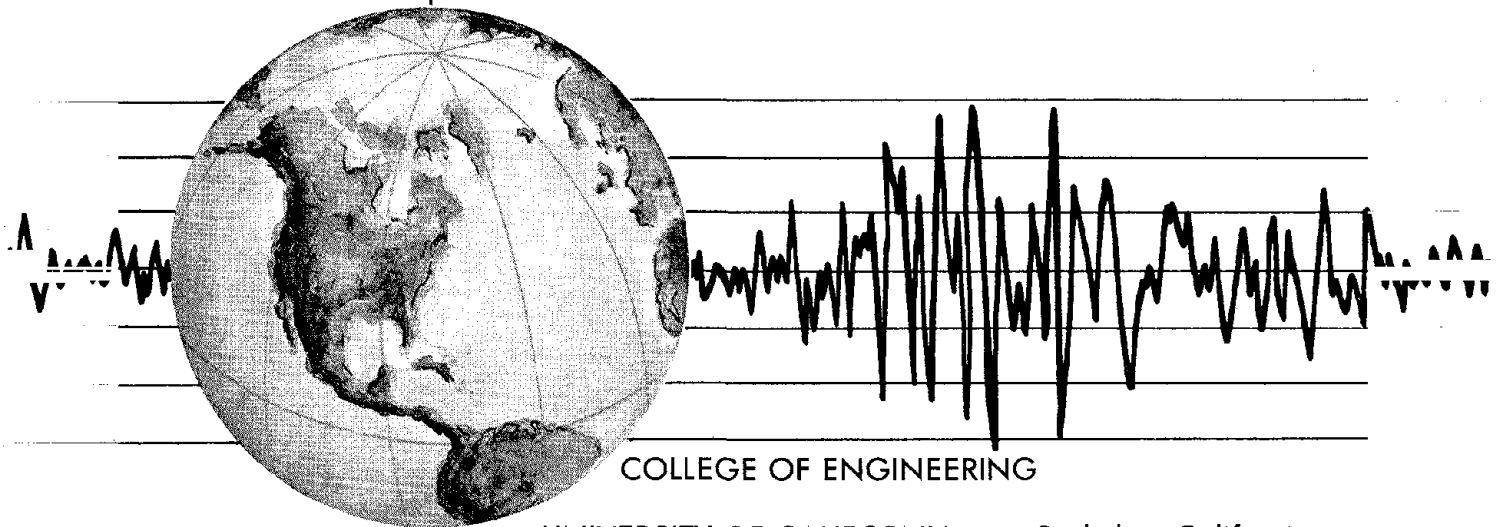
EARTHQUAKE ENGINEERING RESEARCH CENTER

EARTHQUAKE SIMULATOR TESTING OF A BASE-ISOLATED BRIDGE DECK

by

JAMES M. KELLY
IAN G. BUCKLE
HSIANG-CHUAN TSAI

Report to the National Science Foundation



COLLEGE OF ENGINEERING

UNIVERSITY OF CALIFORNIA • Berkeley, California

REPRODUCED BY
U.S. DEPARTMENT OF COMMERCE
NATIONAL TECHNICAL
INFORMATION SERVICE
SPRINGFIELD, VA. 22161

For sale by the National Technical Information Service, U.S. Department of Commerce, Springfield, Virginia 22161.

See back of report for up to date listing of EERC reports.

DISCLAIMER

Any opinions, findings, and conclusions or recommendations expressed in this publication are those of the authors and do not necessarily reflect the views of the National Science Foundation or the Earthquake Engineering Research Center, University of California, Berkeley

REPORT DOCUMENTATION PAGE	1. REPORT NO. NSF/ENG 85029	2.	3. Recipient's Accession No. PB87-124152/AS
4. Title and Subtitle Earthquake Simulator Testing of a Base-Isolated Bridge Deck		5. Report Date January, 1986	
7. Author(s) James M. Kelly, Ian G. Buckel, Hsiang-Chuan Tsai		8. Performing Organization Rept. No. UCB/EERC-85/09	
9. Performing Organization Name and Address Earthquake Engineering Research Center University of California, Berkeley 1301 South 46th Street Richmond, California 94804		10. Project/Task/Work Unit No. 11. Contract(C) or Grant(G) No. (C) (G) NSF No. CEE-8213604	
12. Sponsoring Organization Name and Address National Science Foundation 1800 G. Street, N.W. Washington, D.C. 20050		13. Type of Report & Period Covered Final	
15. Supplementary Notes			
16. Abstract (Limit: 200 words) <p>This report describes a series of tests carried out on the shaking table at Earthquake Engineering Research Center in which a base-isolated bridge deck model representing a typical highway bridge superstructure was subjected to a variety of earthquake inputs representing both real and artificially generated earthquake signals. Two different forms of isolation system were used in the testing program. One used natural rubber elastomeric layers reinforced by steel plates and the other set used the same bearings but with a lead plug inserted in a central hole.</p>			
17. Document Analysis a. Descriptors base-isolated earthquake bridge deck rubber model isolation bearing highway bridge dynamic response b. Identifiers/Open-Ended Terms Earthquake Engineering Research Center c. COSATI Field/Group			
18. Availability Statement: Release Unlimited		19. Security Class (This Report) Unclassified	21. No. of Pages 123
		20. Security Class (This Page) Unclassified	22. Price



2/1-a

**EARTHQUAKE SIMULATOR TESTING
OF A BASE-ISOLATED BRIDGE DECK**

by

James M. Kelly

Professor of Civil Engineering
Earthquake Engineering Research Center
University of California, Berkeley

Ian G. Buckle

Professor of Civil Engineering
University of Auckland, Auckland, New Zealand

and

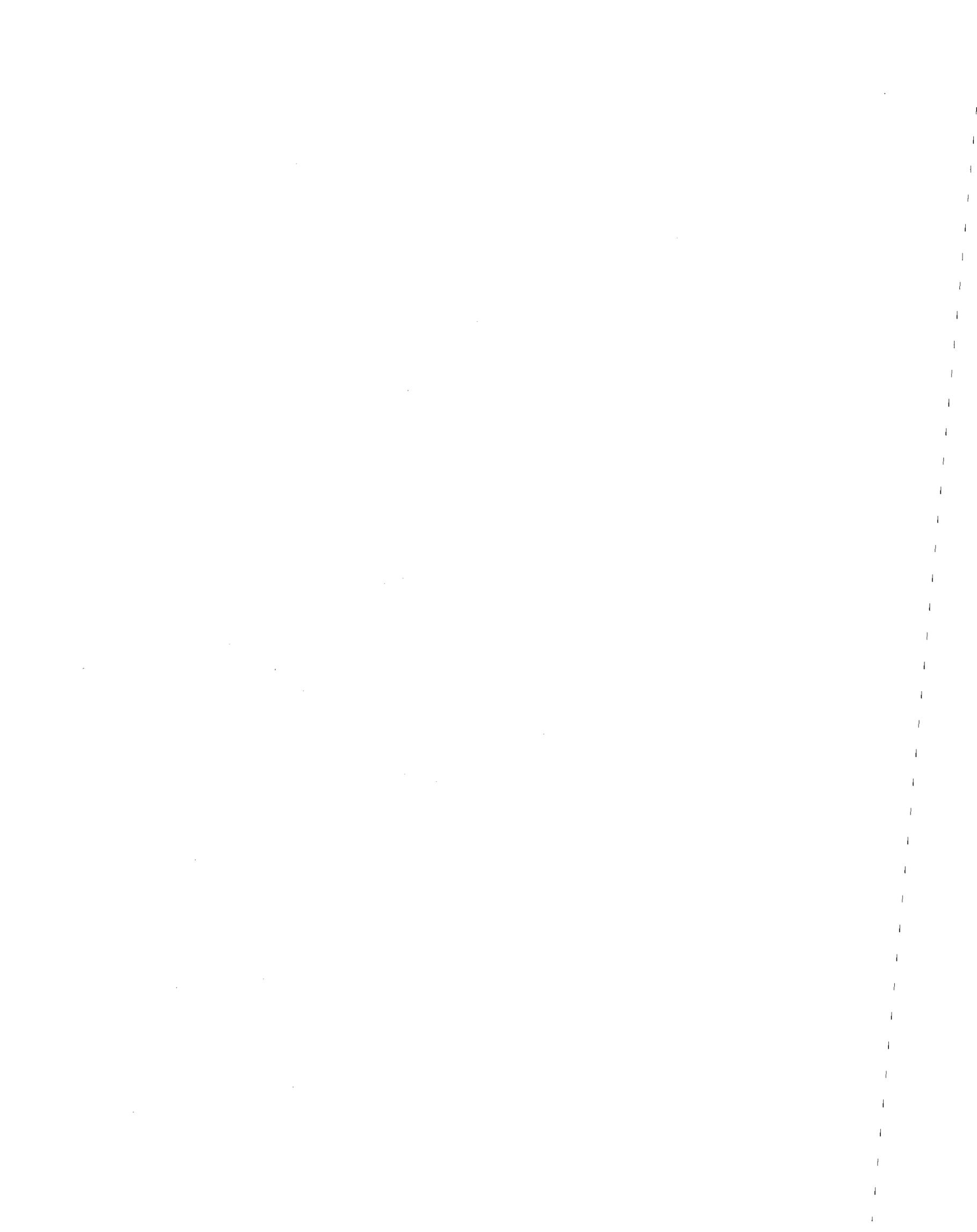
Hsiang-Chuan Tsai

Department of Civil Engineering
University of California, Berkeley

Report to the National Science Foundation

Report No. UCB/EERC-85/09
Earthquake Engineering Research Center
College of Engineering
University of California, Berkeley

January 1986



Abstract

This report describes a series of tests carried out on the shaking table at Earthquake Engineering Research Center in which a base-isolated bridge deck model representing a typical highway bridge superstructure was subjected to a variety of earthquake inputs representing both real and artificially generated earthquake signals. Two different forms of isolation system were used in the testing program. One used natural rubber elastomeric layers reinforced by steel plates and the other set used the same bearings but with a lead plug inserted in a central hole.

The report describes the results of these tests and compares responses of the bridge deck when carried on each system. The report also describes a simple analysis of limit state of an isolation bearing and gives results of tests specifically carried out to verify this analysis.

Another feature of the experimental program is a parameter identification routine designed to provide an equivalent linearization of the dynamic response of the non-linear isolation system. This has been developed with a view to providing elementary design rules for preliminary design of base isolated buildings and bridges. Comparisons of the time histories of the equivalent linear systems and the actual model show that the method gives accurate maxima in displacement and acceleration and at the appropriate times.

Acknowledgments

The research described in this report was supported by the National Science Foundation through Grant No. CEE-8213604. The bearing was provided by Oil States Industries Inc., Athens, Texas. The authors of report are grateful for this support.

Table of Contents

Abstract	i
Acknowledgments	ii
Table of Contents	iii
List of Tables	v
List of Figures	vi
Chapter 1 INTRODUCTION	1
Chapter 2 CHARACTERISTICS OF ISOLATION BEARINGS	3
Chapter 3 EXPERIMENTAL MODEL AND PROGRAM	6
3.1 Test Facilities and Instruments	6
3.2 Bridge Deck Model	7
3.3 Test Programs for Plain Rubber Bearing System	9
3.4 Test Programs for Lead-Filled Rubber Bearing System	11
Chapter 4 TEST RESULTS OF PLAIN BEARING SYSTEM	12
4.1 Results of Longitudinal and Torsional Pull-Back Tests	12
4.2 Decay Curves for Harmonic Input	13
4.3 Results of Steady-State Sinusoidal Loading	14
4.4 Influence of Vertical Excitation	16
4.5 Results of Horizontal Real-Time Earthquake Input	17
4.6 Results of Horizontal Time-Scaled Earthquake Input	18
Chapter 5 TEST RESULTS OF LEAD-FILLED BEARING SYSTEM	21
5.1 Influence of Vertical Excitation	21
5.2 Results of Horizontal Real-Time Earthquake Input	21
5.3 Results of Horizontal Time-Scaled Earthquake Input	23
5.4 Comparison between Plain and Lead-Filled Systems	24
Chapter 6 PARAMETER IDENTIFICATION ROUTINE	26
6.1 Parameter Identification for Linear Viscous Model	26

6.2	Parameter Identification of Plain Rubber Bearing	27
6.3	Parameter Identification of Lead-Filled Rubber Bearing	29
6.4	Influence of Earthquakes on Response of Isolation Systems	30
Chapter 7	LIMIT RESPONSE OF BASE ISOLATION SYSTEMS	31
7.1	Limit State of Rubber Bearing Deformation	31
7.2	Limit Response of Plain Rubber Bearing	32
7.3	Limit Response of Lead-Filled Rubber Bearing	34
Chapter 8	CONCLUSIONS	36
References	40
Tables	41
Figures	58

List of Tables

- Table 1 List of Instrumentation
- Table 2 Summary of Horizontal Earthquake Input Test Programs for Plain Bearing System
- Table 3 Summary of Horizontal Earthquake Input Test Programs for Lead-Filled Bearing System
- Table 4 Logarithmic Decrement of Longitudinal Pull-Back Test for Plain Bearing System
- Table 5 Logarithmic Decrement of Harmonic Motion for Plain Bearing System
- Table 6 Steady-State Sinusoidal Response of Plain Rubber Bearing
- Table 7 Influence of Vertical Excitation on Plain Bearing System Excited by El Centro Signals
- Table 8 Peak Responses of Real-Time Signal Inputs for Plain Bearing System
- Table 9 Peak Responses of Time-Scaled Signal Inputs at Span 750 for Plain Bearing System
- Table 10 Influence of Vertical Excitation on Lead-Filled Bearing System Excited by El Centro Signals
- Table 11 Peak Responses of Real-Time Signal Inputs for Lead-Filled Bearing System
- Table 12 Peak Responses of Time-Scaled Signal Inputs at Span 750 for Lead-Filled Bearing System
- Table 13 Comparison of Peak Response under Real-Time Signal Inputs
- Table 14 Comparison of Peak Response under Time-Scaled Signal Inputs at Span 750
- Table 15 Comparison of Peak Acceleration under Vertical Excitation
- Table 16 Parameter Identification of Plain Rubber Bearing
- Table 17 Parameter Identification of Lead-Filled Rubber Bearing

List of Figures

- Figure 1 Plan and Cross Section of Bearing
- Figure 2 Cross Section of Bridge Deck Model
- Figure 3 Elevation of Bridge Deck Model
- Figure 4 Location of Instrumentation
- Figure 5 Beat Phenomenon during Start-up of Harmonic Input at Frequency 0.65 Hz
- Figure 6 Displacement Time History in Longitudinal Pull-Back Test
- Figure 7 Acceleration Time History in Longitudinal Pull-Back Test
- Figure 8 Displacement Fourier Spectrum in Longitudinal Pull-Back Test
- Figure 9 Time History of Displacement Difference in Torsional Pull-Back Test
- Figure 10 Time History of Acceleration Difference in Torsional Pull-Back Test
- Figure 11 Fourier Spectrum of Displacement Difference in Torsional Pull-Back Test
- Figure 12 Displacement Decay Curve of Harmonic Input
- Figure 13 Damping Factors from Longitudinal Pull-Back Test and Harmonic Decay Test
- Figure 14 Hysteresis Loops of Plain Bearing in Steady-State Sinusoidal Test
- Figure 15 Amplification Factors of Plain Bearing
- Figure 16 Hysteresis Loops of Plain Bearing under Real-Time ATC-3 Signal at Span 400
- Figure 17 Table and Deck Acceleration Time Histories of Plain Bearing System under Real-Time ATC-3 Signal at Span 400
- Figure 18 Table and Deck Displacement Time Histories of Plain Bearing System under Real-Time ATC-3 Signal at Span 400
- Figure 19 Table and Deck Acceleration Fourier Spectra of Plain Bearing System under Real-Time ATC-3 Signal at Span 400
- Figure 20 Responses of Plain Bearing under Increasing Earthquake Intensity
- Figure 21 Time-Scaled San Francisco Displacement Record at Span 750
- Figure 22 Time-Scaled San Francisco Acceleration Record at Span 750
- Figure 23 Hysteresis Loops of Plain Bearing under Time-Scaled El Centro Signal at Span 750
- Figure 24 Hysteresis Loops of Plain Bearing under Time-Scaled Pacoima Dam Signal at Span 750

- Figure 25 Hysteresis Loops of Lead-Filled Bearing System under Real-Time ATC-3 Signal at Span 400
- Figure 26 Deck Displacement Time History of Lead-Filled Bearing System under Real-Time ATC-3 Signal at Span 400
- Figure 27 Deck Acceleration Time History of Lead-Filled Bearing System under Real-Time ATC-3 Signal at Span 400
- Figure 28 Deck Acceleration Fourier Spectrum of Lead-Filled Bearing System under Real-Time ATC-3 Signal at Span 400
- Figure 29 Response Network for Parameter Identification
- Figure 30 Correlation between Plain Bearing and Linear Viscous Model under El Centro Earthquake
- Figure 31 Correlation between Plain Bearing and Linear Viscous Model under Parkfield Earthquake
- Figure 32 Correlation between Plain Bearing and Linear Viscous Model under Pacoima Dam Earthquake
- Figure 33 Relation between Effective Stiffness and Maximum Strain for Plain Natural Rubber Bearing
- Figure 34 Relation between Loss Factor and Maximum Strain for Plain Natural Rubber Bearing
- Figure 35 Correlation between Lead-Filled Bearing and Linear Viscous Model under El Centro Earthquake
- Figure 36 Correlation between Lead-Filled Bearing and Linear Viscous Model under Parkfield Earthquake
- Figure 37 Correlation between Lead-Filled Bearing and Linear Viscous Model under Pacoima Dam Earthquake
- Figure 38 Relation between Effective Stiffness and Maximum Strain for Lead-Filled Natural Rubber Bearing
- Figure 39 Relation between Damping Ratio and Maximum Strain for Lead-Filled Natural Rubber Bearing
- Figure 40 Response Network of El Centro Time-Scaled Record at Span 750
- Figure 41 Response Network of Caltech A1 Time-Scaled Record at Span 750
- Figure 42 Response Network of Taft Time-Scaled Record at Span 750

- Figure 43 Response Network of Parkfield Time-Scaled Record at Span 750
- Figure 44 Response Network of Pacoima Dam Time-Scaled Record at Span 750
- Figure 45 Response Network of San Francisco Time-Scaled Record at Span 750
- Figure 46 Forces Acting on Deformed Bearing
- Figure 47 Forces Acting on Bearing in Limit State
- Figure 48 Relation between Shear Force and Lateral Displacement in Limit State
- Figure 49 Force-Displacement Curves for Roll-out and Slide Failure Modes
- Figure 50 Force-displacement Curve in Roll-out Test of Plain Bearing System
- Figure 51 Response Time Histories in Plain Bearing System under Real-Time ATC-3 Input at Span 400
- Figure 52 Deck Displacement Time History in Slide Test of Lead-Filled Bearing System
- Figure 53 Lead-Filled Rubber Bearing after Slide
- Figure 54 Force-Displacement Curve for Slidged Lead-Filled Bearing
- Figure 55 Force-Displacement Curve for Unslidged Lead-Filled Bearing
- Figure 56 Force-Displacement Curve in Roll-out Test of Lead-Filled Bearing System
- Figure 57 Lead-Filled Rubber Bearing before Roll-out

Chapter 1 INTRODUCTION

The use of base isolation for the seismic protection of buildings and other structures has become the subject of considerable interest in the structural engineering profession since it offers a method of seismic design which could both reduce costs and increase safety. It can reduce costs by permitting the use of simpler framing systems such as braced steel frames or ordinary reinforced concrete frames rather than moment resisting steel frames or ductile concrete frames. It may increase the degree of protection offered to the structure by allowing the structure to be designed elastically for any earthquake that may be anticipated at the site within the lifetime of the structure and would allow the structure to be designed for an extreme earthquake with reduced ductility demand (and hence reduced damage).

It has been proposed for buildings and a few have been built or are in the planning stages but its most extensive use has in fact been for bridges. At this time there are twenty-six highway bridges in New Zealand that use base isolation devices. Some of these bridges have been retrofitted but most are new construction.

The reason why base isolation is more readily accepted for bridge structures than for buildings is clear. Bridges already use elastomeric bearings to reduce thermal or shrinkage loads and so the use of seismic isolation bearings is straightforward. Since the loads transmitted to the piers and foundation structures will be smaller, the use of isolation will reduce the cost of the bridge substructures and foundations. Thus in contrast to buildings which need a double foundation system and new components, namely the isolation bearings, all of which add to the total cost, in the case of bridges it is possible to achieve substantial improvements in seismic safety with decreased cost by use of this technique.

When used in bridges in New Zealand, seismic isolation is generally effected through the use of lead-rubber bearings. In this device a multilayer elastomer bearing is provided with a central hole into which a cylindrical plug of lead is inserted. The lead plug acts as an elastic-perfectly plastic yielding element and provides the isolation system with a high initial elastic stiffness thus supporting wind loads and when yielding acts as an energy dissipator thus

providing increased damping. The lead-rubber bearings tend to control the relative displacements between deck and piers and while doing so do not produce increased accelerations (over those for plain elastomeric bearings) in the bridge superstructure.

It has been shown, in earlier shake table testing with building structure models, that use of lead-rubber isolators tends to induce higher mode response in the models and in that case the model accelerations are increased over those when plain bearings are used. In bridge decks however the higher modes are very much higher than the fundamental mode and are not important in the dynamic response of an isolated deck.

There are a number of open questions on the response of base-isolated bridge decks that can only be answered by shake table testing of large models. Among these are the dynamic response of skew bridge decks. It has been anticipated that there could be problems with rotation (about a vertical axis) if the bridge has a large skew. The precise failure mode of isolation bearings with and without lead plugs needs to be studied and there is also the question of differential seismic input between the two ends of a bridge.

An experimental test program to address these matters and others has recently been carried out at the Earthquake Simulator Laboratory of the Earthquake Engineering Research Center of the University of California using the 20 foot by 20 foot shake table of that facility.

In this test program a half-scale model of a bridge deck supported on seismic isolation bearings both with and without lead plug inserts was subjected to a large number of real and artificial earthquake input signals. The model was designed so that it could in addition be supported on a wide range of skewed supports and it was also possible to have different input motions at each end of the bridge.

The present report describes the non-skewed test results. The results for skewed supports and differential input will be given in subsequent reports.

Chapter 2 CHARACTERISTICS OF ISOLATION BEARINGS

Two types of isolation system were used in the shake table test, one with bearings having no lead plug inserts and the other using bearings with inserts. Identical elastomeric bearings were used for both systems and thus the response of the two systems will not be perfectly comparable since the effective period of the system in the two situations will be different, the lead plug producing as it does a considerable stiffening of the plain bearing. Nevertheless, some comparisons can be legitimately made and, since the major cost of a bearing is in the construction of a mold, the expense of having two sets of bearings of different size was beyond the resources of the project.

The isolators are multilayer natural rubber bearings and a plan and cross section of a bearing are shown in Figure 1. They have fourteen layers of 0.375 in. (9.53 mm) thick rubber and thirteen 0.125 in. (3.18 mm) thick steel plates. At each end is a 0.5 in. (12.7 mm) steel plate with holes for dowels which are used to transfer shear loads. In the test model these dowels key the bearings to load cells below and to the bridge deck main girders above. The total rubber thickness is 5.25 in. (133 mm) and the total height of the bearing is 7.875 in. (200 mm). A hole with a diameter of 1.5 in. (38.1 mm) is provided in the center of the bearing to hold the lead plug.

The natural rubber compound used for these bearings is EDS 39 [1] which has a nominal shear modulus of 100 psi (0.690 Mpa) at a shear strain of 50%. Tests on small samples of the compound before the bearings were manufactured gave a shear modulus of 103 psi (0.710 Mpa) at 50% strain and 0.5 Hz and, 99 psi (0.683 Mpa) at 100% strain and 0.5 Hz. The rubber contains 25 parts of carbon black filler per 100 parts of rubber. The hardness of the rubber as compounded was 50 IRHD.

The horizontal stiffness of a single bearing was measured in a static test rig and found to be 1.18 kips/in. (0.207 kN/m) based on the secant slope at 50% shear strain. For the dimensions of this bearing this is equivalent to a shear modulus of 99.5 psi (0.686 Mpa). In a later

section we will discuss the dynamic testing of the system; in these tests the stiffness was measured as 1.21 kips/in. (0.212 MN/m) corresponding to a modulus of 102 psi (0.703 Mpa). This shows that the stiffness of the natural rubber is not sensitive to the rate of loading.

The vertical stiffness of a bearing from a static test was found to be 135 kips/in. (23.6 MN/m). The shape factor, S , for these bearings including the effect of the central hole is 5 and the compressive modulus is 11.6 ksi (80.2 Mpa), calculated by using the standard formula

$$E_c = E_o (1 + 2KS^2)$$

where, for a hardness of 50, the value of K is 0.73 [2-2] and E_o is 310 psi (2.14 Mpa). So that the predicted vertical stiffness is

$$K_v = E_c \frac{A}{h_r} = 138 \text{ kips/in. (24.2 MN/m)}$$

where the cross-section area of the bearing, A , is 62.2 in.² (0.04 m²) and the total rubber thickness, h_r , is 5.25 in. (0.133 m). This is almost exactly the average between the loading value (135 kips/in.) above and the unloading value of the vertical stiffness. The buckling load of a bearing was determined to be 70 kips (311 kN) and since the total weight of the model as tested was 96 kips (427 kN) and four bearings were used the ratio of vertical load to buckling load is 0.34. Theoretical analysis of the stability of multilayer bearings predicts that the vertical load will reduce the horizontal stiffness by a factor that depends on the ratio of vertical load to buckling load. At this value of the ratio the predicted reduction in horizontal stiffness is around 10% but as noted above the measured horizontal stiffness of the bearing is consistent with the measured modulus of the rubber so that either there are compensating factors in the bearings as manufactured or the effect is masked by the non-linearity of the rubber response.

The lead plug when inserted increases the elastic stiffness of the bearing substantially and, having a yield shear stress of 1.5 ksi (10.3 Mpa), produces a nominal yield shear force of 2.6 kips (11.6 kN) per bearing. The yield shear force for the entire base is thus 10.5 kips (46.7

kN) and constitutes 11% of the weight of the superstructure.

Chapter 3 EXPERIMENTAL MODEL AND PROGRAM

3.1 Experimental Model of Bridge Deck

The structural model of the bridge deck comprised two twenty foot long WF16 girders spaced six feet apart and connected transversely by WF8 cross beams with angle cross-bracing. A set of light precast concrete blocks, eight inches thick, were attached to this steel frame work to form the deck. The reinforced concrete blocks were loaded by lead ballast to produce a bridge deck with a total weight of 96 kips (427 kN) which is a typical figure for a short span reinforced concrete deck. The cross section of the bridge deck model is shown in Figure 2 and an elevation of the model is shown in Figure 3. Stiffener plates were added to the WF16 at the several support locations needed for the straight and skew bridge tests. In the straight bridge tests, the supports used corresponded to a clear span of twelve feet with overhangs of four feet on each end.

Since the primary purpose of the test program was to answer several questions regarding the dynamic response of straight and skew decks on non-linear isolators and since non-linear systems are not easily scaled (different components can scale differently), it was decided to treat the deck as full scale (scale factor unity). The base isolation bearings were thus designed to give an effective period of around 1.5 seconds so that real time unscaled records of ground motion could be used as table input. The bridge deck as a full-scale bridge is of course somewhat short but length-related factors may be expected to be unimportant to base-isolated response, since higher modes will be very much higher in frequency in a real structure than the isolation mode which is of predominant interest.

The bridge deck can also be consider as a scaled model of a structural system with an essentially rigid superstructure. The advantage of the model for this purpose is that, in contrast to the tall frame models used in previous testing [2,3,4], the model can be driven to the point of bearing failure without risk of collapse of the frame. In this phase of the test program, the model was considered to be a half-scale model.

3.2 Test Facilities and Instrumentation

The experiments reported here were carried out on the shaking table at the Earthquake Engineering Research Center of the University of California, Berkeley, at the Richmond Field Station. The table is 20 ft x 20 ft (6.1 m x 6.1 m) in plan dimension. Simulated seismic ground excitation to structures weighing up to 100 kips (444.8 kN) can be applied in one horizontal direction and vertical direction with maximum acceleration 1.5g horizontally and 0.5g vertically.

The shaking table is constructed of a combination of reinforced and prestressed concrete. The table is driven in one horizontal direction by three hydraulic actuators and vertically by four such actuators. During operation the dead weight of the table and test structure is carried on air pressure, so that the actuators apply the seismic accelerations and do not carry gravity loads. The shaking table is electronically controlled in five degrees of freedom. Movement in the other horizontal direction is prevented by sliding mechanism. Normally, the pitch, roll and yaw (twist) commands are zero, and the horizontal and vertical command signals represent translation and displacement time histories of earthquake record.

The table is displacement controlled and the primary control is the span setting. Span setting refers to the maximum table displacement during the signal. The extreme table displacement is ± 5 in. (± 127 mm) and this is assigned span 1000. Other spans produce proportionally smaller peak displacements.

The scaling that is used in shaking table experimentation is based on constant stress. It is assumed that the model carries additional loads which will compensate for the reduction in inertia produced by the geometrical scaling. In constant-stress scaling, the frequency of the system varies with the square root of the geometrical scale factor. Thus, if the time scale is increased by the square root, displacement will be decreased by the scale factor and acceleration and stresses are the same for prototype and model. It is possible in the tests both to use a real-time earthquake input treating the model as if it were a full-scale structure and also by use of this time-scaling process and geometrical scaling to use the model to predict the

response of a larger structure.

The Earthquake Simulator Laboratory is equipped with a NOVA-1200 minicomputer that operates in conjunction with a Diablo-31 moving head magnetic disc unit. A maximum of 128 data channels can be sampled at rates up to 100 samples per second. The analog signals are fed to amplifiers, multiplexers and to an analog digital converter. The digitized data are temporarily stored on magnetic disc before being transferred to tape. After each test run, the positive and negative extreme values of each channel can be searched and can be printed with the corresponding time to when they occurred.

The important instrumentation for the straight-deck experiments consists of four horizontal accelerometers, two in the longitudinal direction and two in the transverse direction, located above each bearing. Vertical accelerations were recorded by four accelerometers, also located above the isolation bearings. Four horizontal potentiometers measured displacement relative to the table in the longitudinal and transverse directions. There were also four vertical potentiometers but their output was difficult to use since the vertical displacement on a bearing is extremely small and is accompanied by a horizontal displacement which is at least an order of magnitude greater. They are useful in a test in which the only input signal is vertical. The horizontal shear forces in each bearing are monitored continuously during a test by force transducers under each bearing. The transducers provide shear loads in both longitudinal and transverse directions. The axial force output from these force transducers was not reliable when horizontal forces were present and they were used only in the tests with purely vertical input.

The location diagram for the instrumentation is shown in Figure 4. A summary of the instrumentation used in the tests on the straight deck is given in Table 1.

3.3 Experimental Program for Plain Rubber Bearing System

The dynamic test program on the bridge deck model with plain rubber bearing system involved a very extensive range of types of test. Pull-back tests were performed first to obtain an estimate of the natural frequencies of the system, both longitudinal and torsional, and to obtain the damping associated with these modes. The frequencies and damping factors that can be obtained by pull-back tests are restricted to those for small strains since it is not possible to produce static deflections in pull-back tests that exceed one inch or strains greater than 20%. In the torsional pull-back tests a large pin was located at the center of the bridge deck preventing lateral displacement with respect to the table. The torsional oscillations took place around this pin. Some degree of friction will have developed at the pin and will have contributed to the damping measured by logarithmic decrement, but this is not felt to be important since the lever arm of the frictional forces will be small leading to a negligible couple.

To obtain logarithmic decrement results from larger initial displacements, the model was subjected to harmonic motion close to resonance to a specified maximum displacement. The table motion was then abruptly halted and the model allowed to perform free vibrations. An interesting aspect of this test was the appearance of a beat phenomenon during the start-up of these tests; these are at first sight unexpected but result from an interaction of the steady-state response with the damped free vibration response at a very closely adjacent frequency. An example of the beats is shown in Figure 5 showing time history of the longitudinal displacement when the input frequency was 0.65 Hz. These beats eventually disappear but they persist for a long enough period of time to make it necessary to take care in determining the final steady-state displacements and accelerations when the input frequencies are close to resonance.

Following these tests, steady-state harmonic tests at fixed table displacement over a frequency range from 0.2 Hz to 2.8 Hz were carried out. These tests allowed the determination of stiffness and damping at different strain ranges.

Earthquake input tests were then carried out and in the first series of the tests both horizontal and vertical signals were used. The purpose of these tests was to assess the influence of vertical motion on the horizontal motion. Tests were run with a purely horizontal input, purely vertical input and the combination of the two. The El Centro 1940 NS record was used for this test series at span setting that varied from 100 to 400.

It was found that when both horizontal and vertical signals were used the horizontal response of the system was essentially identical to that when horizontal input alone was used. It was determined that in all subsequent tests only horizontal signals would be used in order to reduce the quantity of data to be collected.

An extensive series of horizontal earthquake input tests were carried out to investigate the response of bridge deck on the plain rubber bearing system. The signals used were

- (1) El Centro 1940 N-S record
- (2) ATC-3, Soil type 2, spectrum-compatible record [5]
- (3) Caltrans spectrum-compatible record [6]
- (4) Caltech A1 artificial record
- (5) Taft 1952 S69E record
- (6) Parkfield 1966 N65E record
- (7) Pacoima Dam 1971 S14W record
- (8) San Francisco 1957 Golden Gate Park S80E record

The first five records are long-period records whereas the last three are short-period records. The two spectrum-compatible records are derived by modifying the El Centro 1940 N-S signal to produce a response spectrum consistent with the corresponding design spectrum.

The complete test program of horizontal only earthquake inputs for the plain rubber bearing system is summarized in Table 2. Two basically different series, real time signals and $\sqrt{2}$ time scaled signals, were used in the tests within the displacement capacity of the bearings.

Since the center of mass of the model was quite low, it is possible to push the bearings to the limit without fear of great damage to the model or to the shaking table as would be the case if a tall frame model were being tested. The $\sqrt{3}$ time scaled El Centro 1940 NS signal at span 750 was used to study the limiting displacement capacity of the isolation system.

3.4 Experimental Program of Lead-Filled Rubber Bearing System

Only earthquake signal inputs were used in testing the lead-filled rubber bearing system. The first series of tests was to investigate the influence of vertical excitation on the horizontal response of the lead-filled bearing system. Tests were run with a purely horizontal input, purely vertical input and the combination of the two. The El Centro 1940 NS record was used for this test series at spans varying from 100 to 500.

The second series was the horizontal only excitation tests using different real time earthquake signals and $\sqrt{2}$ time-scaled earthquake signals. The complete test program for horizontal only inputs is shown in Table 3. Mainly, the real time earthquake test used four real time signals at different spans: Parkfield, El Centro and two spectrum-compatible El Centro type signals with enhanced low frequency contents. The $\sqrt{2}$ time-scaled earthquake test included six different time scaled signals, long period and short period, at span 750. The Caltrans signals at spans 650 and 800 were used in the limiting tests. The bearing system slid under the excitation of span 650 input and under stronger signal, at span 800, the bearing system was made to roll out.

Chapter 4 TEST RESULTS OF PLAIN BEARING SYSTEM

In this chapter, the results of the various test routines for the plain rubber bearing system will be described in detail. Each of the following sections will cover one of the test routines described in the previous chapter.

4.1 Results of Longitudinal and Torsional Pull-Back Tests

The maximum pull-back force that could be used was 6 kips (26.7 kN) producing a displacement of roughly 1 in. (25.4 mm). Displacement and acceleration time histories were recorded after release of pull-back tension. An example of the longitudinal displacement record averaging channels 48 and 49 is shown in Figure 6. The corresponding acceleration, the average of channels 42 and 43, is shown in Figure 7. The Fourier transform of the displacement time history is shown in Figure 8 with a strong peak at 0.86 Hz.

Logarithmic decrement analysis

$$\beta = \frac{1}{2\pi} \ln \frac{v_{n-1}}{v_n}$$

is used to obtain the damping factor β from successive cycles of the free vibrations as shown in Table 4. It is clear that the damping factors decrease with decreasing strain. The strains here are not large; at the maximum they are 19% and at small strains the data reduction becomes very difficult due to the small difference between v_{n-1} and v_n . Over this range of strain the average damping factor is about 6.9%. The frequency measured by length of time between peaks steadily increases with decreasing strain from 0.80 Hz at 15% to 0.97 Hz at 0.3% strain.

The rotation of the bridge deck during the torsional pull-back test is shown by the difference between channels 50 and 51 in Figure 9, and the acceleration computed from the difference between 40 and 41 corresponding to these rotations is shown in Figure 10. The Fourier transform of the rotation is shown in Figure 11 and indicates a strong peak frequency

at 0.86 Hz and, from the logarithmic decrement averaged over the first five cycles, a damping factor of 6.4%.

The frequencies in the longitudinal and torsional modes are practically the same, and it might be expected that strong torsional lateral coupling would develop (after the central pin was removed, of course). However, no torsional lateral coupling was evident during the tests, nor could it be developed. The lack of torsional coupling is presumably due to the small eccentricity between center of mass and center of stiffness and the damping available in the bearings. An analysis of the phenomenon of torsional lateral coupling in base-isolated systems is given in [7].

After considerable earthquake testing over a period of nine days these pull-back tests were repeated to determine to what extent the response of the bearings had been changed by a considerable history of deformation up to very large strains, up to a maximum of 131%. Under the same 6 kips (26.7kN) pull-back force, the strain becomes 1.3 times the strain obtained from the first pull-back test. That is, the bearing stiffness decreased after a considerable history of deformation, but the damping ratio remained almost the same even though the strain has increased.

4.2 Decay Curves for Harmonic Input

Due to limitations in the force available for pull-back it was only possible to produce an initial displacement of 1 in. (25.4 mm) corresponding a strain of less than 20%. In order to develop higher starting strains in a logarithmic test, the system was set into motion by the table at a frequency close to resonance, the table stopped and the displacement measured. Using this technique initial displacements around 4 in. (102 mm) and strains above 70% could be achieved.

The time history of deck displacement after the table stopped is shown in Figure 12, which shows the decrement of deck displacement in free vibration. Using logarithmic decrement analysis the damping factor β obtained from successive cycles of the free vibrations is

shown in Table 5. The range of the measured strain is from 70.6% to 1.9%. Over this range of strain the average damping factor is about 6.4%. The frequency measured by length of time between peaks steadily increases with decreasing strain from 0.63 Hz at 70.6% to 0.76 Hz at 1.9%. The damping factors obtained from the longitudinal pull-back test and the harmonic decay test are plotted in Figure 13 versus logarithmic strain. Except some values determined from the first cycle and at small strains, which create large errors, the damping factors obtained from these two tests show a smooth variation with respect to the logarithmic strain from 1% to 60%.

4.3 Test Results of Steady-State Sinusoidal Loading

Steady-state sinusoidal tests were carried out at frequencies from 0.2 Hz to 2.8 Hz. In these tests purely horizontal input was used. The maximum shaking table displacement was fixed at 0.35 in. (8.89 mm) and the resultant relative displacements and absolute accelerations of the model recorded. As shown in Table 6, there are two sets of steady-state sinusoidal test. The second set was carried out after the first set was finished. Even under the same excitation frequency, the relative displacements of the second set were larger than those of the first set. Since the rubber bearings had experienced a history of large deformations before the second set of tests, the inconsistent results of these two test sets indicates that the rubber bearing can memorize the experienced strain and the future behavior of the rubber bearing will be affected by this memory.

The amplification factor, defined as the ratio of the maximum relative displacement of model response to the maximum absolute displacement of table input, is listed in Table 6, which indicates that the resonant frequency is roughly 0.7 Hz. Figure 14 compares the hysteresis loops under the frequencies, 0.65 Hz, 0.7 Hz and 0.8 Hz. The reduction in stiffness of the bearing as a function of peak strain is very clear from these plots. The bearing stiffness shown in Table 6 is calculated from the maximum shear force in the bearing divided by the maximum relative displacement of deck. Based on these stiffnesses, the natural frequency of

the base isolation system can be estimated.

The nature of the rubber damping is more accurately modeled by using the so-called hysteretic model of damping [8] where the shear stress τ is related to the shear strain γ through

$$\tau = G(1 + i\delta)\gamma$$

in which G is the shear modulus and δ is the loss factor. The damping force and the energy loss per cycle of hysteretic damping are independent of the input frequency whereas those of viscous damping are linearly dependent on the input frequency. The loss factor can be estimated by measuring the area of the hysteresis loop using the formula

$$\delta = \frac{\text{Area of Loop}}{\pi f_{\max} v_{\max}}$$

where f_{\max} and v_{\max} are the maximum force and maximum displacement in the loop. The loss factors listed in Table 6 are from this equation. They have the same tendency as effective stiffness to decrease with increasing maximum strain. The damping ratios are calculated from the loss factors by the following equation

$$\beta = \frac{\delta}{2\Omega}$$

where Ω is the ratio of input frequency to natural frequency. High fluctuation in the damping ratios, from 1.8% to 44.7%, indicates that the representation of the response by the conventional model of linear viscous damping is not an accurate one.

For a linear hysteresis damping system, the theoretical amplification factor is equal to

$$A = \frac{\Omega^2}{\sqrt{(1 - \Omega^2)^2 + \delta^2}}$$

Using the loss factor of 7.4%, obtained from the second set of test at the resonant frequency 0.7 Hz, the theoretical amplification factor at resonance, $\frac{1}{\delta}$, should be equal to 13.5. However, as shown in Table 6, the amplification factor at 0.7 Hz is only 9.85. For the small loss

factor, the amplification factor in the above equation is very sensitive to slight changes in frequency near resonance. The Fourier spectrum of input displacement record at 0.7 Hz shows that the real input frequency is 0.68 Hz. Using this real input frequency, the theoretical amplification factor calculated from the above equation is 10.1, which is very close to the experimental result 9.85. The curve of theoretical amplification factor based on a linear model with natural frequency 0.7 Hz and loss factor 9% is plotted in Figure 15, along with the experimental results of Table 6. Because of the nonlinear stiffness of the rubber bearing, the experimental results for low amplification factors tend to shift towards the curve of higher natural frequency.

4.4 Influence of Vertical Excitation

The natural frequency of the system in purely vertical input was found to be 7.8 Hz corresponding to a vertical stiffness of 150 kip/in. (26.3 MN/m) for a single bearing. The results for the El Centro signal at span settings of 100 to 400 for horizontal only, vertical only and horizontal and vertical combined are given in Table 7. The results show that the horizontal accelerations when both signals are used do not differ greatly from those for horizontal input only and the vertical accelerations for vertical loading only are similarly unaffected by simultaneous horizontal input. This lack of cross coupling between horizontal and vertical loading justified the subsequent restriction to horizontal input only to limit the amount of data to be collected.

There is in fact a high degree of inconsistency in the table input. The peak horizontal table acceleration, when both inputs are combined, is not the same as when horizontal input only is used.

4.5 Results of Horizontal Real-Time Earthquake Tests

The test results of four real time signals, Parkfield, El Centro and two artificial El Centro type signals with enhanced low-frequency components, are given in Table 8. The peak accelerations, peak displacements and bearing forces are tabulated with peak table values and the corresponding reduction factors for acceleration and amplification factors for displacement. The ratio of peak bearing force to peak displacement is also shown to provide an estimate of the bearing stiffness during the test. The tests were carried out at various span settings.

The results for the El Centro and the two El Centro type artificial inputs are substantially the same with the artificial signals (ATC-3 and Caltrans) producing more accelerations in the model and larger displacements than the real signal (El Centro). This is to be expected since the artificial records are obtained from the El Centro record by enhancement of the lower frequency components. The largest relative displacement measured at the bearings was during the ATC-3 at span 400, and was 6.88 in. (175 mm), corresponding to a strain of 131% and a displacement that is 86% of the bearing width. The force displacement curve for the bearing during this test is shown in Figure 16. The characteristic behavior of the bearing at these large displacements is shown. This will be treated in detail later.

The results for the Parkfield signal are significantly higher for the same span than for the other three input signals. For example, comparing the results for Parkfield at span 300 with the most severe of the other three, namely ATC-3 at span 300, they have the same peak table displacement of around 1.5 in. (38.1 mm) but the deck relative horizontal displacement is 5.0 in. (127 mm) for Parkfield and 4.6 in. (117 mm) for ATC-3. The peak table acceleration of Parkfield at span 300 is 0.227g and the deck acceleration 0.184g, a reduction of only 0.81. For ATC-3, we have 0.251g and 0.173g, a reduction of 0.69. The Parkfield is a relatively short duration signal with a large acceleration pulse at the beginning of the signal. The response spectrum has a substantial peak at 0.6 Hz which is the frequency of the isolated system so that the severity of the results is not unexpected. This earthquake had a magnitude of

5.6 Richter and occurred on the San Andreas fault. The acceleration was recorded 200 feet from the fault trace on alluvial soil overlying rock roughly 100-200 feet below.

As an example of the response of the system to these inputs, Figure 17 shows the table acceleration and model acceleration of ATC-3 at span 400. The corresponding displacements are shown in Figure 18 and the Fourier transforms of table acceleration and model acceleration in Figure 19.

To illustrate the action of the isolation system with increasing earthquake intensity we plot the ratios of model to table acceleration and model relative displacement to table displacement and the bearing stiffness in Figure 20. These are shown for the El Centro input and represent results for two sets of input, one set of tests done before the skew tests were carried out and one set after the skew tests. The stiffness of the bearings was somewhat reduced in the later set since they had undergone a very extensive amount of work. The displacement ratio increases with increasing span and the acceleration decreases and there is, as indicated in other tests, a reduction in stiffness with increasing span and thus increasing shear strain in the elastomer.

4.6 Results of Horizontal Time-Scaled Earthquake Tests

Since the time scaled earthquakes can be used to predict the response of full scale structural systems, the results of this test series can be used for bridge decks roughly twice the size of the experimental model. The results of these tests are summarized in Table 9 in which peak relative displacements and peak deck accelerations are listed and compared to the table values. The isolation system reduces the accelerations by a factor which varies from 0.679 for the Caltech signal (a long duration record) to 0.109 for the San Francisco signal (a short duration signal). The average reduction factor is 0.331 over all six records. The relative displacements experienced by the bearings are, with the exception of the San Francisco record, larger than the absolute displacements of the table, with the maximum amplification factor being that for the El Centro record at 1.838. The average amplification factor is 1.291. The

reduction of displacement which occurs in the San Francisco record is somewhat unexpected but reference to the displacement and acceleration time histories Figures 21 and 22 show that very high accelerations occur very early in the signal with high-frequency components and negligible displacements and the large displacements which occur in this record are produced by low-frequency displacement pulses having a period of around six seconds. Thus for acceleration the isolation system is a low-frequency system and attenuates it and for displacement the system is a high-frequency system and rides with the ground motion producing small relative displacements.

The measured peak forces in the bearings divided by measured peak displacements are also shown in Table 9, providing an estimate of the effective stiffness of the bearings under the transient loading. This varied from 0.9 kips/in. (0.158 MN/m) to 1.3 kips/in. (0.228 MN/m) indicating the non-linearity of the system.

In this case the Parkfield record is no longer the most severe input, reflecting the fact that Parkfield has energy in a limited frequency ratio and time scaling moves this away from the resonant range of the system, whereas El Centro with a wide band of frequencies with high energy continues to be a severe input to the system. The maximum displacement under El Centro input was 6.91 inches which represents a shear strain of 132% and a displacement of 86% of the width of the bearing. The hysteresis loop for the whole system under this loading is shown in Figure 23 where the instability of the bearing is seen. The force displacement curve is diminishing, indicating incipient roll-out of the bearing. The dynamics of the situation at that instant are such that the bearing can recover without damage. A detailed analysis of the roll-out behavior of the bearings will be given in a following section.

Another demonstration of the non-linear response of this system is shown in Figure 24 where the hysteresis loops of the first few cycles of response to the Pacoima Dam record are shown. The loops are averaged over all four bearings. The initial response has a stiffness of 1.77 kips/in. (0.31 MN/m), 7.08 kips/in. (1.24 MN/m) for the system, and after one cycle the stiffness drops to 1 kip/in. (0.175 MN/m), 4 kips/in. (0.7 MN/m) for the system. The

maximum strain on the first cycle is 6% and on the second 84%.

Chapter 5 TEST RESULTS OF LEAD-FILLED BEARING SYSTEM

In this chapter, the results of the test routines for the lead-filled rubber bearing system will be described in detail. Real-time earthquake inputs and $\sqrt{2}$ time-scaled earthquake inputs are the two test series carried out on the lead-filled rubber bearing system. These test results will be compared with those of the plain rubber bearing system.

5.1 Influence of Vertical Excitation

The natural frequency of the system for the vertical vibration mode was found to be 11 Hz corresponding to a vertical stiffness of 300 kips/in. (52.5 MN/m) for a single bearing. Due to the insertion of lead plug, the vertical stiffness of the lead-filled bearing is twice that of the plain bearing. To investigate the influence of vertical excitation on the horizontal motion of the bridge deck with the lead-filled bearing system, a series of tests for the El Centro real-time signal at spans varying from 100 to 500 for horizontal only, vertical only and horizontal and vertical combined were carried out and the results of test are given in Table 10.

The results show that the horizontal accelerations when both horizontal and vertical signals are used do not differ greatly from those for horizontal input only. Similarly, the vertical accelerations are almost unaffected by the excitation of vertical loading only or simultaneous horizontal and vertical inputs. Similar results were found for the plain bearing system. This uncoupled response between horizontal and vertical loading suggests that the later earthquake input tests could be horizontal input only to limit the amount of data to be collected.

5.2 Results of Horizontal Real-Time Earthquake Tests

The test results of four real-time signals at different spans are shown in Table 11. These four real-time signals are Parkfield, El Centro, ATC-3 and Caltrans, where the last two are artificial El Centro type signals with enhanced low-frequency components. This table shows the peak displacements and peak acceleration of the shaking table input and the measured

response of the bridge deck. The corresponding reduction factors for acceleration and amplification factors for displacement are computed from the ratio of the bridge deck response to the shaking table input. Also shown is the peak shear force measured in a single bearing and the ratios of peak bearing force to peak displacement to provide an estimate of the bearing stiffness during the test.

The results for the Parkfield, ATC-3 and Caltrans inputs are substantially the same whereas the result for the El Centro input is completely different. For the same span, the El Centro signal has a much higher input acceleration than the other three signals, but produces less relative deformation of the deck and only slightly higher deck acceleration. The El Centro signal thus has smaller amplification factor for displacement and reduction factor for acceleration. For example, comparing the results at span 400, the deck relative displacement for El Centro is 3.06 in. (77.7 mm) whereas it is between 3.75 in. (95.3 mm) and 4.00 in. (102 mm) for the other three inputs. The deck acceleration for El Centro, 0.245g, is almost the same as that of the other three, from 0.238g to 0.241g, but the input acceleration of El Centro is 0.509g which is much higher than the other three signals, varying from 0.302g to 0.315g. Thus, the amplification factor of displacement for El Centro, 1.514, is lower than the average of the other three, 1.887, and the reduction factor of acceleration for El Centro, 0.481, is lower than the average of the other three, 0.777. The smaller response for the El Centro signal is expected because the three other signals -- Parkfield, ATC-3 and Caltrans -- have considerable lower frequency energy which is severe to the base isolation system.

The other main difference of the test results between the El Centro input and the other three inputs shown in Table 11 is the variation of isolation effect with increasing span. For the El Centro signal, the reduction factors of acceleration decrease with increasing span but the amplification factors of displacement remain almost the same. This implies that the effect of the lead-filled rubber bearing system on the protection of bridge deck increases when the intensity of the El Centro input signal increases. However, the opposite effect occurs with the other three signals, for which both the amplification factor of displacement and the reduction

factor of acceleration increase with increasing input intensity.

The relation between the shear force and shear deformation of the lead-filled rubber bearing during the ATC-3 test at span 400 is shown in Figure 25. This relation is approximately bilinear. For small excitation, the lead plug does not yield and confers high stiffness on the bearing. As the intensity of the motion increases, the lead plug yields and the stiffness of the bearing drops to that produced by the rubber. Large hysteresis loops are formed due to yielding of the lead and dissipate more energy than the plain rubber bearing. The phenomenon of stiffness hardening is illustrated in Figure 25. At the lead yielding stage, when the bearing has returned to its undeformed shape and is moving to the opposite side, the stiffness of bearing is found to increase slightly. This stiffness hardening will reduce the isolation effect of lead-filled rubber bearing.

As an example of the response of the system to these real-time inputs, the displacement time history of bridge deck response under the excitation of the ATC-3 signal at span 400 is shown in Figure 26. The corresponding acceleration time history is plotted in Figure 27, and the Fourier response spectrum of this acceleration time history in Figure 28. Unlike the plain bearing case, the Fourier spectrum does not have a concentrated frequency content near the natural frequency.

5.3 Results of Horizontal Time-Scaled Earthquake Tests

The results of the $\sqrt{2}$ time-scaled earthquake tests are summarized in Table 12 in which peak relative displacements and peak accelerations of bridge deck are listed and compared to the table input values. Since the bridge deck model is approximately one-half scale of the prototype, the acceleration response of the $\sqrt{2}$ time-scaled earthquake tests can be used to predict the response of the full-scale structure. The isolation system reduced the accelerations by a factor which varied from 0.713 for the Caltech signal (a long duration record) to 0.200 for the San Francisco signal (a short duration signal). The average reduction factor was 0.532 over all six records. The relative displacements experienced by the lead-filled rubber bearing

are smaller than the absolute displacements of the table input. The average displacement ratio was 0.747.

The measured peak shear forces in the single lead-filled bearings divided by measured peak displacements shown in Table 12 provide an estimate of the effective stiffness of the bearings under the transient loading. This varied from 2.0 kips/in. (0.35 MN/m) to 2.7 kips/in. (0.473 MN/m).

5.4 Comparison between Plain and Lead-Filled Systems

The amplification factor of displacement and the reduction factor of acceleration for the plain and lead-filled bearing system are compared in Table 13 for the four real-time earthquake inputs at different spans, as are the ratios of the lead-filled bearing values to the plain bearing values. The ratios of the displacement amplification factor vary from 0.43 to 0.75 with an average of 0.58. The ratios of the acceleration reduction factor vary from 0.80 to 1.22 with an average of 1.06. This indicates that, while the lead plug insert can reduce the relative displacement of the bridge deck, acceleration response will remain nearly the same. However, the acceleration response of real-time earthquake inputs represents the response of the size of the model, which can not be applied to predict the response of a full-scale structure.

The results for the six $\sqrt{2}$ time-scaled signal at span 750 are compared in Table 14. The ratios of the displacement amplification factor vary from 0.35 to 1.10 and have an average of 0.67. The ratios of the acceleration reduction factor vary from 0.87 to 1.83 with an average of 1.35. This shows that, although the lead plug can reduce displacement response by one-third, it also increases acceleration response by one-third. Although the lead-filled rubber bearing can reduce the relative displacements of the bridge deck, this reduction is at the cost of increased deck accelerations.

The vertical acceleration responses of the plain and lead-filled bearing systems are compared in Table 15 for the El Centro vertical only real-time signal at spans varied from 100 to

400. The ratios of the deck response acceleration to the table input acceleration shown in Table 15 indicate that the amplification factor of vertical acceleration for the plain bearing system, with an average of 1.66, is larger than that for the lead-filled bearing system, with an average of 1.20.

Chapter 6 PARAMETER IDENTIFICATION ROUTINE

6.1 Parameter Identification for Linear Viscous Model

Since the bridge deck model has a uniformly distributed dead load and is excited in the longitudinal direction, lateral or torsional vibrations will be negligible. Thus, the entire system can be idealized as a single degree-of-freedom system. There are considerable advantages in analysis and design to modeling the base isolation system as a linear viscously damped system. The natural frequency and the damping ratio are then the only two parameters needed to describe the model. If these two parameters are identified from the experimental results of the base isolation system, the model they describe should simulate the real system. Also from these identified parameters, the extent to which the real system differs from the ideal model can be estimated.

To obtain the parameters for each test, the response spectrum of the table input is calculated for a range of frequency and a range of damping ratio which are around the identified values. The maximum acceleration and maximum displacement for each frequency and damping ratio are used as two coordinates. The contour plots of constant damping ratios at varying frequencies and those of constant frequencies with different damping ratios form two sets of intersecting curves. This produces a network the intersections of which represent the maximum displacement and maximum acceleration for a specific frequency and a specific damping ratio as shown in Figure 29, the example for the Parkfield time-scaled signal at span 750. This response network has twenty frequencies, from 0.35 Hz to 1.30 Hz with an interval of 0.05 Hz, and four damping ratios, 3%, 5%, 7% and 9%. The actual experimental results for this signal were 4.99 in. (178 mm) peak displacement and 0.177g peak acceleration. When these results are plotted on Figure 29, the estimated frequency is 0.60 Hz and the damping ratio is 5%. By this response network approach, the effective frequency and damping ratio are determined by satisfying the following two conditions: the maximum displacement and maximum acceleration of the linear viscous model are the same as those in the real base isolation

system.

6.2 Parameter Identification of Plain Rubber Bearing

This identification procedure has been carried out on the plain rubber bearing system for the thirteen real-time and time-scaled signals. The results, namely effective frequencies, damping ratios and the effective stiffness of a bearing derived from the effective frequency, are shown in Table 16. The large variation of effective stiffness and damping ratio indicates that the real system is far from the linear viscous model. There is a tendency for the effective stiffness to decrease when the maximum strain increases. This is consistent with the observation in the steady state sinusoidal tests mentioned in section 4.3. However, damping ratios fluctuate too much, from 2% to 10%. Since the rubber damping is more accurately modeled using the hysteretic model of damping illustrated in section 4.3, the loss factors are also listed in Table 16, which are measured from the largest loop of each test as shown in Figures 16, 23 and 24. They tend, as does the effective stiffness, to decrease with increasing maximum strain.

The actual experimental response and the computed model responses based on these values of effective frequency and damping ratio are compared in Figures 30, 31 and 32 for the El Centro, Parkfield and Pacoima Dam time-scaled signals at span 750. These time history plots show that the maximum response is well fitted, but away from the maximum peak the actual response and the computed response differ, the differences being in the rapidity with which the response dies away. At lower displacements the effective damping of the system is underestimated due to the nature of damping in rubber-like materials. In contrast to the idealized linear viscous model, the damping in rubber is independent of frequency. Thus selecting the damping factor on the basis of the low effective frequencies and the large strains at peak displacement has the effect of underestimating the damping at the smaller strains and the higher effective frequencies away from the peak response.

The stiffness of a single plain rubber bearing as estimated from the parameter identification routine for the earthquake input tests is plotted in Figure 33 as a function of maximum strain. This figure also shows the stiffness as calculated from the steady-state sinusoidal tests. The sinusoidal tests cover a smaller maximum strain whereas the earthquake tests cover a range of strain up to 141%. The results from these two types of test are seen to be mutually consistent which suggests that results of steady-state sinusoidal tests can be used to infer the peak response values under transient loading. When the least squares method is used to fit these data, an approximate functional relationship between the shear stiffness K_h and the maximum strain ϵ_{\max} can be calculated by the expression

$$K_h = 0.894 - 0.790 \log \epsilon_{\max}$$

in which the unit of shear stiffness is kip/in. This function is plotted in Figure 33 and seen to fit the experimental results very well. It should be noted that this equation does not show the relationship between shear force and shear strain. It only indicates the rule that the stiffness will change if the maximum strains in deformation cycles differ. The hysteresis loops shown in Figures 23 and 24 reveal that the stiffness during a deformation cycle remains constant.

The variation of loss factors, measured in the sinusoidal and earthquake tests, with respect to maximum strain is shown in Figure 34. The result of fitting these data by a curve of the form

$$\delta = 0.894 - 0.790 \log \epsilon_{\max}$$

is also shown in the figure. This equation indicates that the loss factor decreases with increasing maximum strain.

These properties of reducing stiffness and high internal damping make the plain rubber bearing the most suitable mechanism for the earthquake protection of buildings. The shear stiffness of these bearings is high at the low displacement amplitudes associated with wind loading and low at the much larger displacements associated with earthquake excitation.

6.3 Parameter Identification of Lead-Filled Rubber Bearing

Although the behavior of lead-filled rubber bearing can be closely represented by a bilinear model, any nonlinear approach requires considerable computational effort. This section will describe a correlation study between the lead-filled rubber bearing and the linear viscous model, which is the simplest model in structural dynamics. The parameter identification routine described in section 6.1 will be applied to find the equivalent best linear viscous model.

The parameter identification procedure has been carried out on the lead-filled rubber bearing system for the twelve real-time and time-scaled signals. The results, namely effective frequencies, damping ratios and the effective stiffness of a single bearing derived from the effective frequency, are shown in Table 17. The actual experimental responses and the computed model responses based on these parameters are compared in Figures 35, 36 and 37 for the El Centro, Parkfield and Pacoima Dam time-scaled signals at span 750. These time history plots show that the maximum response is well fitted and also that the peak values are achieved at very nearly the same times as in the experiments, but the computed response of the cycles after the maximum peak differs from the actual response. The differences arise because the hysteresis loop of the lead-filled rubber bearing at peak displacement is greater than that of the linear viscous model. At peak response, more energy is dissipated in the actual bearing so that after the peak the response of the linear viscous model is greater than the actual response.

Distributions of the identified effective stiffness and damping ratio with respect to the maximum strain are shown in Figures 38 and 39. The following two equations approximately fit these data

$$K_h = 2.924 - 1.686 \epsilon_{\max}$$

and

$$\xi = 0.1398 - 0.0221 \epsilon_{\max}$$

where the unit of effective shear stiffness K_h is kip/in. With these two formulac, the linear viscous model can be applied to predict the response of lead-filled rubber bearings at different maximum strain levels.

6.4 Influence of Earthquake on Response of Isolation Systems

It can be seen that the effective stiffness and damping ratio of the lead-filled rubber bearing are higher than those of the plain rubber bearing. In general, the plain rubber bearing produces lower acceleration and larger displacement responses, and the lead-filled rubber bearing can be expected to decrease displacement response because of higher damping, but also due to greater stiffness to increase slightly the acceleration response. However, this is not always true. Figures 40 to 45 show the response networks, described in the section 6.1, of six different time-scaled signals at span 750. Networks with coarse subdivisions are plotted so that the responses of plain and lead-filled rubber bearing can be shown in the same figure. As shown in Figures 40 and 41, the lead-filled bearing is the best isolation system for earthquakes such as the El Centro and Caltech A1, because the displacement response is tremendously decreased while the acceleration response remains nearly the same. For the earthquakes such as Taft and Parkfield, shown in Figures 42 and 43, the lead-filled bearing is less efficient. The advantage of reduced displacement is achieved at the cost of increased acceleration. For types of earthquake such as Pacoima Dam and San Francisco, the plain bearing is more attractive than the lead-filled bearing. Greatly increased acceleration and slightly decreased displacement response is found for the lead-filled bearing excited by the Pacoima Dam record as shown Figure 44. For the San Francisco earthquake, shown in Figure 45, the displacement and acceleration responses of the lead-filled bearing are all higher than those of the plain bearing. This result for the Pacoima Dam record was earlier reported when a five-story steel frame was tested in the large-scaled shaking table with lead-filled rubber bearings [4].

Chapter 7 LIMIT RESPONSE OF BASE ISOLATION SYSTEMS

7.1 Limit State of Rubber Bearing Deformation

In order to study the limiting displacement capacity of the base isolation system, the bridge deck model was subjected to large seismic inputs that would exceed the displacement capacity of bearings. In this section, the possible failure modes when a bearing arrives at its limit state will be investigated. Then, experimental results for the plain and lead-filled bearings will be given in the following sections.

As shown in Chapter 2, the bearings are not attached to the load cells below or the bridge deck above. They are keyed to each by dowels which can transmit shear but no tension, a design that ensures that no tensile stresses can be induced in the bearings. When a bearing is under lateral force and vertical load, a moment is developed at the top and bottom surfaces. Since no tension can be developed at the top or bottom surfaces, this moment can only be provided by a shifting of the resultant vertical load, P , as shown in Figure 46. The equilibrium state for a bearing with height h and width b can be described by

$$V h = P d$$

where V is the resultant shear force developed at the top and bottom surfaces and d is the arm of the resultant vertical forces. When the lateral displacement, δ , increases, the increasing shear force V must be balanced by enlarging the arm, d , requiring the resultant vertical forces to move toward the edges and the contact stresses to increase. There is a limit to the extent that the resultant vertical forces acting on the top and bottom surfaces can be moved and this is reached when they are concentrated at the edges of the bearing as shown in Figure 47. Equilibrium at this point requires that

$$V h = P (b - \delta)$$

This equation shows that the shear force will decrease if the shear deformation increases and indicates that the bearing becomes unstable at this limit state. As shown in Figure 48, a plot

of this limit state equation on a plot of lateral force V as a function of lateral displacement δ for different vertical loads P produces a set of downward sloping lines from $V=Pb/h$ at $\delta=0$ to $V=0$ at $\delta=b$. If the lateral deformation is greater than b , the bearing will roll out under even the smallest value of V .

When the lateral deformation of the bearing increases, the bending of the steel plates on the bearing induces openings on the top and bottom surfaces. If this opening is large, the dowels will leave the holes and no longer transmit shear. In this situation, the shear force is taken by the friction force developing on the top and bottom surfaces which can be expressed as

$$V_f = \mu P$$

where μ is the friction coefficient. If the shear force is larger than V_f , there will be a lateral slide movement between the deck and bearing or between the bearing and load cell.

There are thus two kinds of failure mode as shown in Figure 49. For plain bearings with lower stiffness in which the developed shear force is smaller than V_f when the lateral deformation reaches the limit state, the response of the bearing follows the limit state curve and the bearing rolls out. For the higher stiffness bearing in which the developed shear force is larger than V_f and the shear key does not work, the bearing will slide and the shear force in the bearing will suddenly be released. These failure modes have been found in the shaking table tests. Only roll-out was found in testing of the plain bearing system whereas both roll-out and sliding occurred with the lead-filled bearings.

7.2 Limit Response of Plain Rubber Bearing

For the plain rubber bearing, the elastic force-displacement curve can be expressed as

$$F = K_h \delta$$

where K_h is the horizontal stiffness of the plain rubber bearing. This ascending curve will intersect the descending curve for the limit state at the critical point which lateral

deformation is given by

$$\delta_c = \frac{b}{1 + K_h \frac{h}{P}}$$

In other words, the plain rubber bearing becomes unstable when the lateral deformation is greater than δ_c . In these experiments, a bearing has a height of 7.5 in. (179 mm) and a width of 8 in. (203 mm). The vertical loading on each bearing is approximately 24 kips (107 kN) and the horizontal stiffness is around 1 kip/in. (0.175 MN/m). So that the critical deformation δ_c is about 6.1 in. (155 mm).

Roll-out took place when the experimental model was horizontally excited by the $\sqrt{3}$ time-scaled El Centro signal at span 750. The force-displacement curves shown in Figure 50 indicates instability occurs at 6.1 in. (155 mm). The curve approaching roll-out is the same as the predicted curve shown in Figure 49 except for a rounding near the critical deformation.

In the tests there were several examples of instability which did not lead to roll-out. An example of a case where the bearings went beyond the point of instability but did not roll out is shown Figure 16. In this case of the real time ATC-3 signal at span 400, the maximum displacement was 7.42 in. (188 mm). The displacement at which the force-displacement curve becomes negative is 6.2 in. (157 mm). In other cases where instability occurred but no roll-out happened, the point of instability is in the range 6.0 to 6.2 in. (152 to 157 mm). It is interesting to look at the time histories of displacement, acceleration and shear force in this situation. These are shown on the same plot in Figure 51. When the displacement is small, all three graphs are clearly linearly related but when the displacement is close to 6.0 in. (152 mm) the shear force diagram drops and the acceleration also drops but an additional high-frequency acceleration appears. It is clear that in this case the bearings must have lifted up out of their dowels and, when they rolled back in, some impact effects were produced.

These results indicate that the approximate analysis, although based as it is only on a limiting equilibrium concept, seems to be a good indication of the onset of instability in the

bearings. Thus the formula for the critical value of relative displacement, δ_c , can be used as an ultimate design rule for roll-out of the bearing. It will be a conservative estimate for the limiting displacement, since the results show that it is only the displacement at which roll-out could happen but not necessarily that it will happen. In the course of the testing program, the bearing were subjected to displacements in excess of 6.1 in. (155 mm) in 4 runs without roll-out and, in the one instance that roll-out occurred, the predicted peak displacement on the basis of elastic analysis was around 8 in. (203 mm). These results show that the design of the bearings for maximum displacement can be approached with confidence.

7.3 Limit Response of Lead-Filled Rubber Bearings

In the tests of lead-filled bearing system, there were two examples in which the lateral deformation exceeded the limit displacement capacity of the bearings, one of which, excited by the real-time Caltrans signal at span 650, to a slide and the other to a roll-out, the input being the same signal at span 800.

The displacement time history of deck response in the case of span 650 is shown in Figure 52. Two of four bearings actually developed a slide as shown in Figure 53. The isolation system was still working after the slide but left the bridge deck model with about 2 in. (50.8 mm) permanent set. The relation between the deck deformation and the shear force measured on the load cell of the slide bearing is plotted in Figure 54. The shear force reached a maximum value of 9.5 kips (42.3 kN) and was then suddenly released because the friction can not support such a large shear force. Figure 55 shows the force-displacement curve on the bearing which did not slide. Due to the permanent set, this bearing had a residual force which was opposite in sign to the residual force in the bearing which slipped.

The force-displacement curve in the case of roll-out is shown in Figure 56. The maximum shear force is 8 kips (35.6 kN), which is smaller than 9.5 kips (42.3 kN) in the slide case. The critical deformation is about 5 in. (127 mm). Since the stiffness of lead-filled bearing is higher than that of plain bearing, it is to be expected that this critical displacement will

be smaller than that for the plain bearing, 6.1 in. (155 mm). Figure 57 shows the shape of bearing at large deformation where gaps at the top and bottom surfaces of bearing can be seen.

Chapter 8 CONCLUSIONS

In all previous shake table testing of base-isolated models it has been necessary due to scaling to use rubber isolators with fairly soft rubbers. These rubbers would not be practical for actual application to full-scale systems where filled rubber would be used. In this test series because of the use of a bridge deck as the structural system to be modeled it has been possible to increase the mass of the model to the extent that a more realistic filled rubber material could be used in the isolators. In earlier tests the structural response of the isolated system and the dynamic response of flexible attachments were important aspects of the study, but in the present tests these were omitted by using a model that behaved as a rigid block on the isolation system.

The advantage of this is that it is possible to study the performance of an isolation system on a reasonably well-filled rubber. In this case the rubber contained 25 parts of carbon per 100 parts of natural rubber. This is a lightly filled rubber compound but it does have a low strain shear modulus which is much higher than the modulus at large shear strain. The implication of this for seismic protection systems is that the resistance to wind load of the isolation system is provided by the high shear modulus at low strains and the flexibility desired under earthquake loading is provided by the lower large strain modulus. The ratio of the two moduli in the compound used here is around 3. For a full-scale system where a more highly filled rubber would be used this ratio would rise to at least 5 and possibly more. The results also show that the drop in the value of the modulus with strain is very rapid and takes place mainly in the range 2% to 10% strain. The modulus changes less rapidly for strains greater than 10% and thus an isolation system could be designed for seismic loading at least in the preliminary design stage as if it were a linear elastic system.

These conclusions of course apply only to the bearings not having the central lead plug. When the lead plug is present in the bearings the lead behavior dominates the rubber and wind resistance is provided entirely by the lead. Under large seismic loading when the lead

yields the rubber provides an elastic restoring force but the energy dissipation is also dominated by the lead. The lead plug bearings were extremely effective in limiting the displacements experienced by the bridge deck model. For real time input signals, that is, treating the twenty-foot model as a full-scale structure, the system with lead plugs reduced the displacements as compared to the plain bearing system. The range of the reduction was to between 25% and 50%. For these real time signals the reductions were not achieved at the expense of increased accelerations since the accelerations on the filled bearings were generally about the same as those on the plain bearings, exceeding them in only few instances and by no more than 20%.

These results indicate that the use of lead plugs is highly effective for bridge structures, reducing displacements with minimal increases in acceleration. The high-frequency actions which have been observed in previous lead-plug system testing will have no effect on a bridge superstructure. It is essential not to overstate the case on this point since the earthquake inputs used in the real time tests were low-frequency earthquake El Centro and Parkfield and the two artificial earthquakes were specially enhanced low-frequency signals. The presence of the lead plug increases the effective frequency for the system from roughly 0.5 Hz to close to 1.0 Hz and much of the effect may be due to period shift rather than energy dissipation. Nevertheless all four earthquakes conform in their frequency content to design spectra recommended for highway bridge design and the results are therefore of particular interest to seismic design of bridges.

When we compare the plain bearing system with the lead-plug system for the time-scaled earthquake input, that is treating the model as a part of a real building and neglecting the structural vibrations of the building, the results are more evenly balanced between the systems. Over the range of the input signals reduction in displacement is achieved at the expense of a commensurate increase in accelerations. The exceptions are the El Centro record where the lead system is clearly superior and the Pacoima Dam and San Francisco records where the plain bearing system is clearly superior. The implications of these results to

building design are somewhat unfortunate since the choice between the two systems is not clear.

The inclusion of a lead plug in the elastomeric bearing incurs increased costs and other technical problems such as damage to the rubber/steel bond, bending of the steel reinforcing plates and loss of energy dissipation capacity by ovaling of the plug. These problems can be addressed and more elaborate designs of lead-plug system than that used here and the replacement of the lead by other substances have been developed. However, if the simplest system is desired and the displacements predicted by the design spectrum for the site are acceptable, then a plain bearing is probably the better choice. If, as in bridges, displacements must be controlled, then the extra cost and complications are justified and the lead-plug system would be the better choice.

The prediction of the displacement capacity of an isolation system has been an important question since these systems were first considered. The results of this test series show that a very simple formula can be used to predict the roll-out of the bearing system. This suggests that, at least at the present time, it is advantageous to use the doweled system to connect the bearings to the foundation and to the superstructure. The alternative of firmly bolting the bearings to upper and lower sole plates will produce a failure mechanism involving cavitation in the rubber. The displacement may be larger in some cases than when doweled, but the limit state is governed by a very imprecisely predictable mechanism and the reliability of a predicted limit cannot be great. The roll-out mechanism on the other hand is governed by a simple static analysis which can provide a prediction with high reliability. It further shows that the limit displacement can be increased by increasing the size of the bearings while holding the bearing pressure constant or by increasing the bearing pressure while maintaining the same size of bearing. The possibility of sliding of the bearings prior to roll-out, which is a possibility in the lead-plug system, can be avoided by the use of longer dowels.

A high-frequency vibration generated by the dowels when they move in and out of the dowel holes will not be a problem in bridges and most building structures. It could be a

problem in nuclear systems but would not occur until the earthquake input exceeded the safe shut-down earthquake (SSE) level.

A final conclusion is that the method of parameter identification proposed here and tested by correlation with time history analysis is a highly effective one for the bearing system using lead plugs. The fact that it is not so effective for the plain bearing system which is less nonlinear than the other system is surprising and further study of why this should be so is warranted. It is worth noting that, when time history computations are carried out with the parameters obtained by the identification procedure, the peak values of acceleration and displacement are obtained at the correct time as given by the experiments. This is not a necessary result of the parameter identification procedure but confirms that it is an accurate method for linearization of the non-linear system.

In all, the test series has provided a great amount of information on the response of isolation systems. The conclusions given here pertain only to the non-skew bridge deck model and results for the skewed system await future publication.

References

- [1] "Natural Rubber Engineering Data Sheets", Malaysian Rubber Producers Research Association, England.
- [2] J. M. Kelly, K. E. Beucke and M. S. Skinner, "Experimental Testing of A Friction Damped Aseismic Base Isolation System with Fail-Safe Characteristics", *Report No. UCB/EERC-80/18*, Earthquake Engineering Research Center, University of California, Berkeley (1980).
- [3] J. M. Kelly, M. S. Skinner and K. E. Beucke, "Experimental Testing of An Energy-Absorbing Base Isolation System", *Report No. UCB/EERC-80/35*, Earthquake Engineering Research Center, University of California, Berkeley (1980).
- [4] J. M. Kelly and S. B. Hodder "Experimental Study of Lead and Elastomeric Dampers for Base Isolation Systems", *Report No. UCB/EERC-81/16*, Earthquake Engineering Research Center, University of California, Berkeley (1981).
- [5] "Tentative Provisions for the Development of Seismic Regulations for Buildings", Applied Technology Council, ATC 3-06 (1978).
- [6] J. H. Gates, "Factors Considered in the Development of the Seismic Design Criteria for Bridges", *Proceedings of Workshop on Earthquake Resistance of Highway Bridges*, Applied Technology Council (1979).
- [7] T. C. Pan and J. M. Kelly, "Seismic Response of Torsionally Coupled Base Isolated Structures", *Earthquake Engineering and Structural Dynamics*, Vol. 11, 749-770 (1983).
- [8] J. C. Snowdon, "Vibration Isolation: Use and Characterization", U.S. Department of Commerce, National Bureau of Standards (1979).

Channel	Title	Measurement	Direction
28	SHEAR 1EW	bearing shear force	longitudinal
29	SHEAR 2EW	bearing shear force	longitudinal
30	SHEAR 3EW	bearing shear force	longitudinal
31	SHEAR 4EW	bearing shear force	longitudinal
32	SHEAR 1NS	bearing shear force	transverse
33	SHEAR 2NS	bearing shear force	transverse
34	SHEAR 3NS	bearing shear force	transverse
35	SHEAR 4NS	bearing shear force	transverse
36	AXIAL 1	bearing axial force	vertical
37	AXIAL 2	bearing axial force	vertical
38	AXIAL 3	bearing axial force	vertical
39	AXIAL 4	bearing axial force	vertical
40	ACC 1	deck acceleration	transverse
41	ACC 2	deck acceleration	transverse
42	ACC 3	deck acceleration	longitudinal
43	ACC 4	deck acceleration	longitudinal
44	ACC 5	deck acceleration	vertical
45	ACC 6	deck acceleration	vertical
46	ACC 7	deck acceleration	vertical
47	ACC 8	deck acceleration	vertical
48	POT 1	deck relative displacement	longitudinal
49	POT 2	deck relative displacement	longitudinal
50	POT 3	deck relative displacement	transverse
51	POT 4	deck relative displacement	transverse
52	POT 5	deck relative displacement	vertical
53	POT 6	deck relative displacement	vertical
54	POT 7	deck relative displacement	vertical
55	POT 8	deck relative displacement	vertical

Table 1 List of Instrumentation

SERIES	INPUT RECORDS	HORIZONTAL SPANS					
real time	Parkfield	100	150	200	300		
	El Centro	100	200	300	400	450	
	ATC-3	100	150	200	300	350	400
	Caltrans	100	200	300	400		
$\sqrt{2}$ time scaled	El Centro	750					
	Taft	500	750				
	Parkfield	750					
	Pacoima Dam	500	750				
	San Francisco	250	750				
	Caltech A1	750					
$\sqrt{3}$ time scaled	El Centro	750					

Table 2 Summary of Horizontal Earthquake Input Test Programs
for Plain Bearing System

SERIES	INPUT RECORDS	HORIZONTAL SPANS						
Real time	Parkfield	100	200	300	400			
	El Centro	100	200	300	400	450	500	
	ATC-3	100	200	300	400			
	Caltrans	100	200	300	400	500	650	800
$\sqrt{2}$ time scaled	El Centro	500	750					
	Taft	750						
	Parkfield	750						
	Pacoima Dam	750						
	San Francisco	250	750					
	Caltech A1	750						

Table 3 Summary of Horizontal Earthquake Input Test Programs for Lead-Filled Bearing System

Cycle (n)	Displacement (v_n)	Strain (ϵ_n)	Damping Ratio (β_n)	Frequency (Hz)
0	1.007	0.192		
1	0.586	0.112	0.086	0.80
2	0.372	0.071	0.072	0.81
3	0.233	0.044	0.074	0.85
4	0.152	0.029	0.068	0.87
5	0.102	0.019	0.064	0.89
6	0.067	0.013	0.067	0.90
7	0.044	0.008	0.067	0.92
8	0.034	0.006	0.041	0.93
9	0.022	0.004	0.069	0.93
10	0.013	0.002	0.084	0.97

Table 4 Logarithmic Decrement of Longitudinal Pull-Back Test
for Plain Bearing System

Cycle (n)	Displacement (v_n)	Strain (ϵ_n)	Damping Ratio (β_n)	Frequency (Hz)
0	3.779	0.720		
1	3.707	0.706		0.63
2	2.822	0.538	0.043	0.63
3	1.939	0.369	0.060	0.62
4	1.299	0.247	0.064	0.64
5	0.848	0.162	0.068	0.67
6	0.544	0.104	0.071	0.67
7	0.347	0.066	0.072	0.70
8	0.226	0.043	0.068	0.70
9	0.147	0.028	0.068	0.74
10	0.098	0.019	0.064	0.76

Table 5 Logarithmic Decrement of Harmonic Motion
for Plain Bearing System

test set no.	input freqy. (Hz)	amplf. factor	max. strain (%)	bearg. stiff. (kpi)	natur. freqy. (Hz)	dampg. ratio (%)	loss factor (%)
1	0.2	0.07	0.4	2.78	1.06	44.7	16.8
1	0.4	0.23	1.5	2.40	0.99	17.3	14.0
2	0.5	0.48	3.2	2.09	0.92	11.1	12.0
1	0.6	1.06	6.9	1.91	0.88	8.7	11.8
2	0.6	1.17	7.8	1.82	0.86	7.9	11.0
2	0.65	2.86	19.2	1.54	0.79	5.9	9.6
1	0.7	7.81	50.3	1.21	0.70	4.6	9.1
2	0.7	9.85	66.6	1.19	0.70	3.7	7.4
1	0.8	4.03	25.8	1.36	0.75	4.9	10.5
2	0.8	4.17	27.2	1.38	0.75	4.7	10.0
1	0.9	2.67	17.2	1.43	0.76	4.8	11.3
1	1.0	2.35	15.2	1.61	0.81	4.2	10.4
1	1.2	1.68	10.8	1.66	0.82	3.9	11.4
1	1.4	1.42	9.1	1.70	0.83	3.6	12.0
1	1.6	1.29	8.2	1.73	0.84	3.3	12.6
1	1.8	1.22	7.6	1.74	0.84	2.9	12.3
1	2.0	1.17	7.2	1.76	0.85	2.6	12.3
1	2.2	1.13	7.0	1.76	0.85	2.4	12.2
1	2.4	1.10	6.7	1.78	0.85	2.1	11.9
1	2.6	1.09	6.6	1.76	0.85	2.0	12.2
1	2.8	1.07	6.4	1.77	0.85	1.8	11.9

Table 6 Steady-State Sinusoidal Response of Plain Rubber Bearing

(Unit: g)	Table Acc.		Deck Acc.		Ratio (Deck/Table)	
	Horiz.	Vert.	Horiz.	Vert.	Horiz.	Vert.
H100,V0	0.122	0.006	0.062	0.010	0.508	1.667
H0,V100	0.007	0.086	0.009	0.119	1.286	1.324
SUM	0.129	0.092	0.071	0.129	0.550	1.402
H100,V100	0.128	0.075	0.071	0.124	0.555	1.653
H200,V0	0.218	0.038	0.113	0.036	0.518	0.947
H0,V200	0.012	0.133	0.028	0.252	2.333	1.895
SUM	0.230	0.171	0.141	0.288	0.613	1.684
H200,V200	0.246	0.154	0.113	0.275	0.459	1.786
H300,V0	0.328	0.017	0.160	0.039	0.488	2.294
H0,V300	0.015	0.213	0.026	0.368	1.733	1.728
SUM	0.343	0.230	0.186	0.407	0.542	1.769
H300,V300	0.345	0.249	0.160	0.427	0.464	1.715
H400,V0	0.503	0.024	0.200	0.060	0.398	2.500
H0,V400	0.016	0.299	0.045	0.506	2.812	1.692
SUM	0.519	0.323	0.245	0.566	0.472	1.752
H400,V400	0.511	0.310	0.219	0.559	0.428	1.803

Table 7 Influence of Vertical Excitation on Plain Bearing System
under El Centro Signal Inputs

Horzn Span	Displacement (in)			Acceleration (g)			Shear (kip)	Stiff (k/in)
	Table	Deck	Ratio	Table	Deck	Ratio		
(a) Parkfield Input								
100	0.503	1.344	2.672	0.096	0.069	0.719	1.848	1.375
150	0.761	2.186	2.872	0.133	0.102	0.767	2.659	1.216
200	1.015	3.176	3.129	0.159	0.134	0.843	3.440	1.083
300	1.529	5.014	3.279	0.227	0.184	0.810	4.874	0.972
(b) El Centro Input								
100	0.502	1.118	2.227	0.122	0.062	0.508	1.658	1.438
200	1.008	2.221	2.203	0.218	0.113	0.518	3.005	1.353
300	1.513	3.550	2.346	0.328	0.160	0.488	4.050	1.141
400	2.018	5.164	2.559	0.503	0.200	0.398	5.511	1.067
450	2.269	5.996	2.643	0.600	0.214	0.357	6.418	1.070
(c) ATC-3 Input								
100	0.515	1.449	2.814	0.098	0.078	0.796	2.122	1.464
150	0.769	2.186	2.843	0.140	0.103	0.736	2.820	1.290
200	1.018	2.977	2.924	0.178	0.130	0.730	3.595	1.208
300	1.531	4.618	3.016	0.251	0.173	0.689	5.149	1.115
400	2.041	6.882	3.372	0.319	0.232	0.727	5.872	0.853
(d) Caltrans Input								
100	0.513	1.334	2.600	0.107	0.069	0.645	1.859	1.394
200	1.031	2.754	2.671	0.183	0.129	0.705	3.520	1.278
300	1.526	4.189	2.745	0.238	0.168	0.706	4.840	1.155
400	2.041	6.264	3.069	0.308	0.209	0.679	5.660	0.904

Table 8 Peak Responses of Real-Time Signal Inputs
for Plain Bearing System

Record	El Cen	Parkfd	Pac Dm	Taft	San Fr	Caltec
Table Disp. (in)	3.758	3.739	3.748	2.099	3.816	3.604
Deck Disp. (in)	6.906	4.990	4.400	2.386	2.059	5.758
Ratio (Dec/Tab)	1.838	1.330	1.174	1.137	0.540	1.598
Table Acc. (g)	0.426	0.371	0.428	0.294	1.219	0.274
Deck Acc. (g)	0.240	0.177	0.163	0.109	0.133	0.186
Ratio (Dec/Tab)	0.563	0.477	0.381	0.371	0.109	0.679
Shear For. (kip)	6.352	5.123	4.383	2.770	2.575	5.223
Stiff. (kip/in)	0.920	1.033	0.996	1.161	1.251	0.907

Table 9 Peak Responses of Time-Scaled Signal Inputs at Span 750
for Plain Bearing System

(Unit: g)	Table Acc.		Deck Acc.		Ratio (Deck/Table)	
	Input	Horiz.	Vert.	Horiz.	Vert.	Horiz.
H100,V0	0.169	0.018	0.093	0.021	0.550	1.167
H0,V100	0.008	0.103	0.017	0.122	2.125	1.184
SUM	0.177	0.121	0.110	0.143	0.621	1.182
H100,V100	0.135	0.096	0.098	0.129	0.726	1.344
H200,V0	0.238	0.015	0.150	0.024	0.630	1.600
H0,V200	0.014	0.197	0.035	0.249	2.500	1.264
SUM	0.252	0.212	0.185	0.273	0.734	1.288
H200,V200	0.255	0.209	0.151	0.244	0.592	1.167
H300,V0	0.350	0.025	0.201	0.045	0.574	1.800
H0,V300	0.015	0.298	0.050	0.354	3.333	1.188
SUM	0.365	0.323	0.251	0.399	0.688	1.235
H300,V300	0.340	0.277	0.202	0.339	0.594	1.224
H400,V0	0.509	0.029	0.245	0.074	0.481	2.552
H0,V400	0.020	0.364	0.072	0.431	3.600	1.184
SUM	0.529	0.393	0.317	0.505	0.599	1.285
H400,V400	0.509	0.305	0.248	0.424	0.487	1.390
H450,V0	0.614	0.031	0.260	0.094	0.423	3.032
H0,V450	0.023	0.397	0.082	0.482	3.565	1.214
SUM	0.637	0.428	0.342	0.576	0.537	1.346
H450,V450	0.624	0.323	0.270	0.492	0.433	1.523
H500,V0	0.776	0.040	0.276	0.121	0.356	3.025
H0,V500	0.027	0.433	0.076	0.496	2.815	1.145
SUM	0.803	0.473	0.352	0.617	0.438	1.304
H500,V500	0.777	0.327	0.288	0.544	0.371	1.664

Table 10 Influence of Vertical Excitation on Lead-Filled Bearing System
under El Centro Signal Inputs

Horzn Span	Displacement (in)			Acceleration (g)			Shear (kip)	Stiff (k/in)
	Table	Deck	Ratio	Table	Deck	Ratio		
(a) Parkfield Input								
100	0.509	0.666	1.308	0.089	0.066	0.742	1.720	2.583
200	1.018	1.608	1.580	0.153	0.127	0.830	3.330	2.071
300	1.531	2.585	1.688	0.220	0.188	0.855	4.960	1.919
400	2.044	3.768	1.843	0.309	0.241	0.780	6.575	1.745
(b) El Centro Input								
100	0.509	0.851	1.672	0.169	0.093	0.550	2.327	2.734
200	1.018	1.560	1.532	0.238	0.151	0.634	3.977	2.549
300	1.520	2.390	1.572	0.350	0.201	0.574	5.377	2.250
400	2.021	3.060	1.514	0.509	0.245	0.481	6.425	2.100
450	2.272	3.550	1.563	0.614	0.261	0.425	6.870	1.935
500	2.514	3.998	1.590	0.776	0.276	0.356	7.280	1.821
(c) ATC-3 Input								
100	0.512	0.620	1.211	0.106	0.068	0.637	1.746	2.816
200	1.026	1.402	1.366	0.190	0.123	0.647	3.135	2.236
300	1.542	2.618	1.698	0.263	0.190	0.722	4.997	1.909
400	2.046	3.816	1.865	0.315	0.240	0.762	6.475	1.697
(d) Caltrans Input								
100	0.512	0.677	1.323	0.103	0.068	0.660	1.788	2.641
200	1.018	1.600	1.572	0.193	0.130	0.674	3.362	2.101
300	1.534	2.839	1.851	0.249	0.195	0.783	5.083	1.790
400	2.045	3.991	1.952	0.302	0.238	0.788	6.487	1.625
500	2.553	4.122	1.614	0.448	0.296	0.661	7.578	1.838

Table 11 Peak Responses of Real-Time Signal Inputs
for Lead-Filled Bearing System

Records	El Cen	Parkfd	Pac Dm	Taft	San Fr	Caltec
Table Disp. (in)	3.759	3.756	3.755	2.115	3.817	3.138
Deck Disp. (in)	2.416	3.346	3.610	1.482	2.271	2.176
Ratio (Dec/Tab)	0.643	0.891	0.961	0.701	0.595	0.693
Table Acc. (g)	0.484	0.392	0.437	0.321	1.231	0.275
Deck Acc. (g)	0.236	0.264	0.286	0.148	0.246	0.196
Ratio (Dec/Tab)	0.488	0.673	0.654	0.461	0.200	0.713
Shear For. (kip)	5.802	6.682	7.375	3.985	5.908	5.316
Stiff. (kip/in)	2.401	1.997	2.043	2.689	2.601	2.443

Table 12 Peak Responses of Time-Scaled Signal Inputs at Span 750
for Lead-Filled Bearing System

Horzn Span	Disp. Amplif. Factor			Accel. Reduc. Factor		
	Plain	Lead	Ratio	Plain	Lead	Ratio
(a) Parkfield Input						
100	2.672	1.308	0.49	0.719	0.742	1.03
200	3.129	1.580	0.50	0.843	0.830	0.98
300	3.279	1.688	0.51	0.810	0.855	1.06
(b) El Centro Input						
100	2.227	1.672	0.75	0.508	0.550	1.08
200	2.203	1.532	0.70	0.518	0.634	1.22
300	2.346	1.572	0.67	0.488	0.574	1.18
400	2.559	1.514	0.59	0.398	0.481	1.21
450	2.643	1.563	0.59	0.357	0.425	1.19
(c) ATC-3 Input						
100	2.814	1.211	0.43	0.796	0.637	0.80
200	2.924	1.366	0.47	0.730	0.647	0.89
300	3.016	1.698	0.56	0.689	0.722	1.05
400	3.372	1.865	0.55	0.727	0.762	1.05
(d) Caltrans Input						
100	2.600	1.323	0.51	0.645	0.660	1.02
200	2.671	1.572	0.59	0.705	0.674	0.96
300	2.745	1.851	0.67	0.706	0.783	1.11
400	3.069	1.952	0.64	0.679	0.788	1.16

Table 13 Comparison of Peak Response under Real-Time Signal Inputs

Signal	Disp. Amplif. Factor			Accel. Reduc. Factor		
	Plain	Lead	Ratio	Plain	Lead	Ratio
El Cen	1.838	0.643	0.35	0.563	0.488	0.87
Parkfd	1.330	0.891	0.67	0.477	0.673	1.41
Pac Dm	1.174	0.961	0.82	0.381	0.654	1.72
Taft	1.137	0.701	0.62	0.371	0.461	1.24
San Fr	0.540	0.595	1.10	0.109	0.200	1.83
Caltec	1.598	0.693	0.43	0.679	0.713	1.05

Table 14 Comparison of Peak Response under Time-Scaled Signal Inputs at Span 750

El Centro V. Span	Plain Bearing			Lead Bearing		
	Table Acc.	Deck Acc.	Ratio	Table Acc.	Deck Acc.	Ratio
100	0.086	0.119	1.32	0.103	0.122	1.18
200	0.133	0.252	1.89	0.197	0.249	1.26
300	0.213	0.368	1.73	0.298	0.354	1.19
400	0.299	0.506	1.69	0.364	0.431	1.18

Table 15 Comparison of Peak Acceleration Under Vertical Excitation

(a) Real-Time Signals

horzn. span	record name	max. displ. (in)	max. accel. (g)	max. strain (%)	effct. freqy. (Hz)	effct. stiff. (kpi)	dampg. ratio (%)	loss factor (%)
100	El Cen	1.13	.059	22	0.71	1.29	4	9.8
150	Parkfd	2.19	.102	42	0.67	1.15	8	8.7
200	El Cen	2.26	.101	43	0.66	1.11	7	8.4
300	Caltrn	4.19	.167	80	0.62	0.98	5	7.4
400	El Cen	6.28	.195	120	0.55	0.77	5	7.0
400	Caltrn	6.26	.208	119	0.57	0.83	7	6.8
400	ATC-3	7.42	.207	141	0.52	0.69	5	6.6

(b) Time-Scaled Signals

horzn. span	record name	max. displ. (in)	max. accel. (g)	max. strain (%)	effct. freqy. (Hz)	effct. stiff. (kpi)	dampg. ratio (%)	loss factor (%)
750	El Cen	6.91	.234	132	0.56	0.80	10	6.5
750	Caltec	5.76	.185	110	0.57	0.83	2	7.0
750	Taft	2.39	.109	45	0.66	1.11	5	9.9
750	Parkfd	4.99	.177	95	0.60	0.92	5	7.4
750	Pac Dm	4.40	.163	84	0.60	0.92	3	7.4
750	San Fr	2.06	.127	39	0.76	1.48	4	8.8

Table 16 Parameter Identification of Plain Rubber Bearing

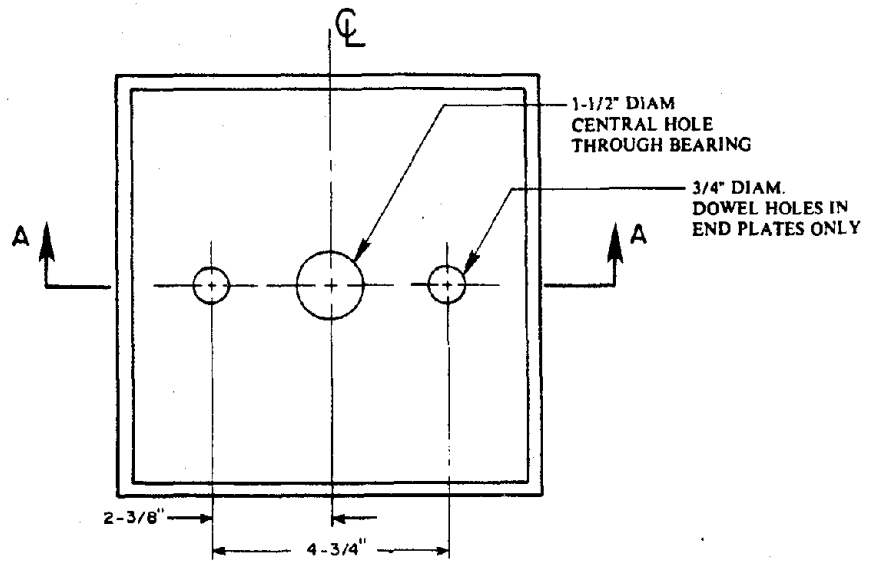
(a) Real-Time Signals

horzn. span	record name	max. displ. (in)	max. accel. (g)	max. strain (%)	effct. freqy. (Hz)	effct. stiff. (kpi)	dampg. ratio (%)
100	El Cen	0.85	.092	16	1.00	2.56	13
300	Caltrn	2.84	.195	54	0.81	1.68	11
400	Caltrn	3.99	.237	76	0.77	1.52	11
500	Caltrn	4.12	.296	79	0.82	1.72	14
400	ATC-3	3.81	.240	73	0.77	1.52	12

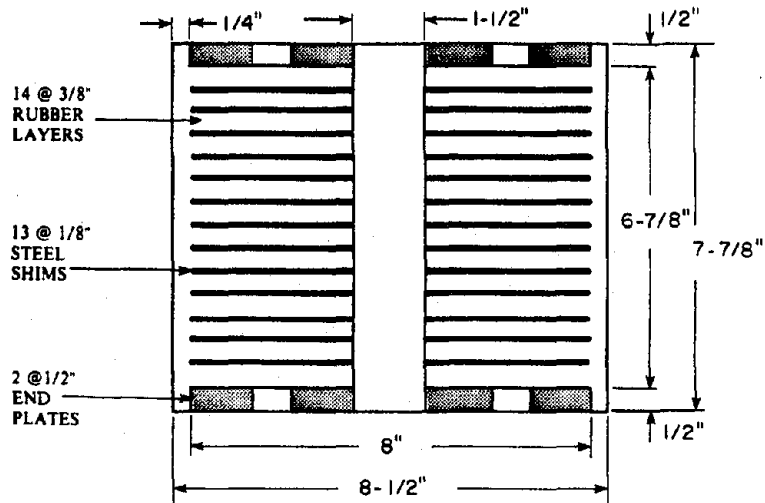
(b) Time-Scaled Signals

horzn. span	record name	max. displ. (in)	max. accel. (g)	max. strain (%)	effct. freqy. (Hz)	effct. stiff. (kpi)	dampg. ratio (%)
500	El Cen	1.60	.170	31	1.00	2.56	13
750	El Cen	2.42	.236	46	0.95	2.31	14
750	Caltec	2.17	.195	41	0.94	2.26	14
750	Taft	1.48	.147	28	0.94	2.26	14
750	Parkfd	3.34	.263	64	0.86	1.89	13
750	Pac Dm	3.61	.285	69	0.86	1.89	12
750	San Fr	2.27	.246	43	0.98	2.46	13

Table 17 Parameter Identification of Lead-Filled Rubber Bearing



PLAN



SECTION A-A

Figure 1 Plan and Cross Section of Bearing

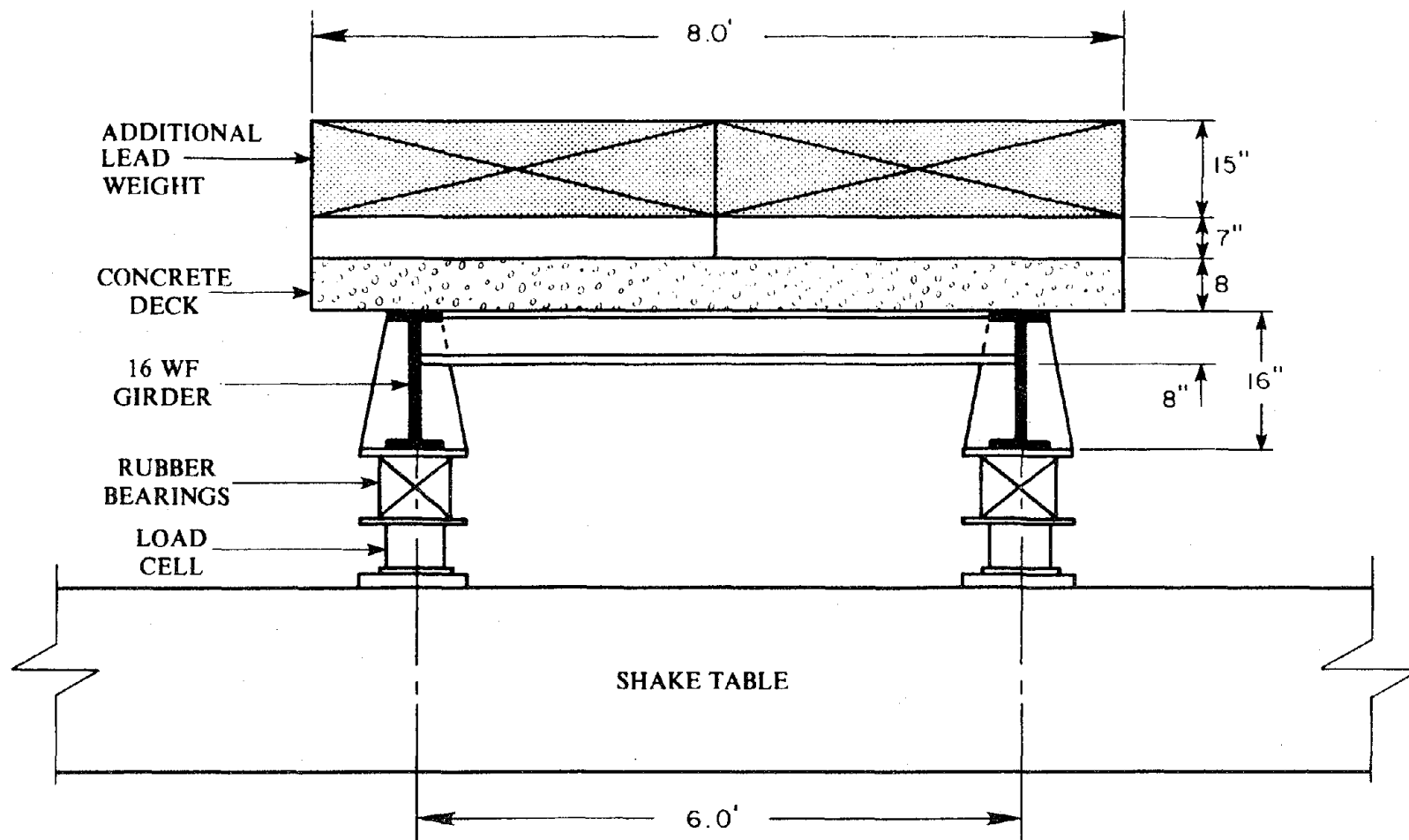


Figure 2 Cross Section of Bridge Deck Model

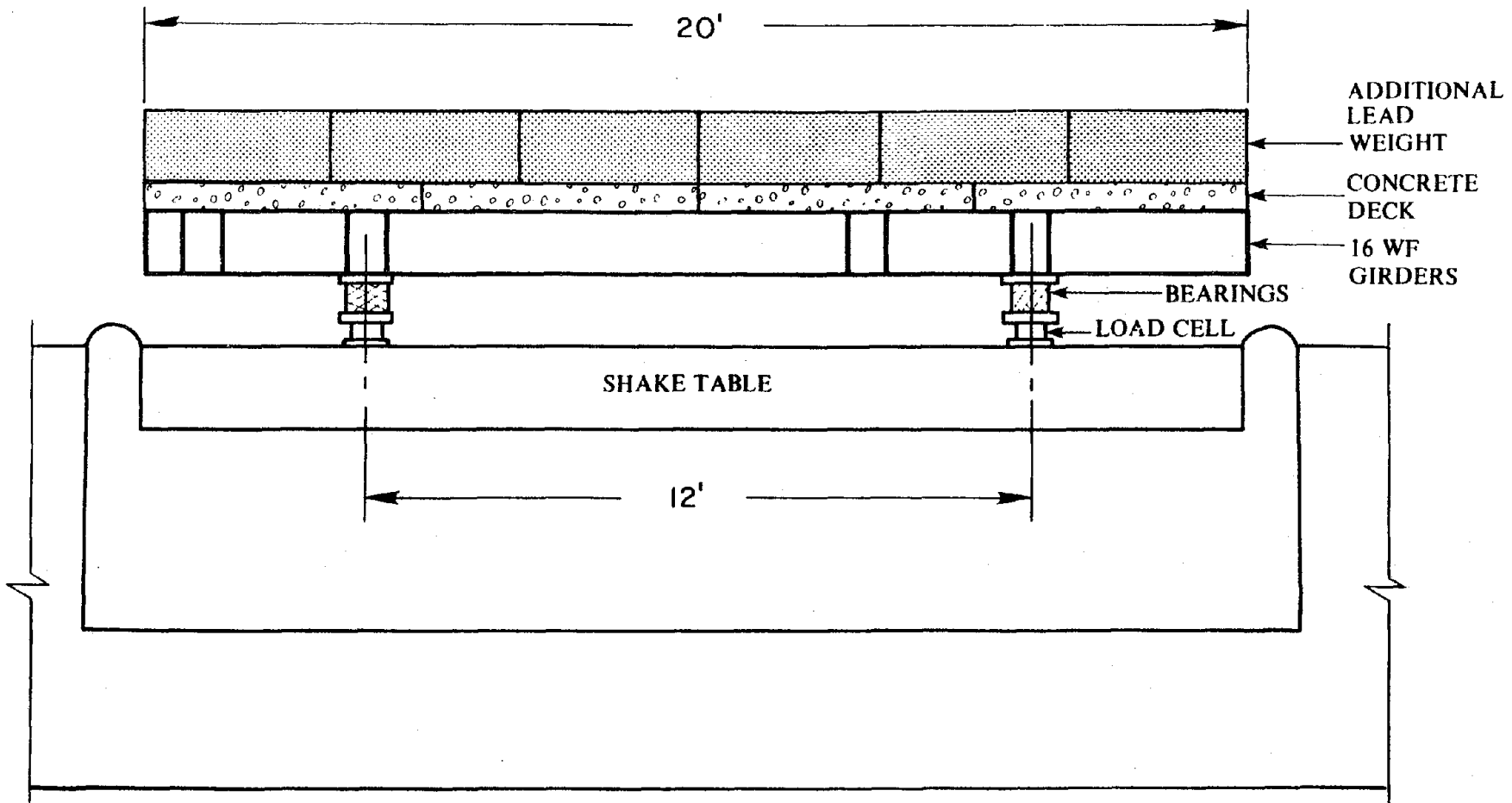


Figure 3 Elevation of Bridge Deck Model

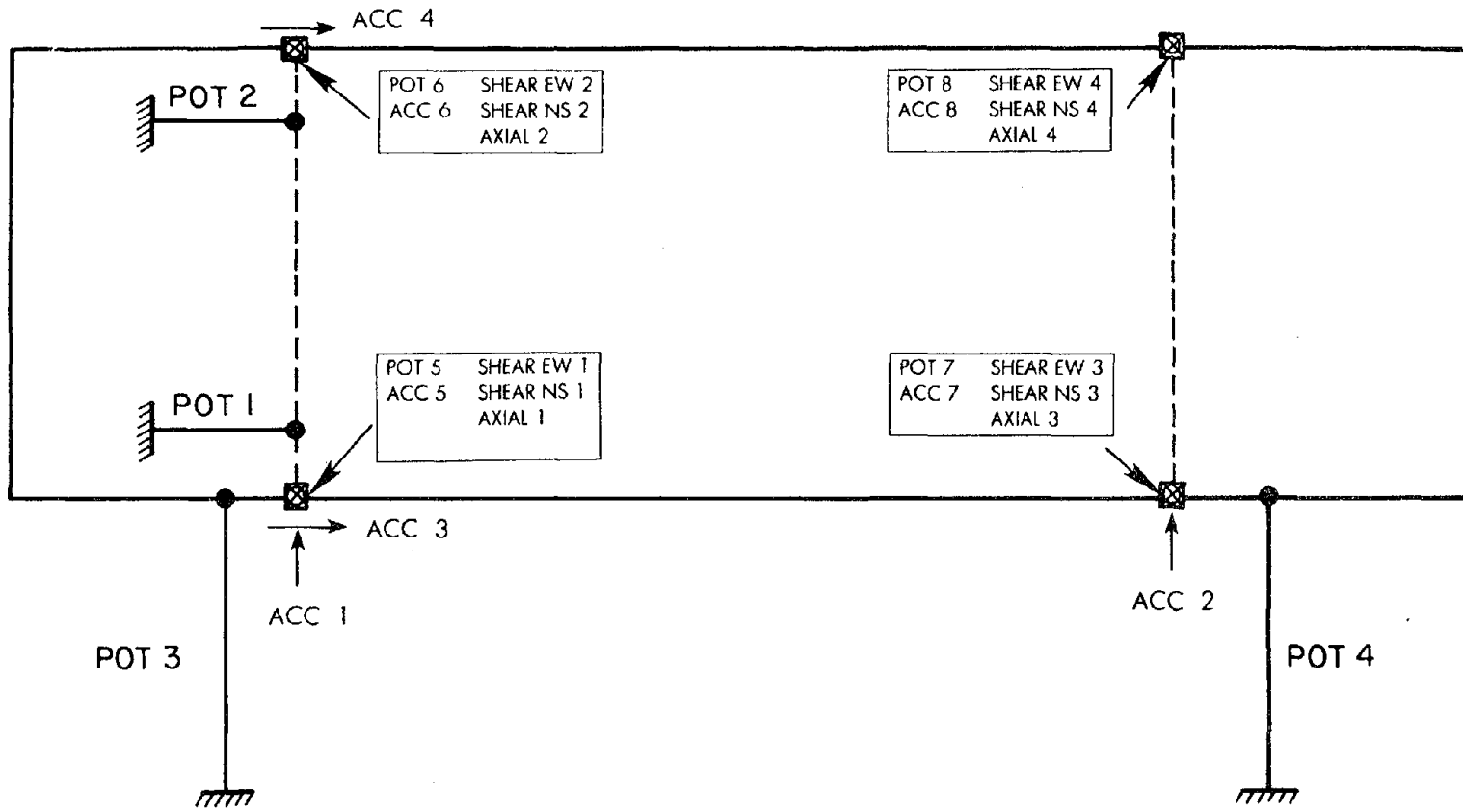


Figure 4 Location of Instrumentation

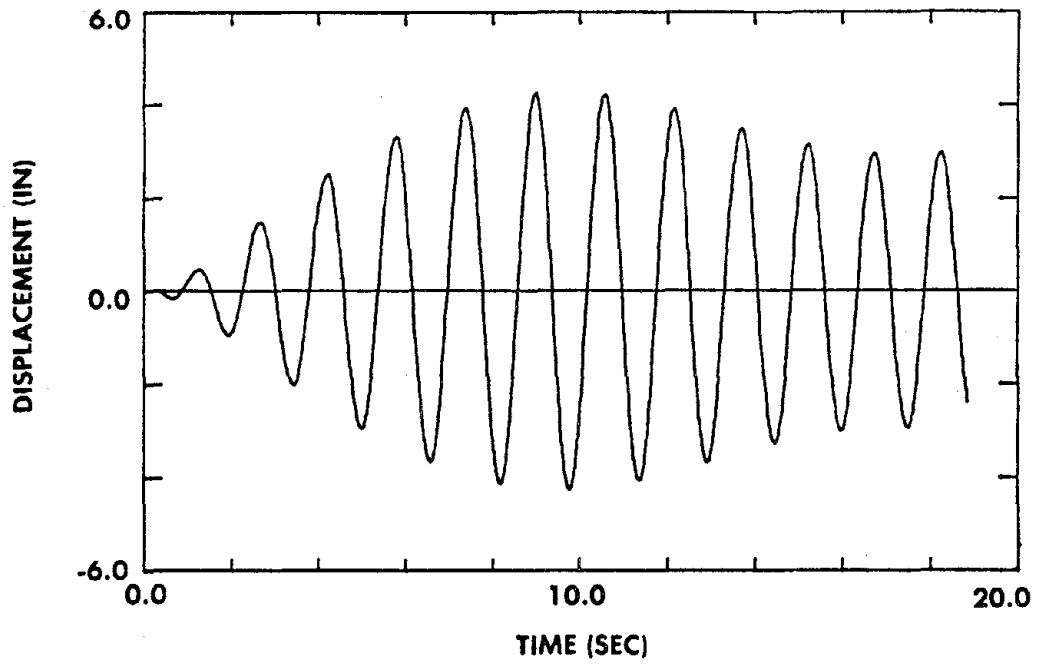


Figure 5 Beat Phenomenon during Start-up of Harmonic Input at Frequency 0.65 Hz

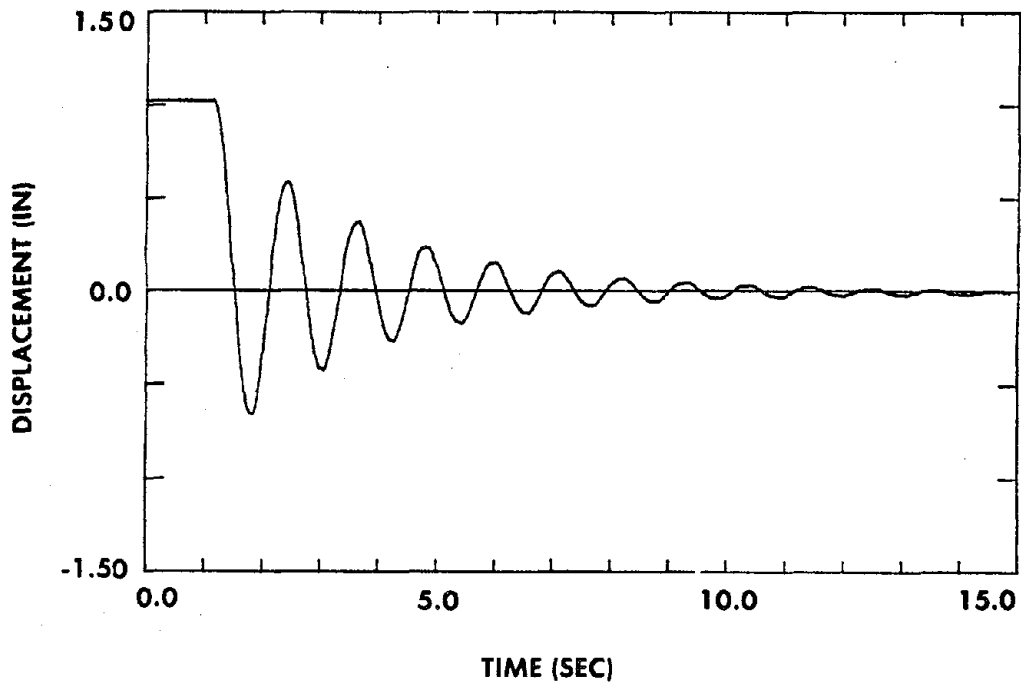


Figure 6 Displacement Time History in Longitudinal Pull-Back Test

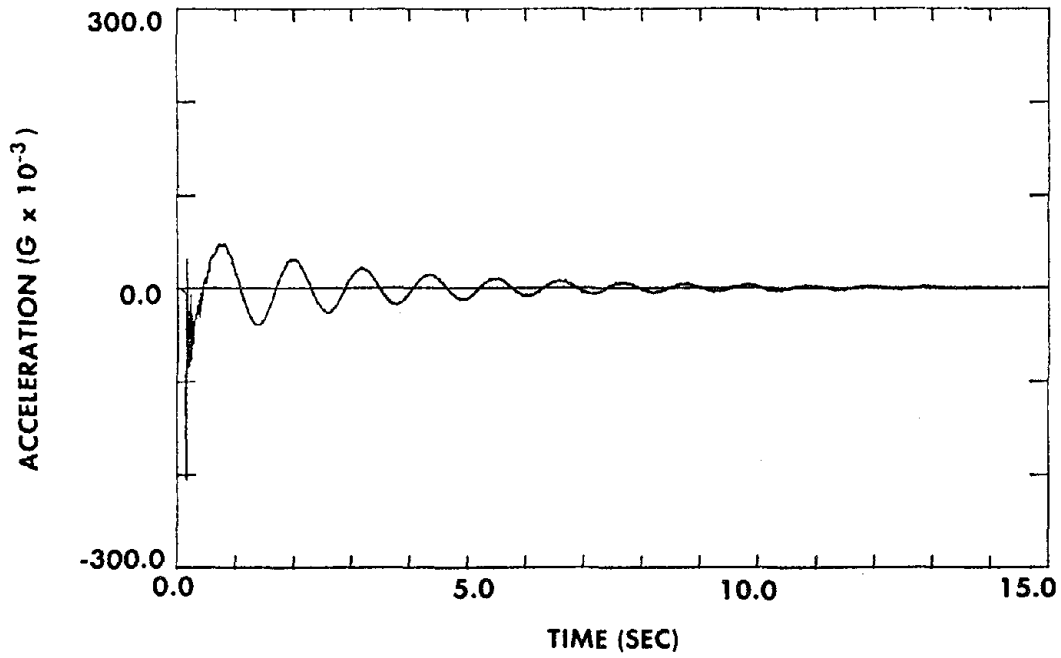


Figure 7 Acceleration Time History in Longitudinal Pull-Back Test

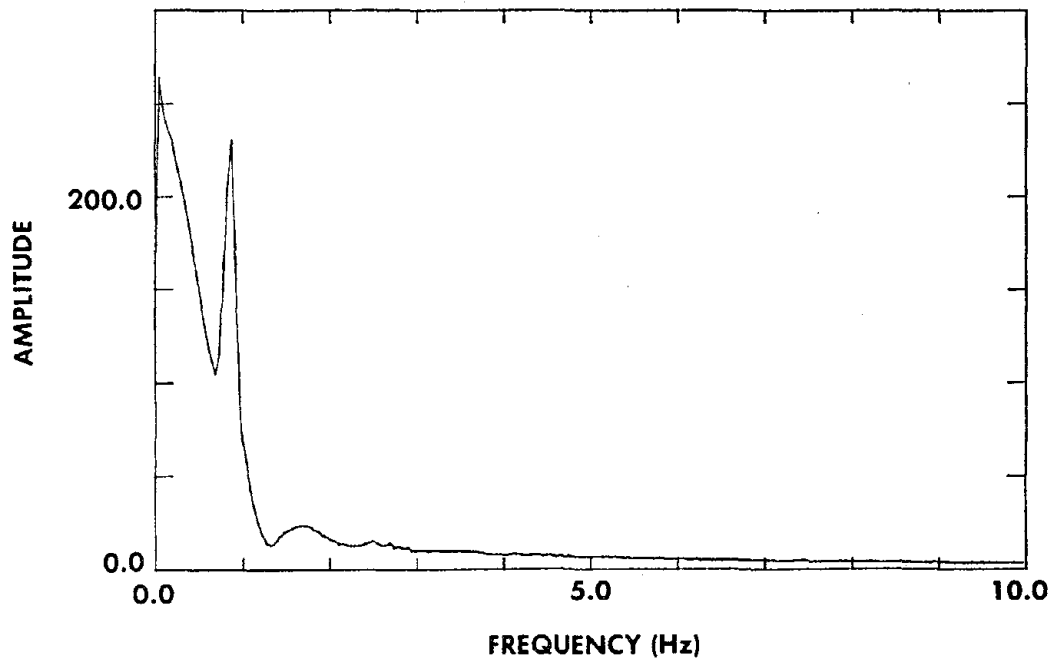


Figure 8 Displacement Fourier Spectrum in Longitudinal Pull-Back Test

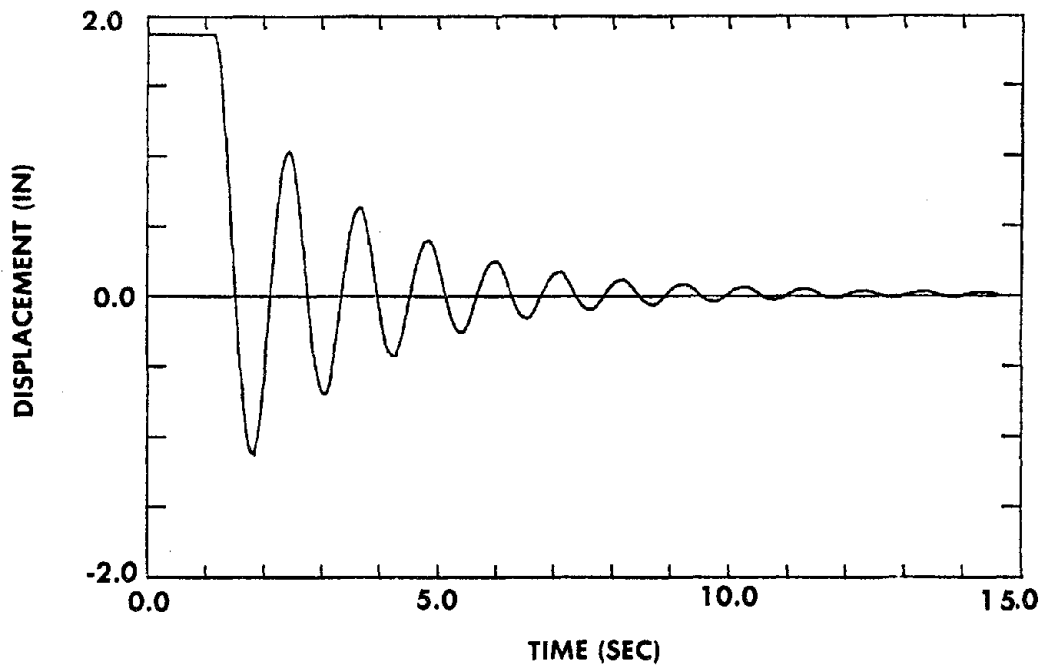


Figure 9 Time History of Displacement Difference in Torsional Pull-Back Test

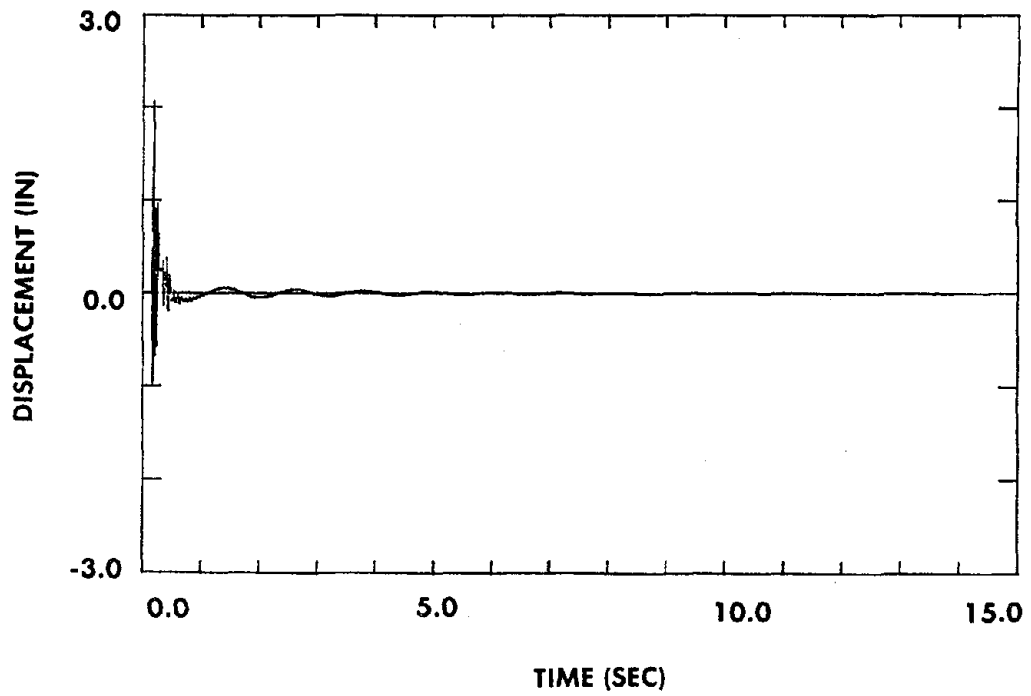


Figure 10 Time History of Acceleration Difference in Torsional Pull-Back Test

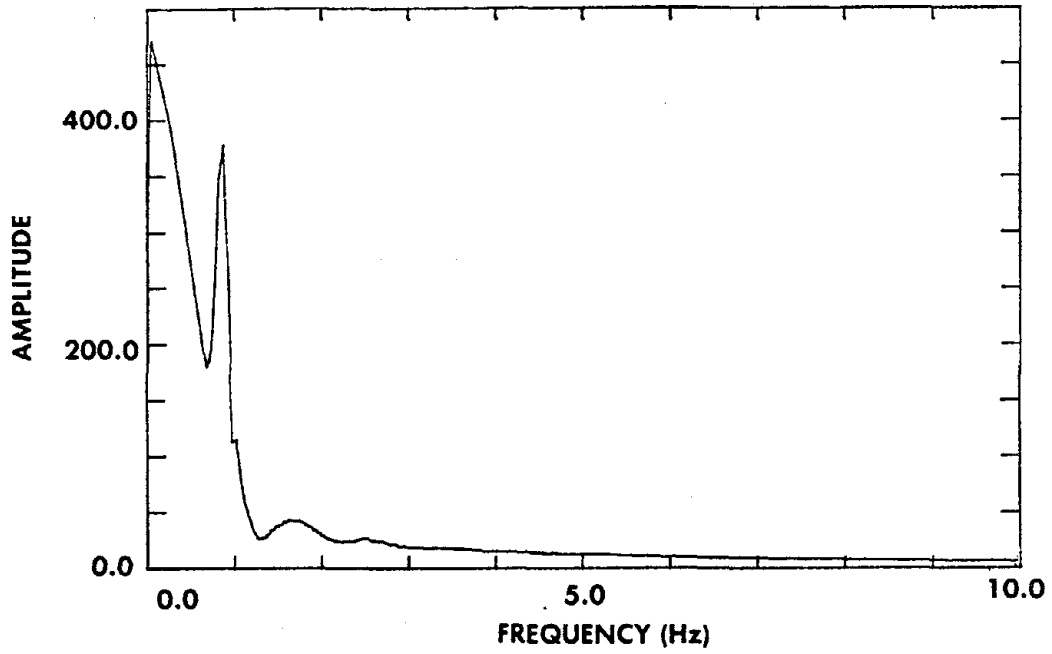


Figure 11 Fourier Spectrum of Displacement Difference in Torsional Pull-Back Test

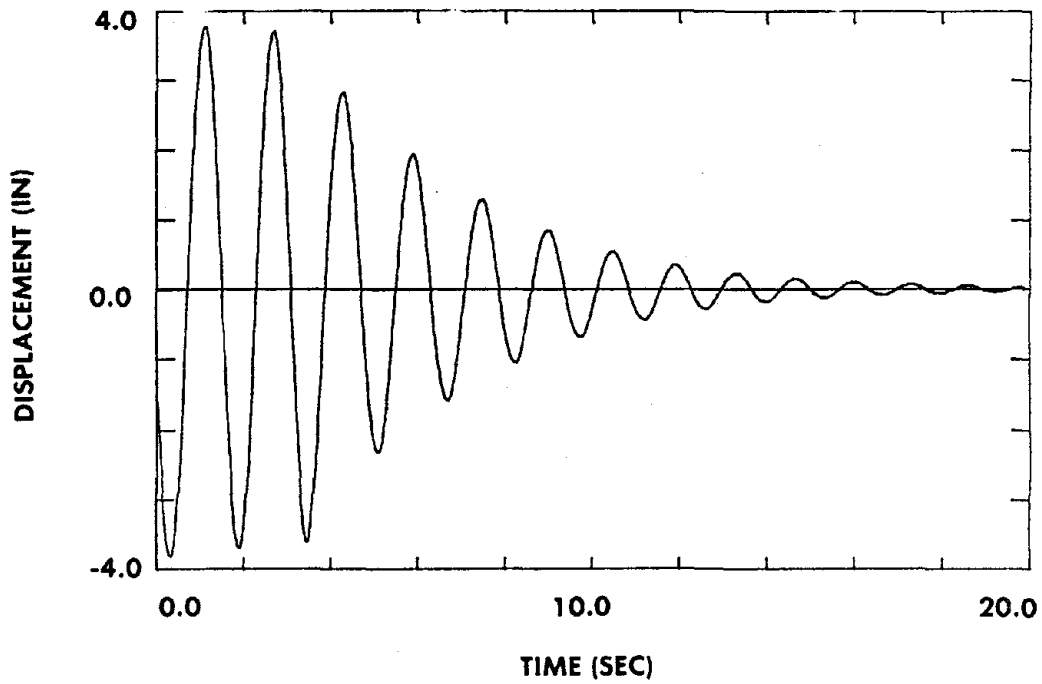


Figure 12 Displacement Decay Curve of Harmonic Input

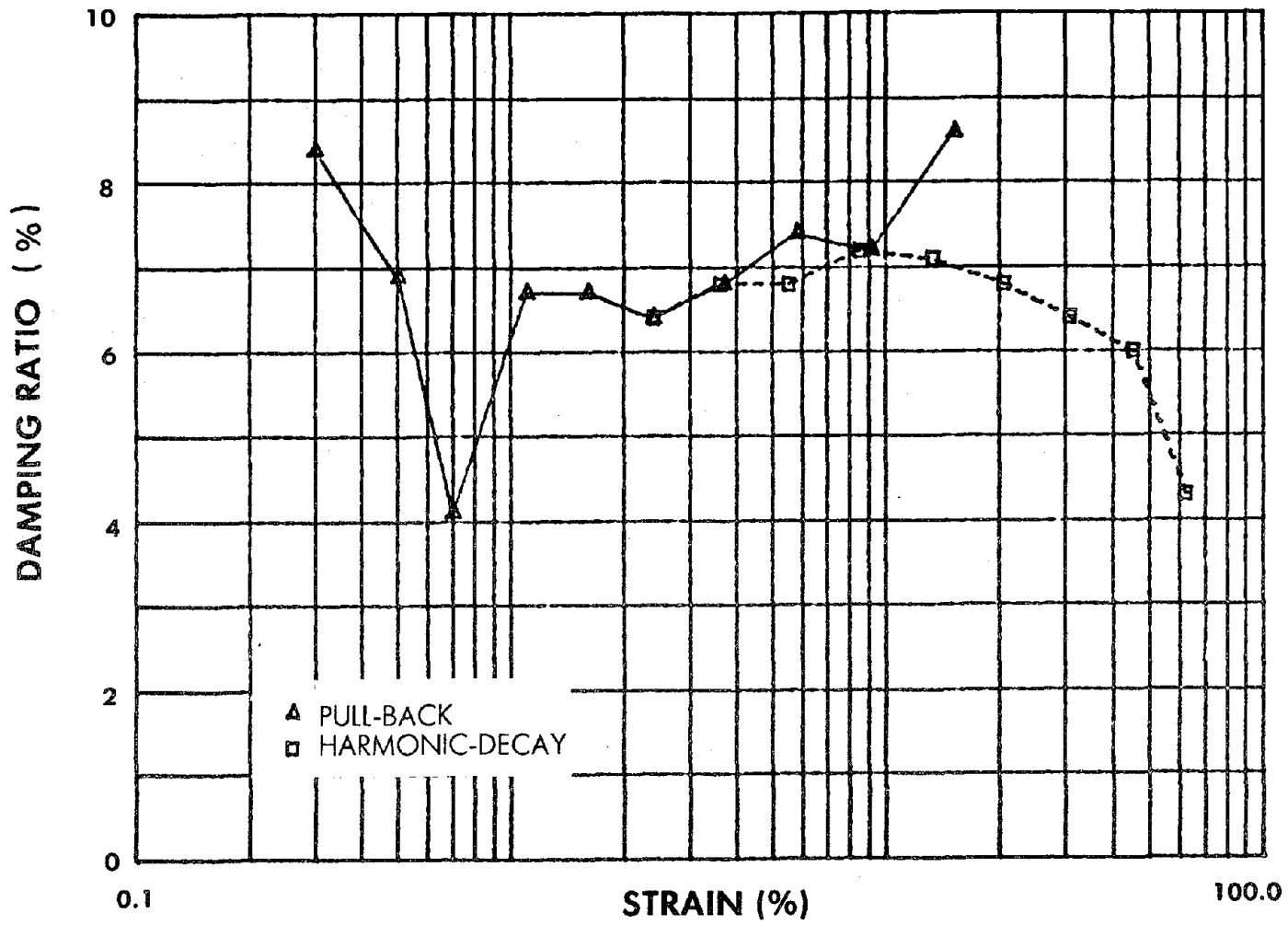


Figure 13 Damping Factors from Longitudinal Pull-Back Test and Harmonic Decay Test

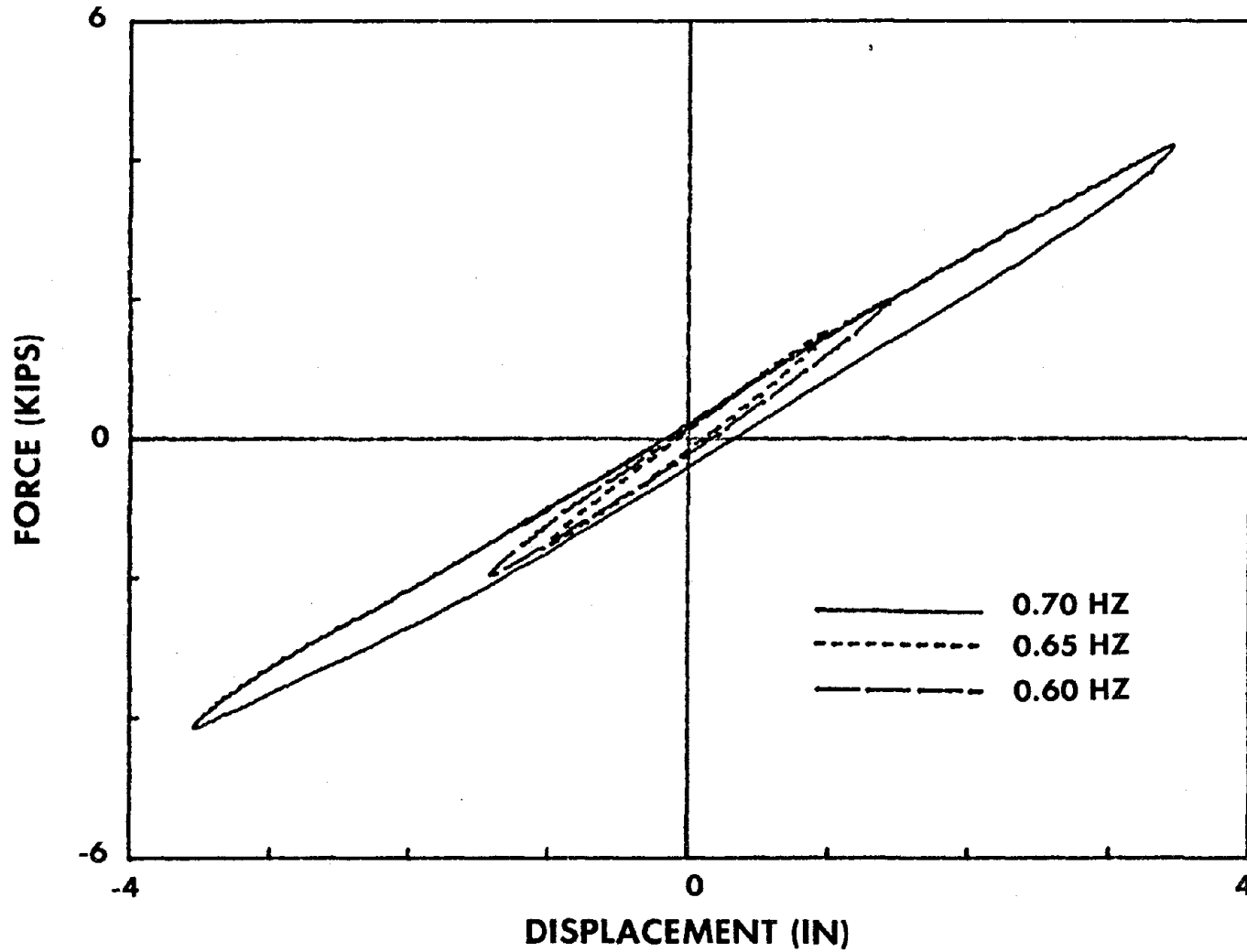


Figure 14 Hysteresis Loops of Plain Bearing in Steady-State Sinusoidal Test

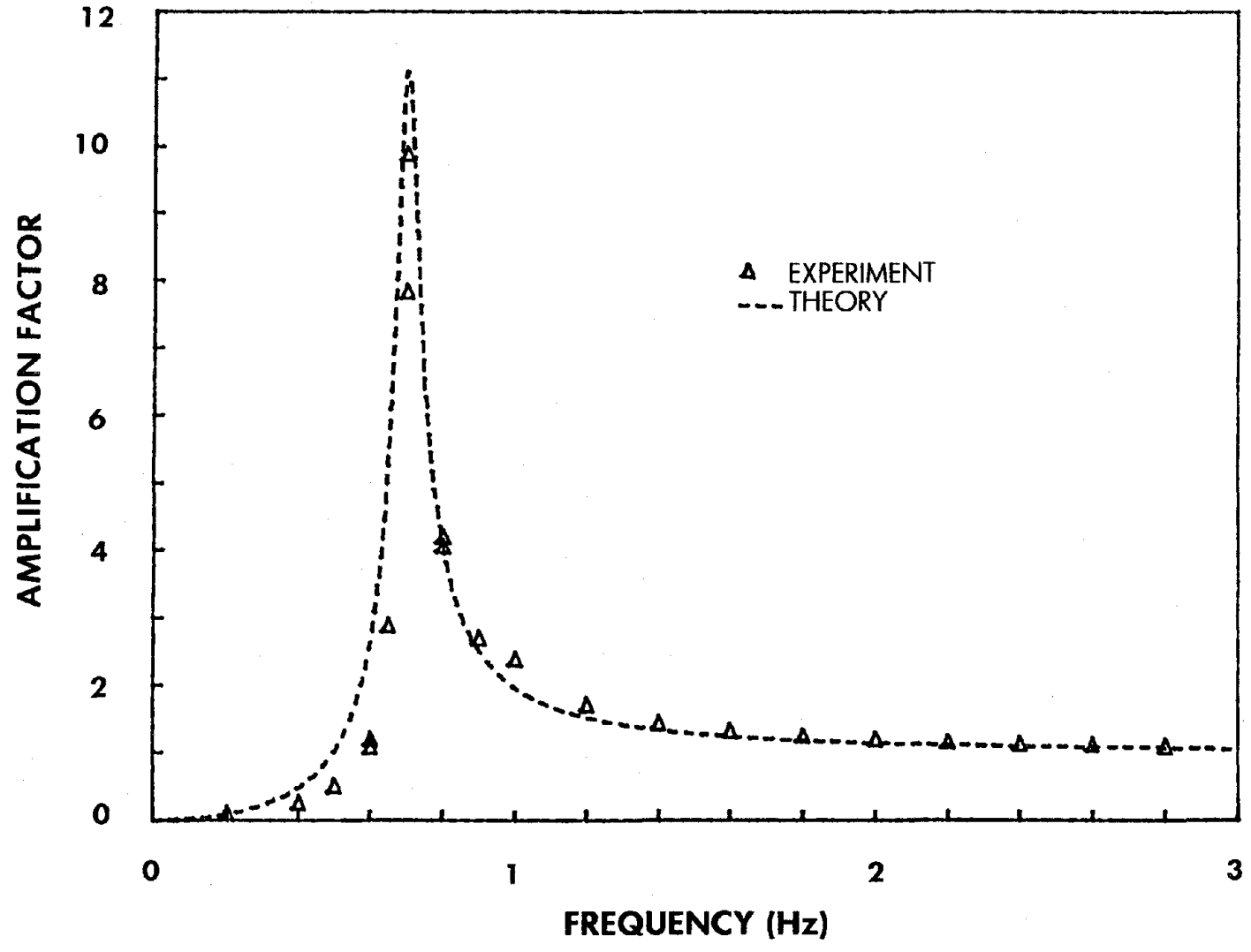


Figure 15 Amplification Factors of Plain Bearing

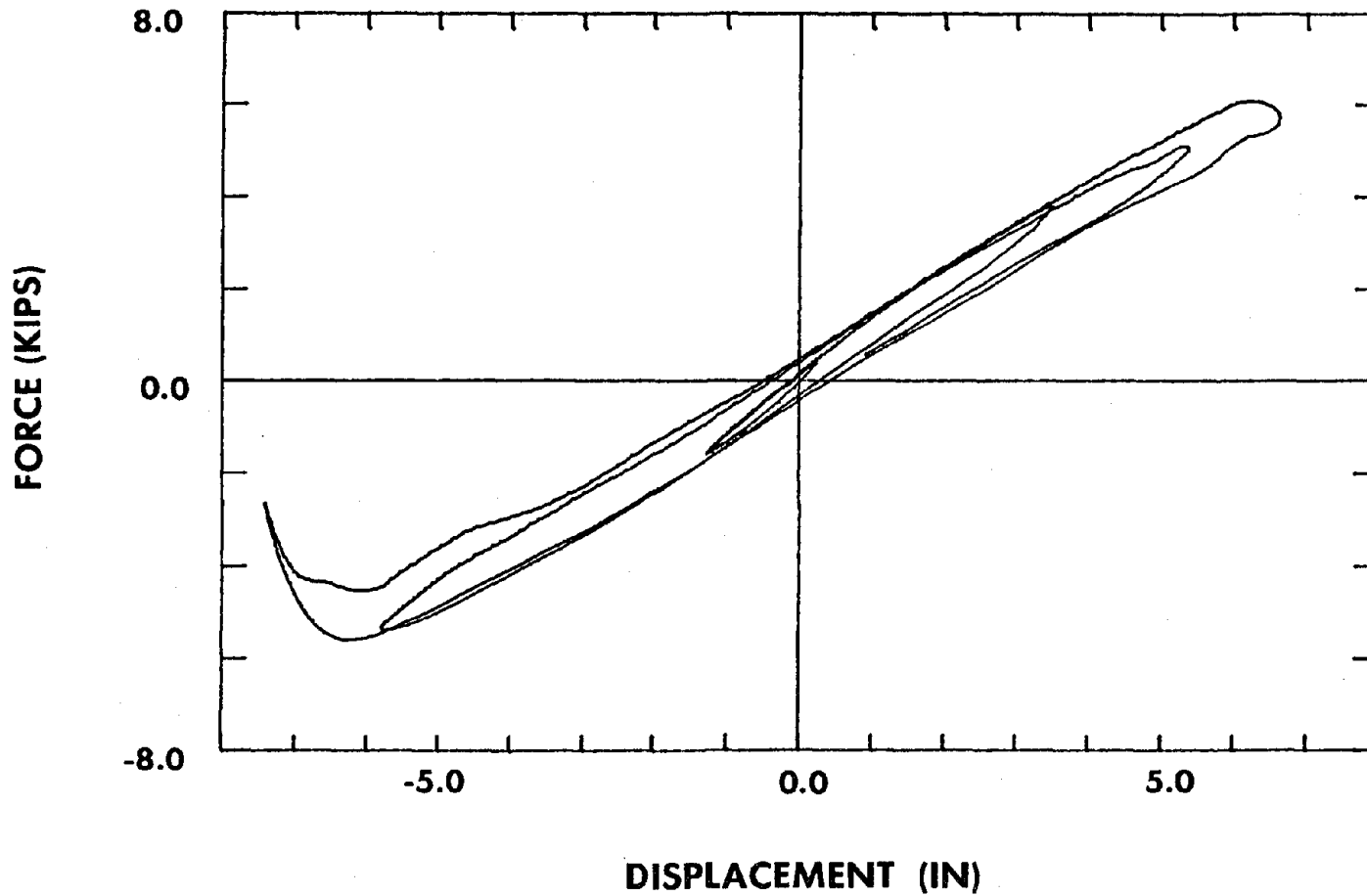


Figure 16 Hysteresis Loops of Plain Bearing under Real-Time
ATC-3 Signal at Span 400

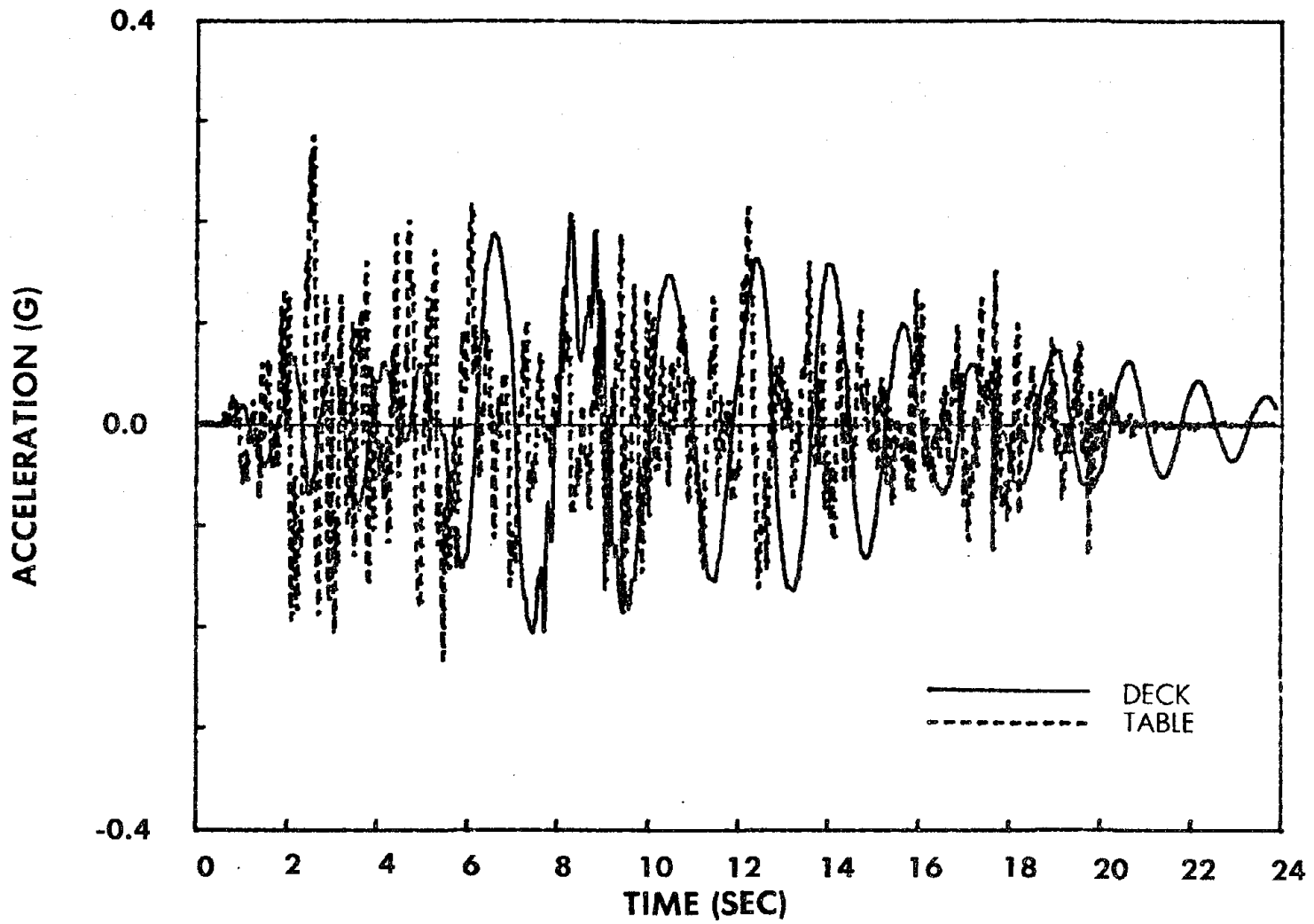


Figure 17 Table and Deck Acceleration Time Histories of Plain Bearing System under Real-Time ATC-3 Signal at Span 400

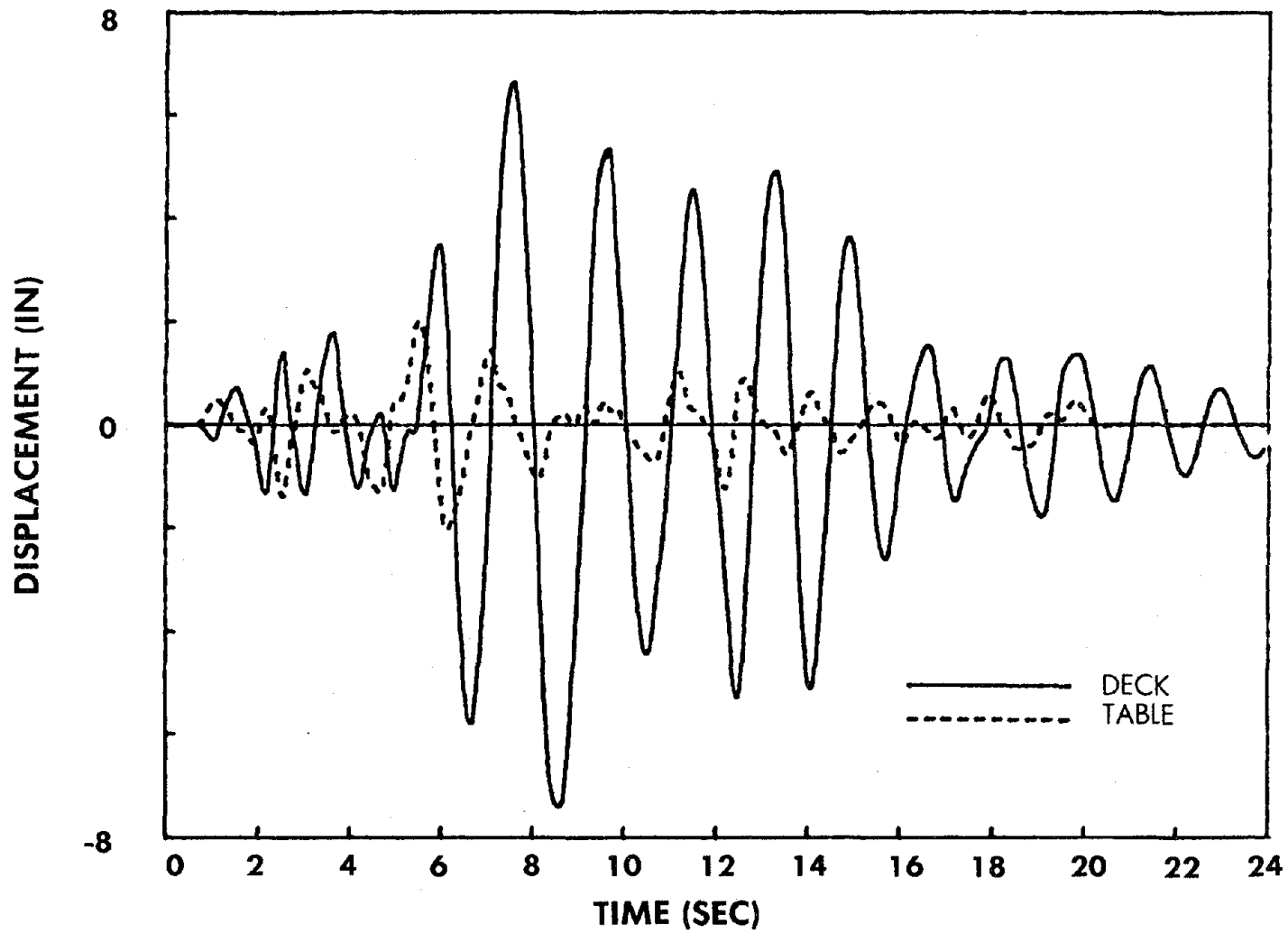


Figure 18 Table and Deck Displacement Time Histories of Plain Bearing System under Real-Time ATC-3 Signal at Span 400

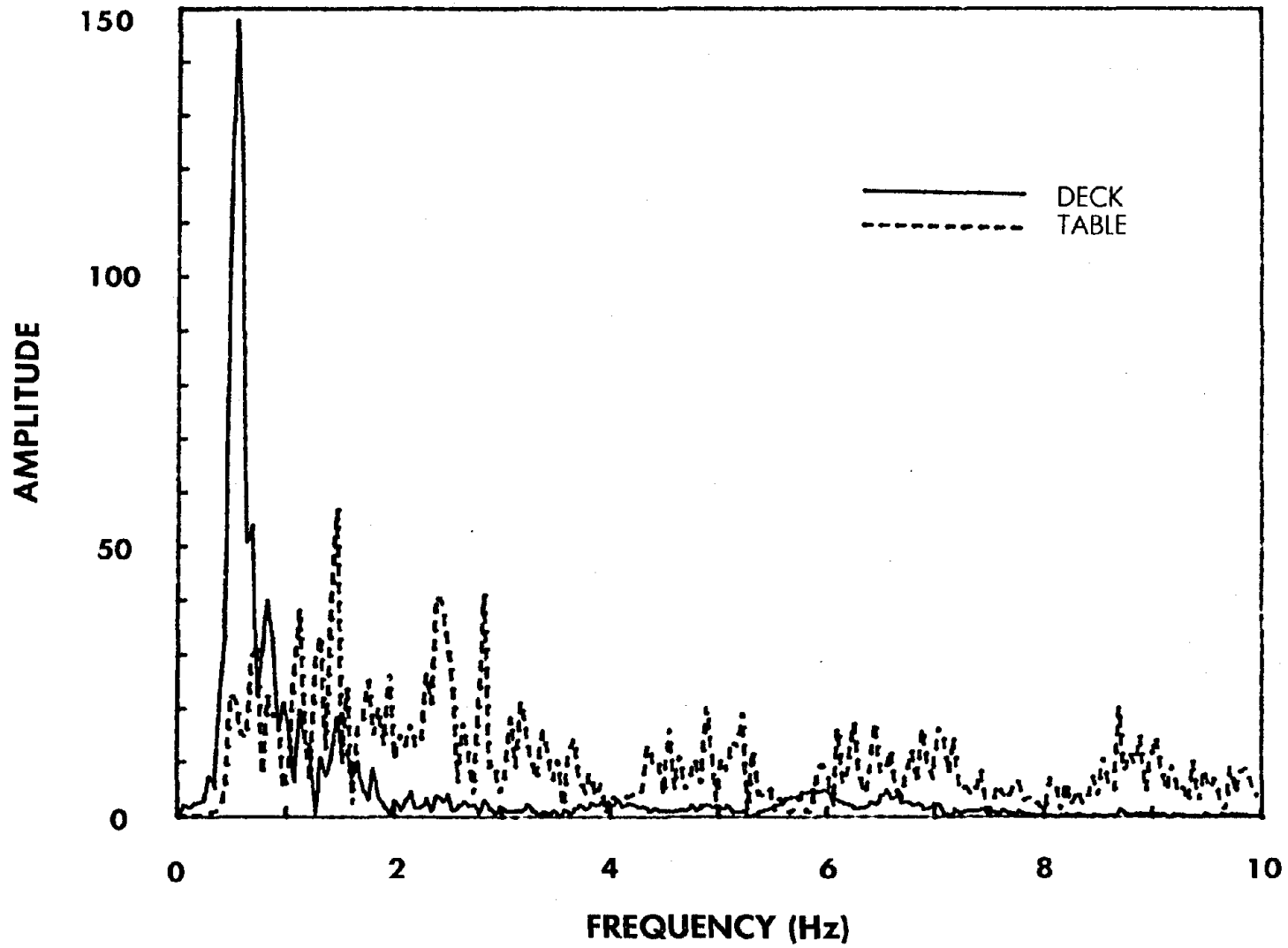


Figure 19 Table and Deck Acceleration Fourier Spectra of Plain Bearing System under Real-Time ATC-3 Signal at Span 400

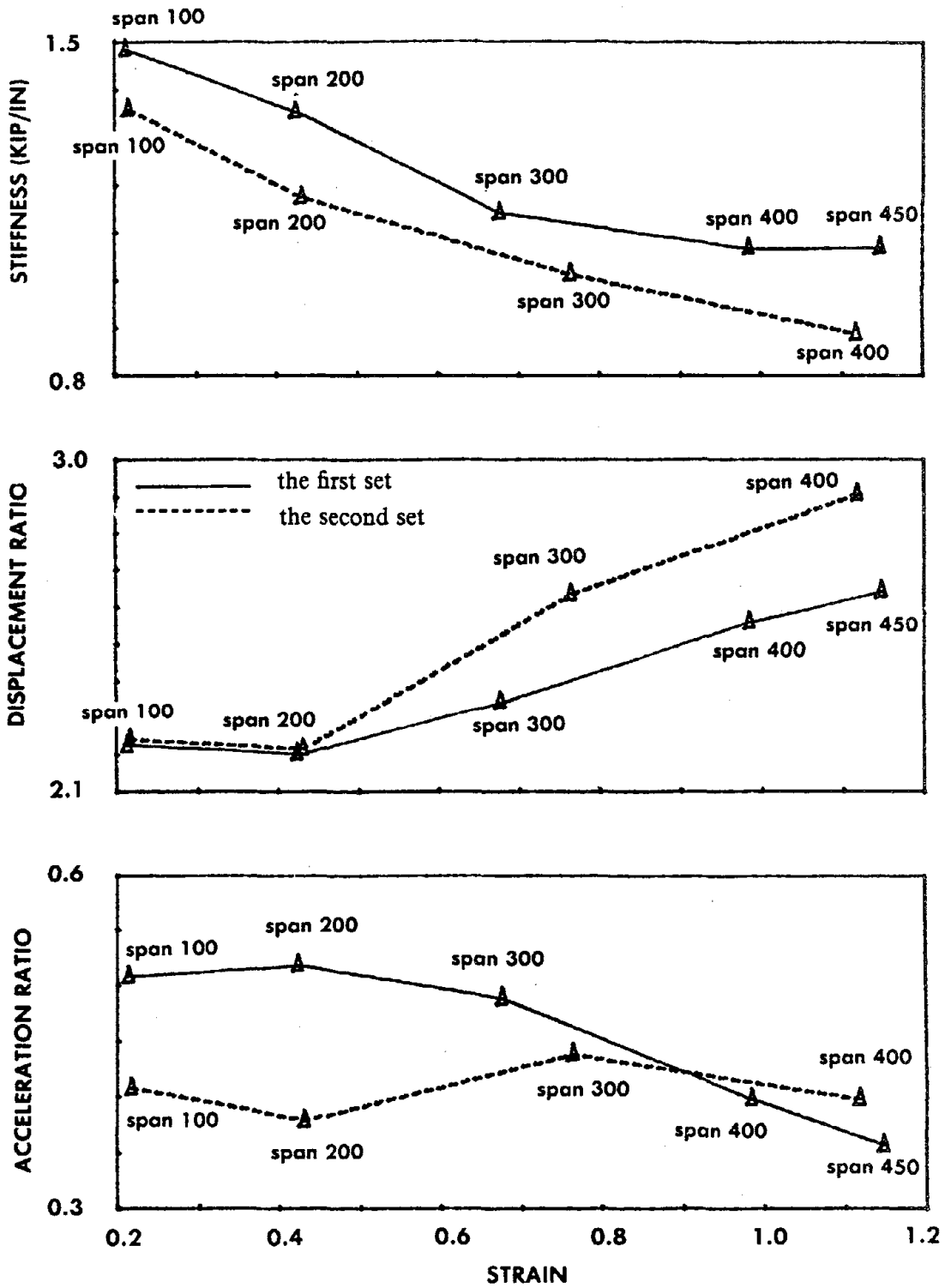


Figure 20 Responses of Plain Bearing under Increasing Earthquake Intensity

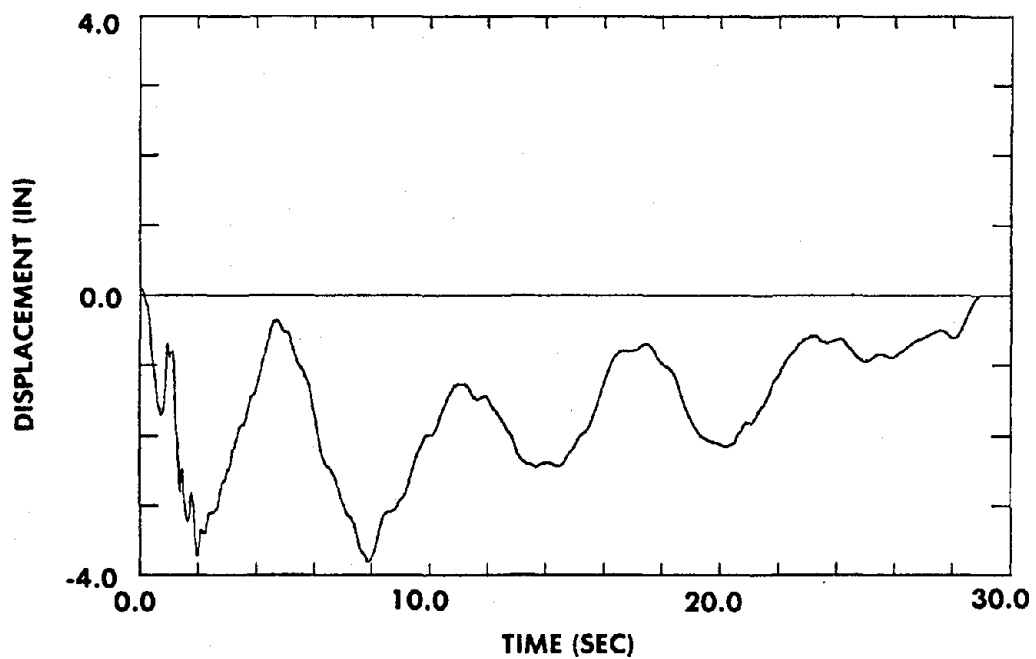


Figure 21 Time-Scaled San Francisco Displacement Record at Span 750

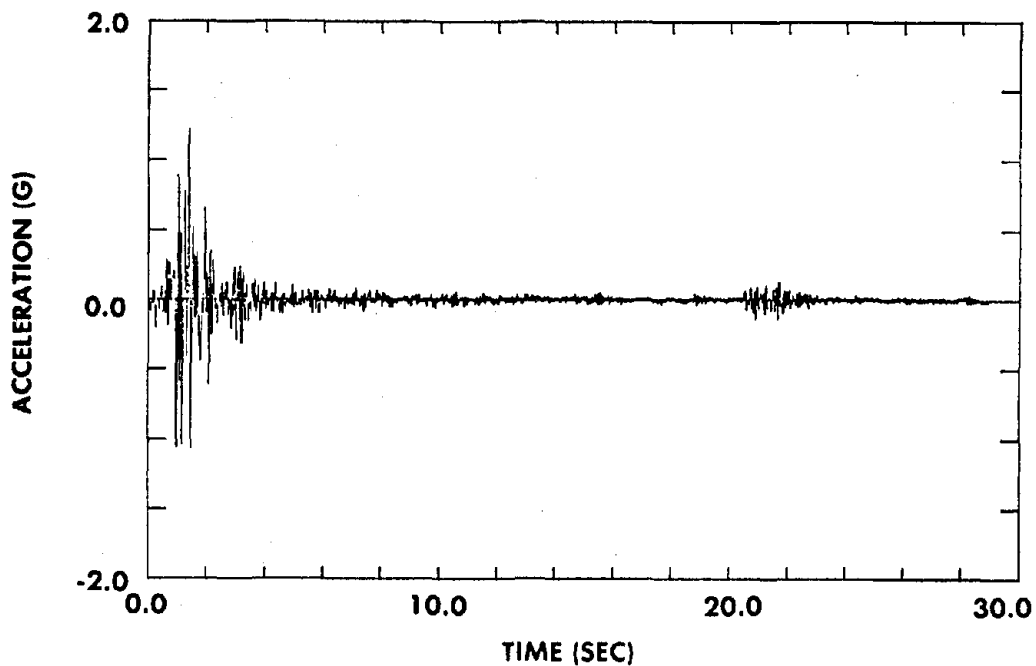


Figure 22 Time-Scaled San Francisco Acceleration Record at Span 750

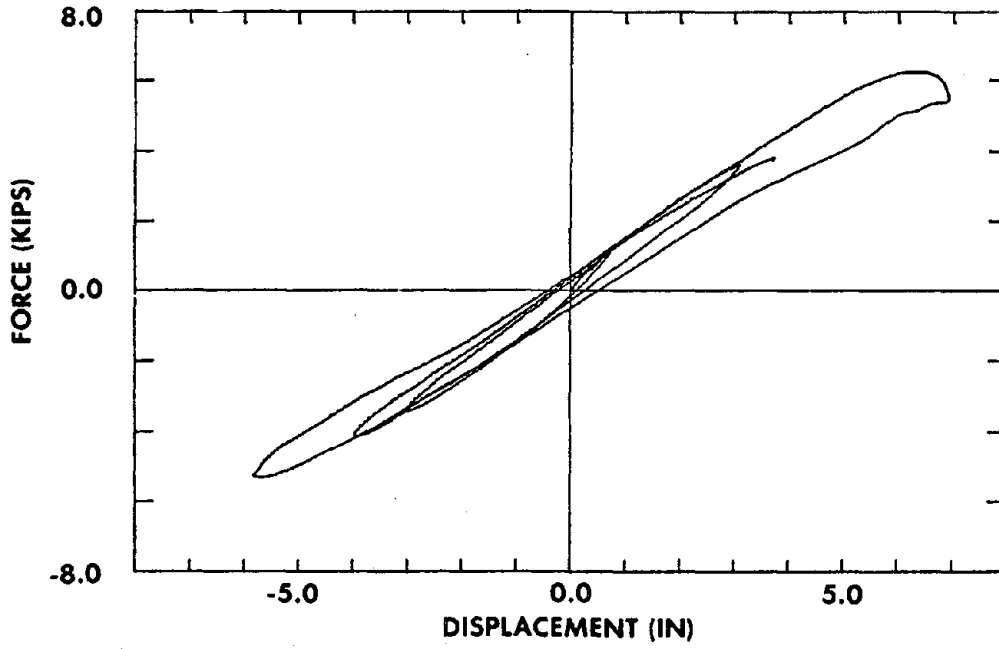


Figure 23 Hysteresis Loops of Plain Bearing under Time-Scaled El Centro Signal at Span 750

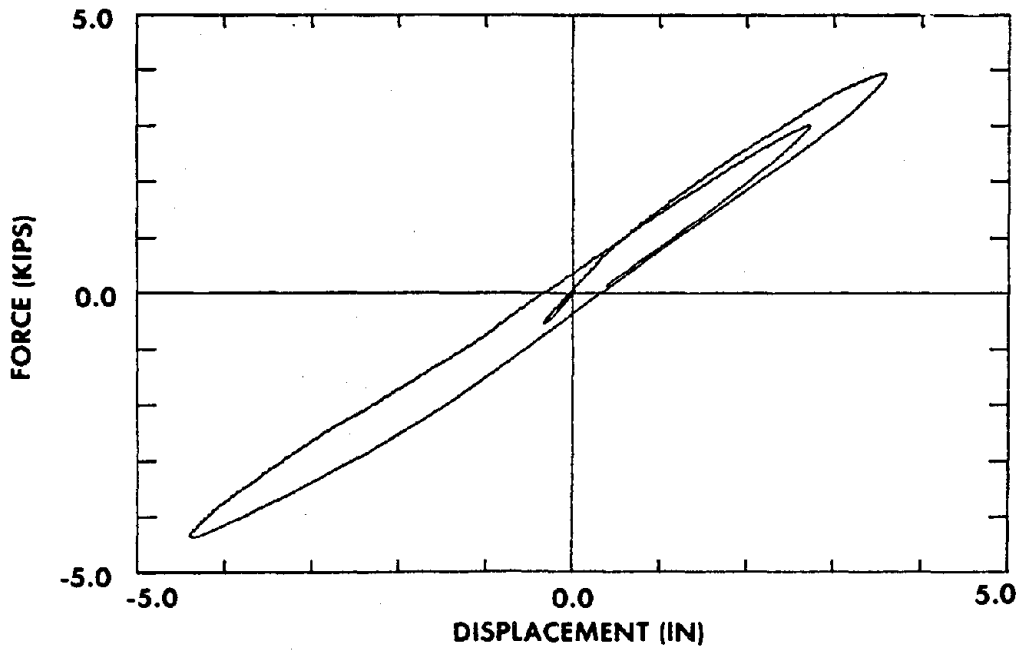


Figure 24 Hysteresis Loops of Plain Bearing under Time-Scaled Pacoima Dam Signal at Span 750

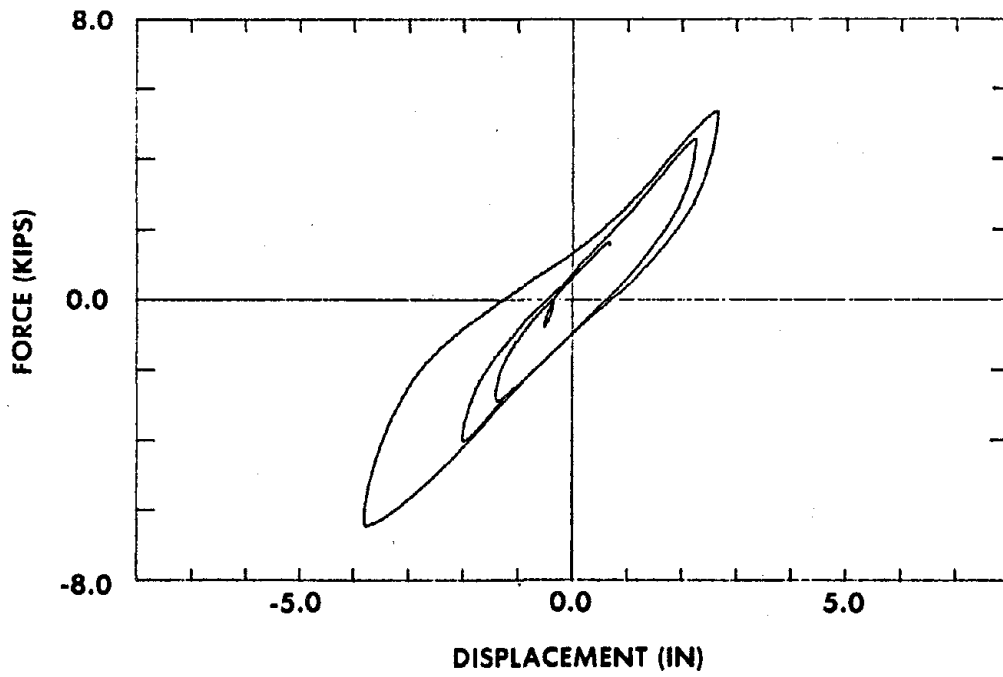


Figure 25 Hysteresis Loops of Lead-Filled Bearing System under Real-Time ATC-3 Signal at Span 400

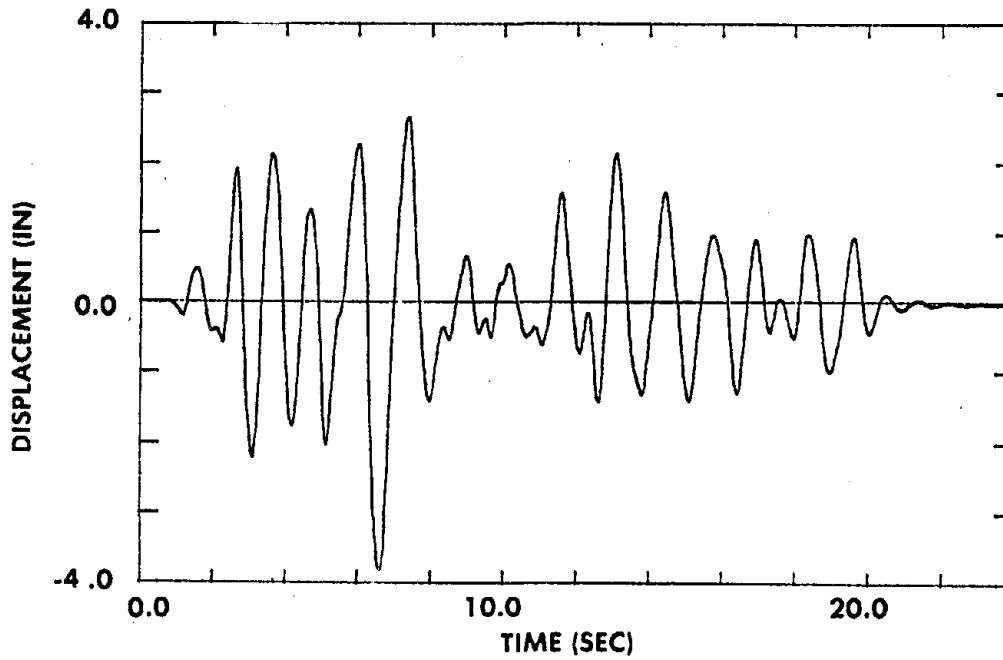


Figure 26 Deck Displacement Time History of Lead-Filled Bearing System under Real-Time ATC-3 Signal at Span 400

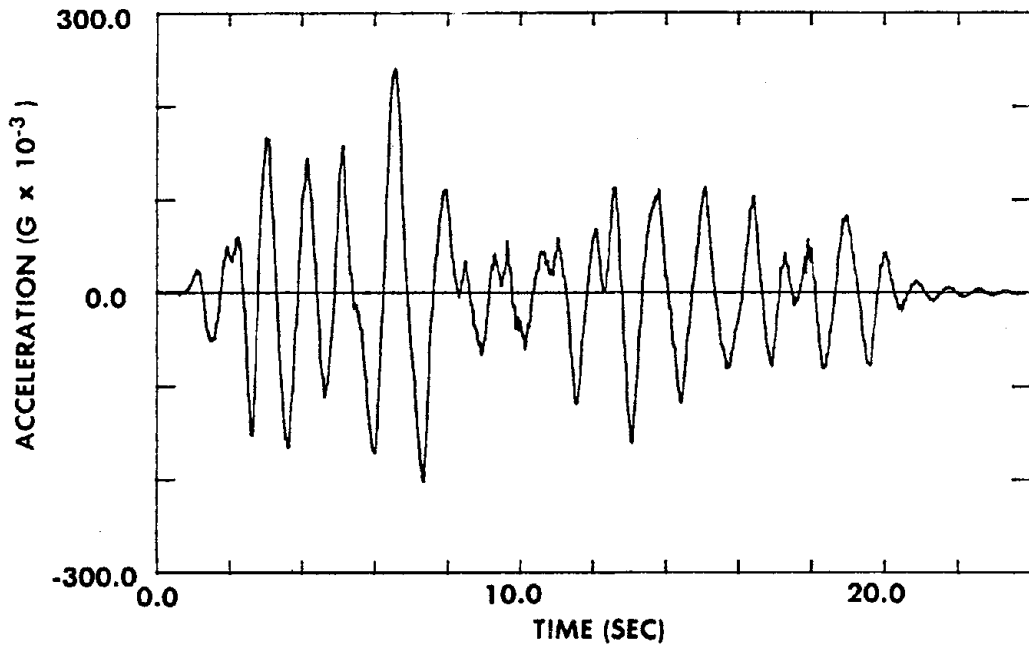


Figure 27 Deck Acceleration Time History of Lead-Filled Bearing System under Real-Time ATC-3 Signal at Span 400

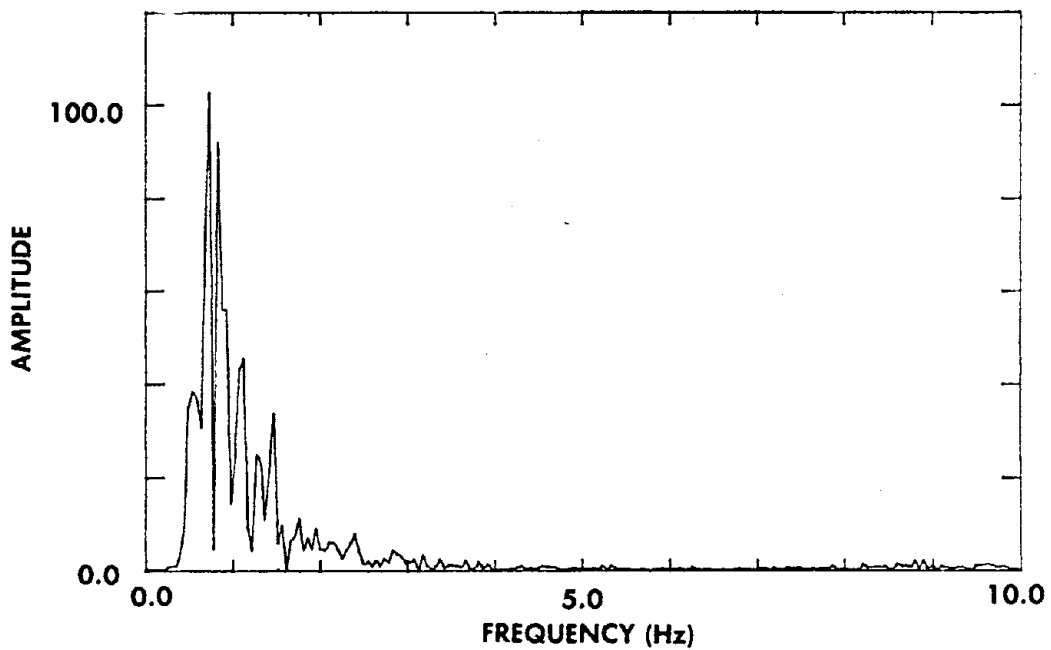


Figure 28 Deck Acceleration Fourier Spectrum of Lead-Filled Bearing System under Real-Time ATC-3 Signal at Span 400

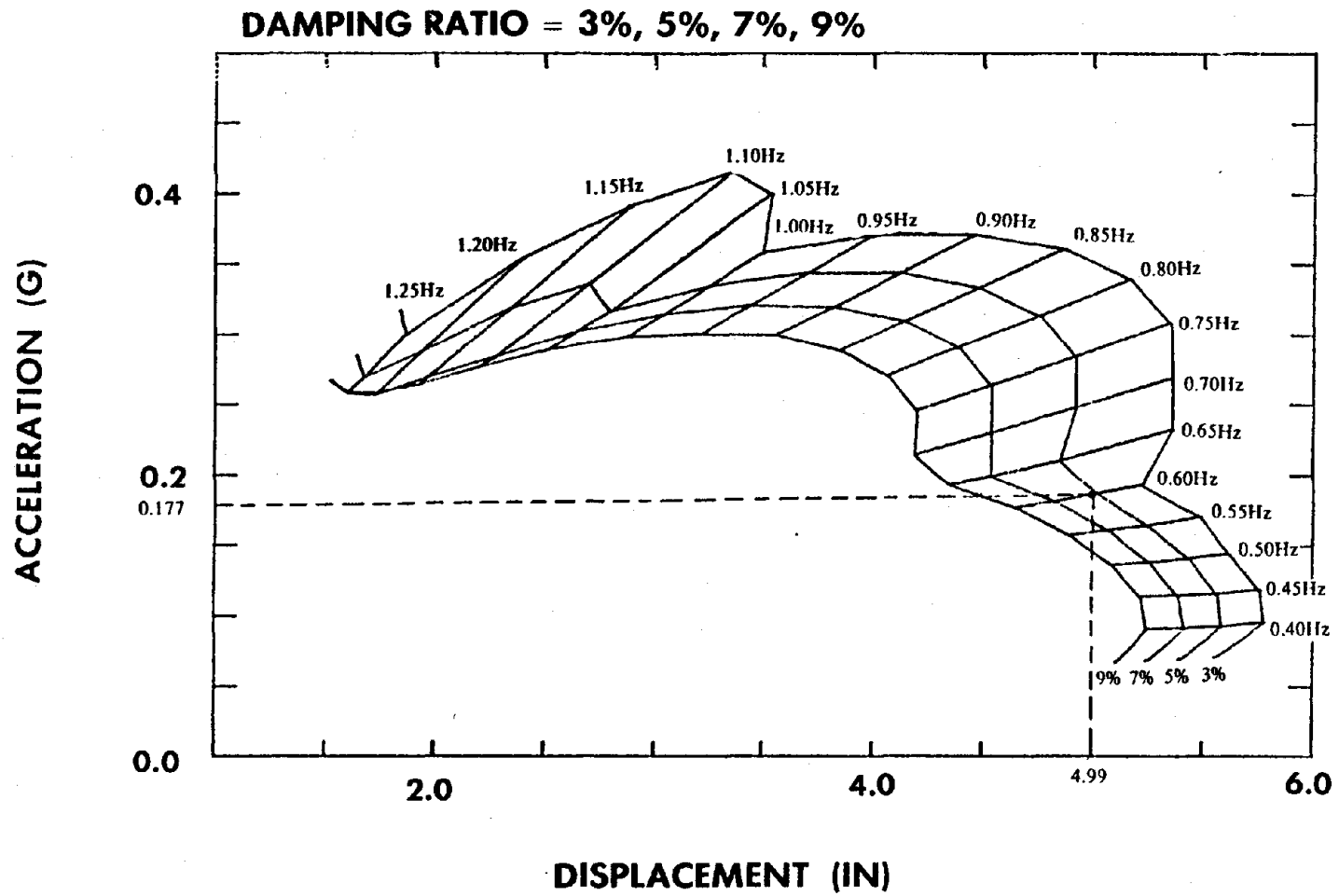


Figure 29 Response Network for Parameter Identification

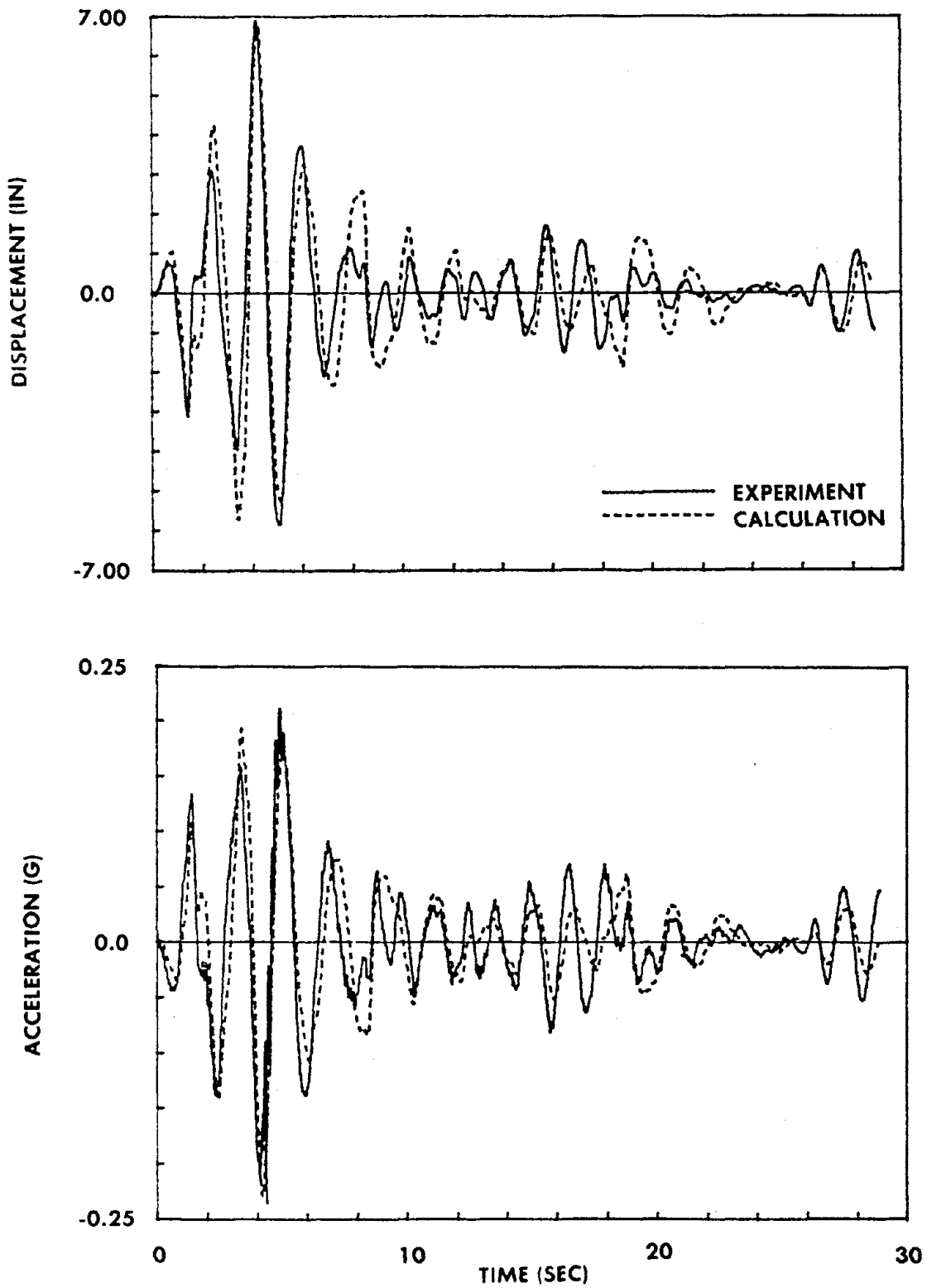


Figure 30 Correlation between Plain Bearing and Linear Viscous Model under El Centro Earthquake

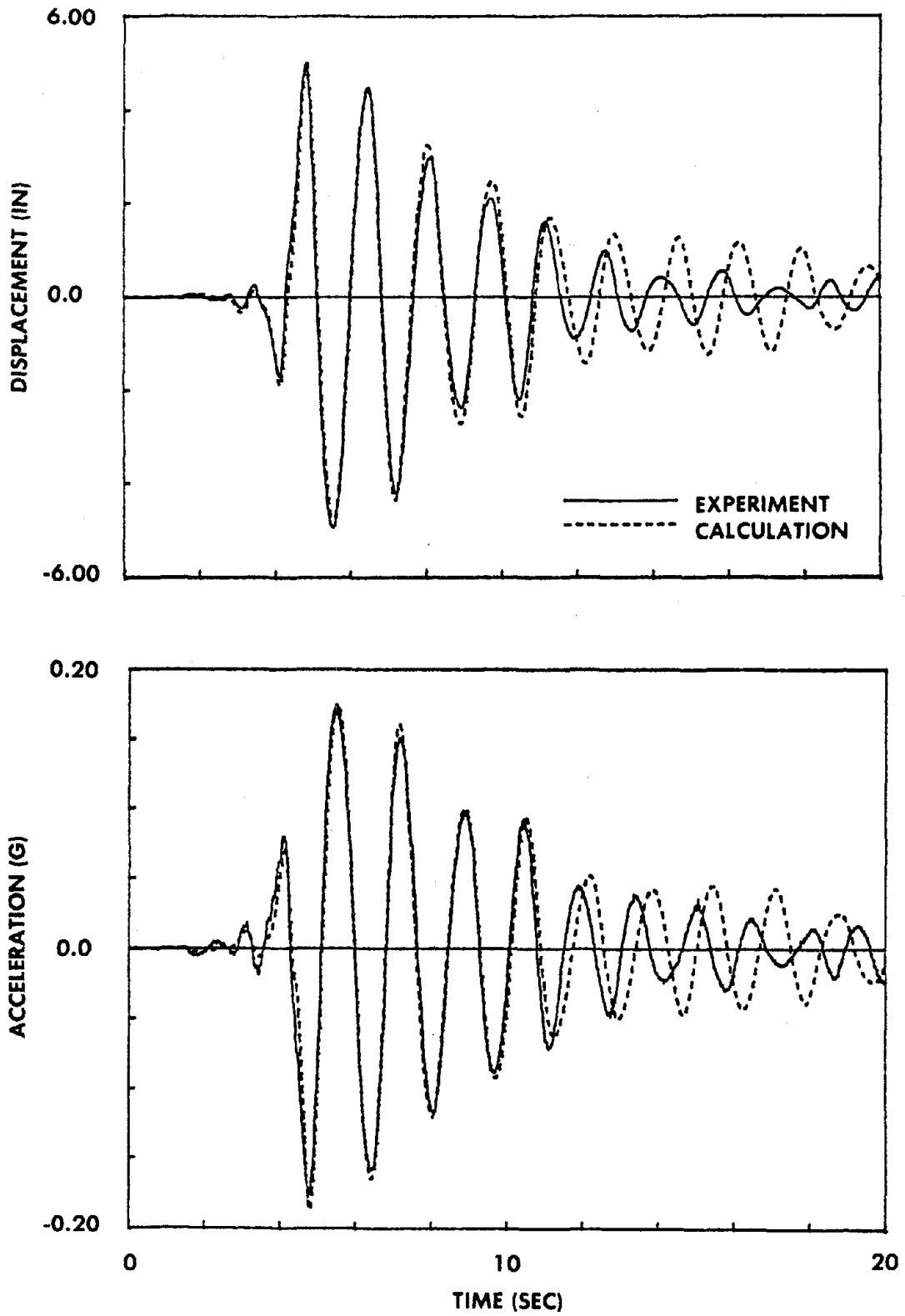


Figure 31 Correlation between Plain Bearing and Linear Viscous Model under Parkfield Earthquake

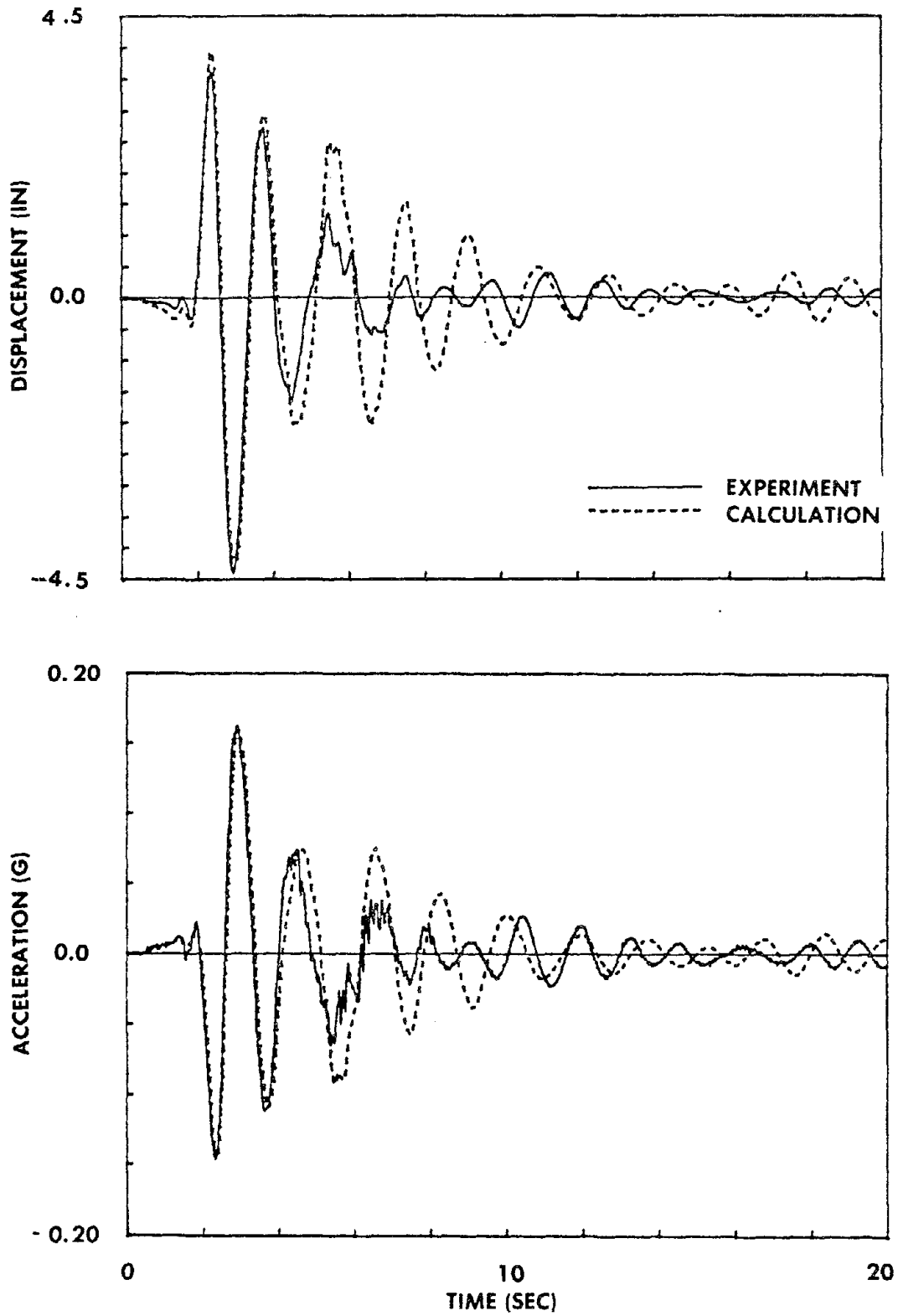


Figure 32 Correlation between Plain Bearing and Linear Viscous Model under Pacoima Dam Earthquake

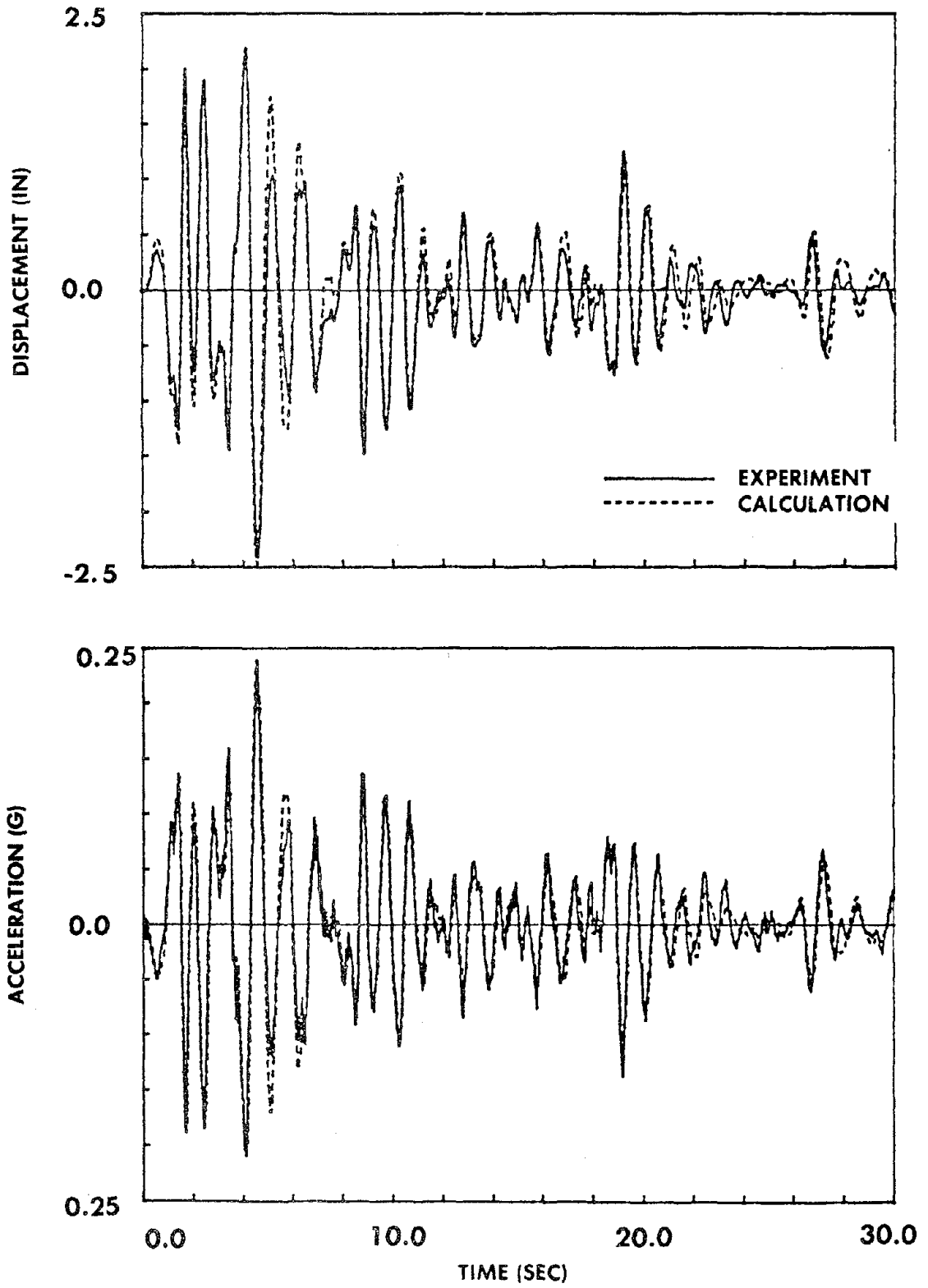


Figure 35 Correlation between Lead-Filled Bearing and Linear Viscous Model under El Centro Earthquake

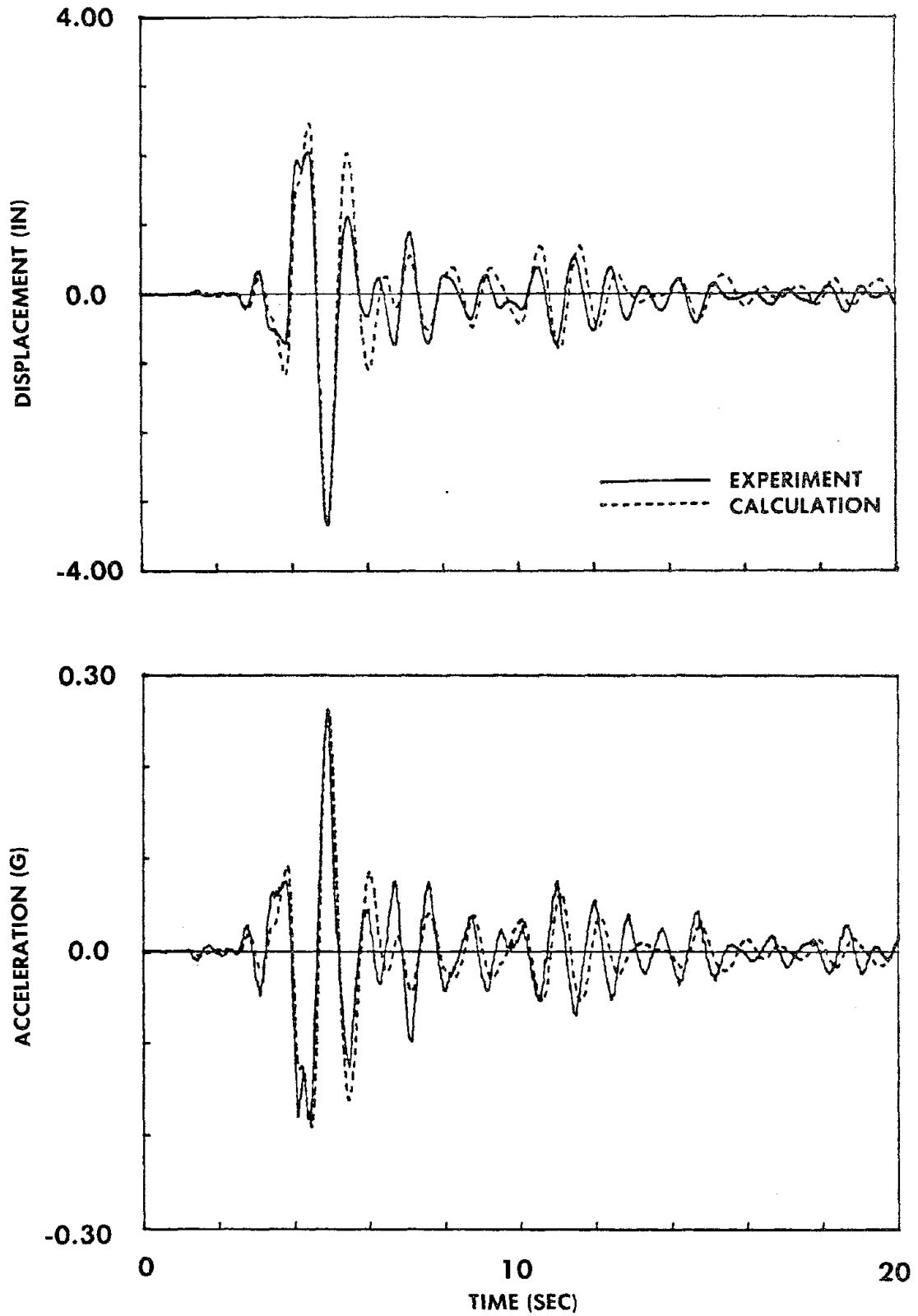


Figure 36 Correlation between Lead-Filled Bearing and Linear Viscous Model under Parkfield Earthquake

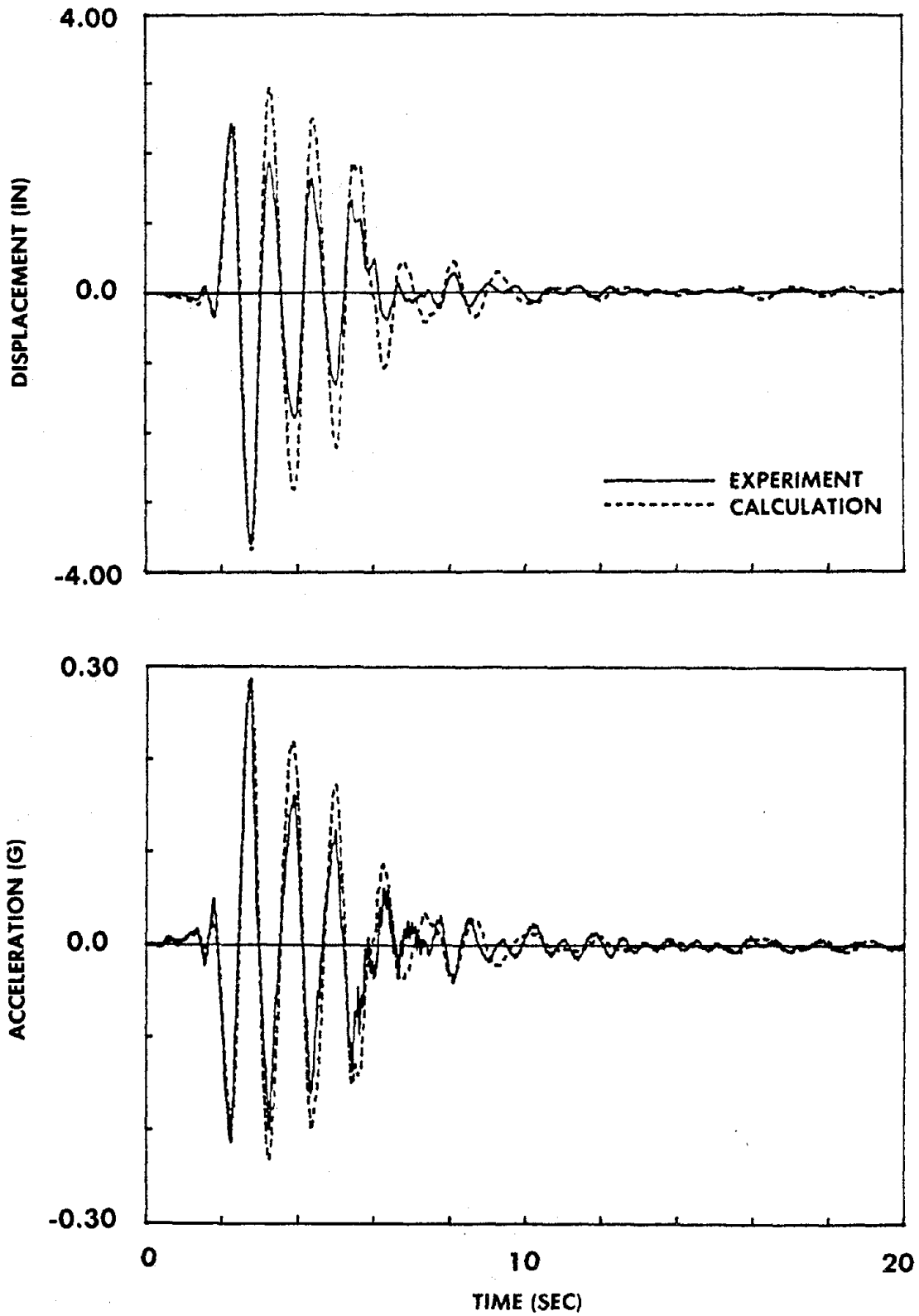


Figure 37 Correlation between Lead-Filled Bearing and Linear Viscous Model under Pacoima Dam Earthquake

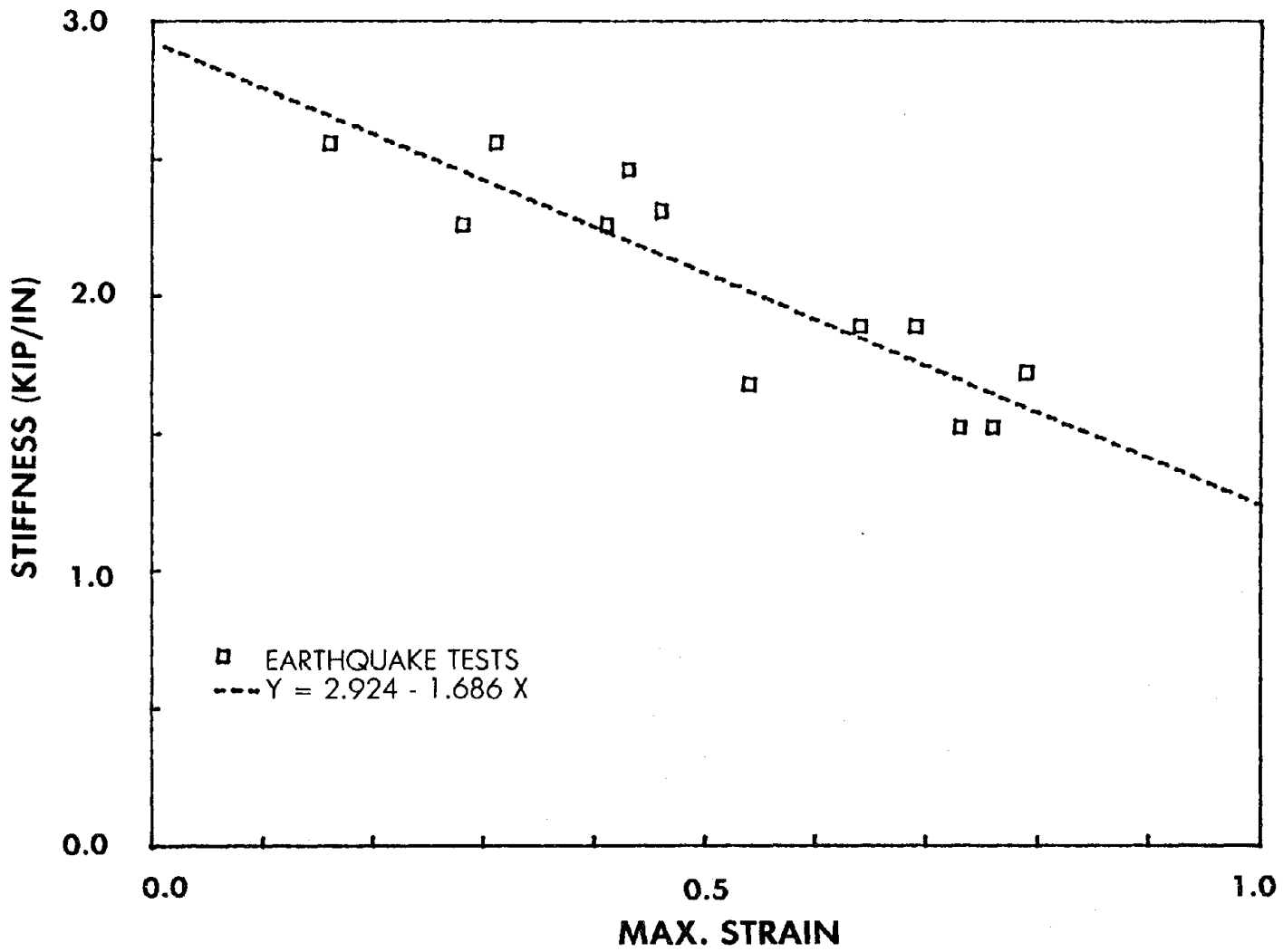


Figure 38 Relation between Effective Stiffness and Maximum Strain for Lead-Filled Natural Rubber Bearing

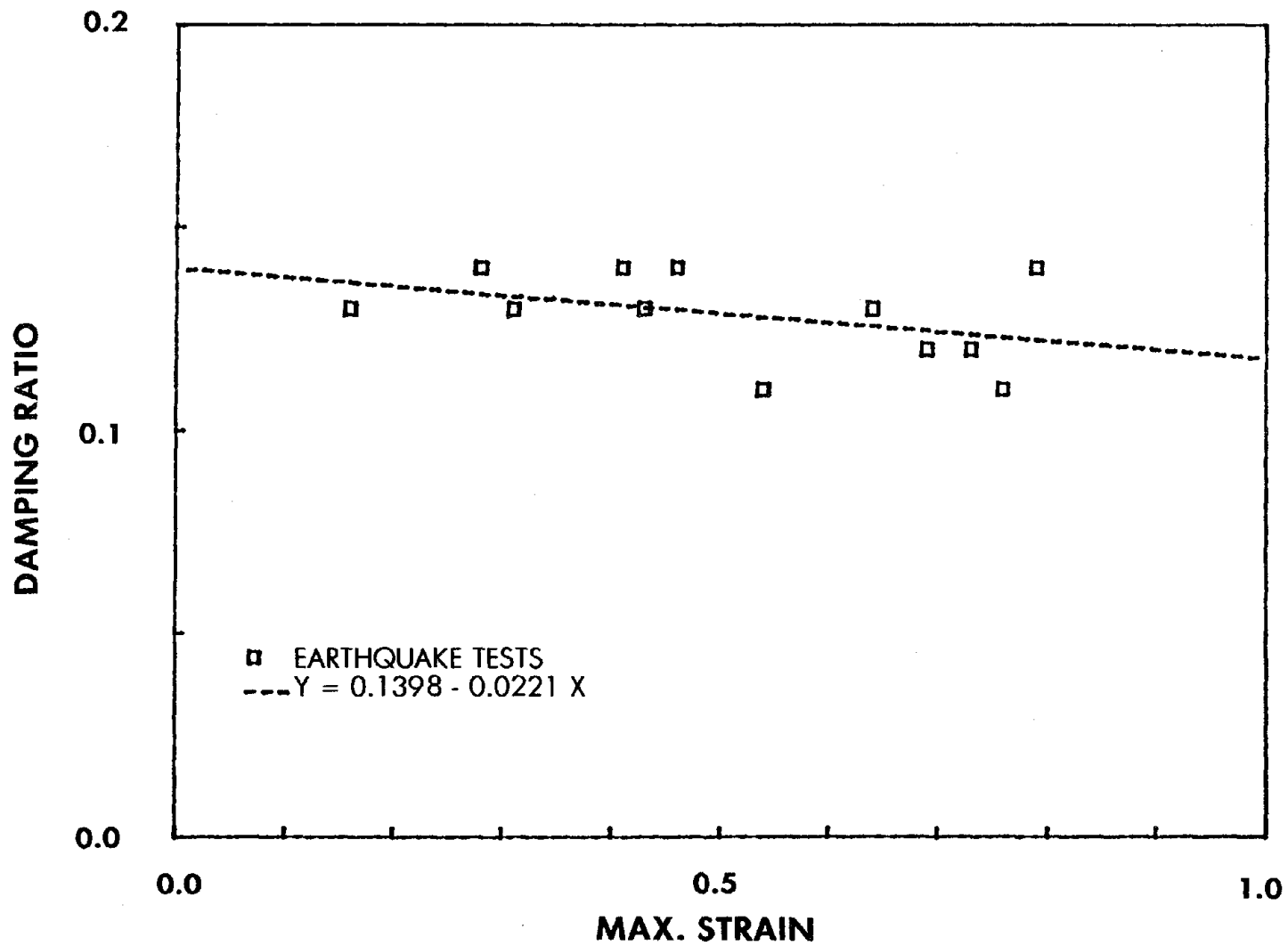


Figure 39 Relation between Damping Ratio and Maximum Strain for Lead-Filled Natural Rubber Bearing

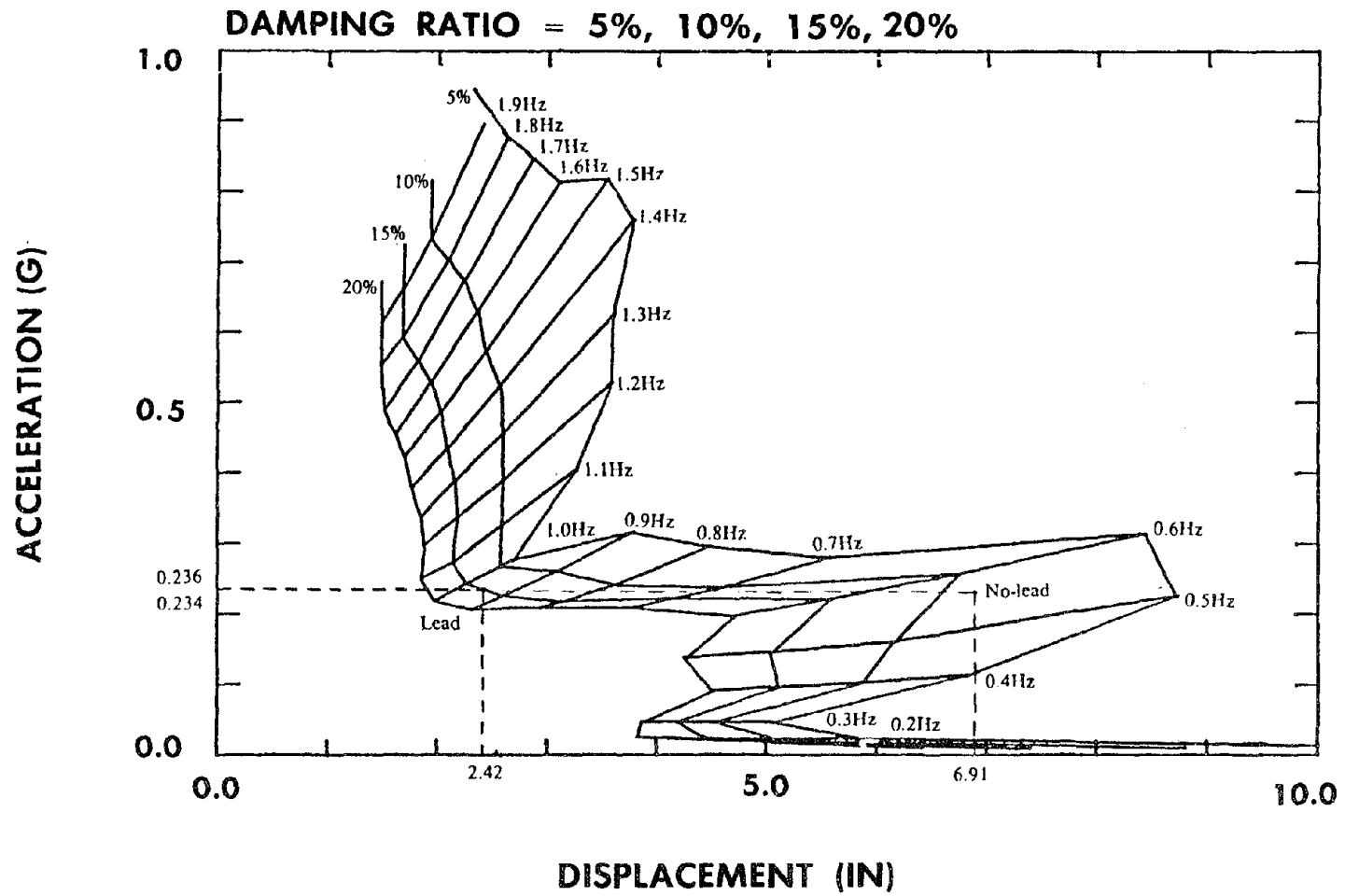


Figure 40 Response Network of El Centro Time-Scaled Record at Span 750

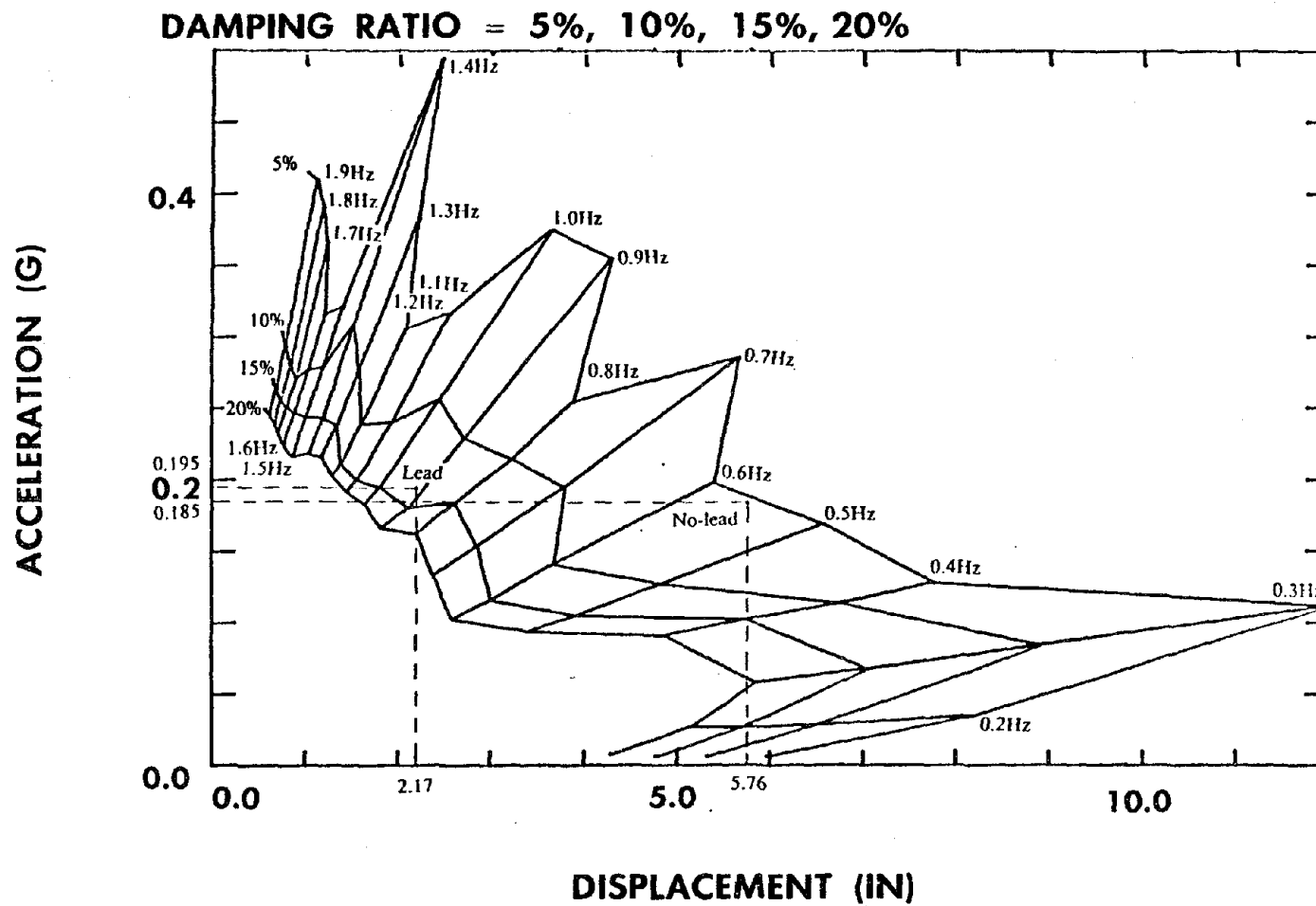


Figure 41 Response Network of Caltech A1 Time-Scaled Record at Span 750

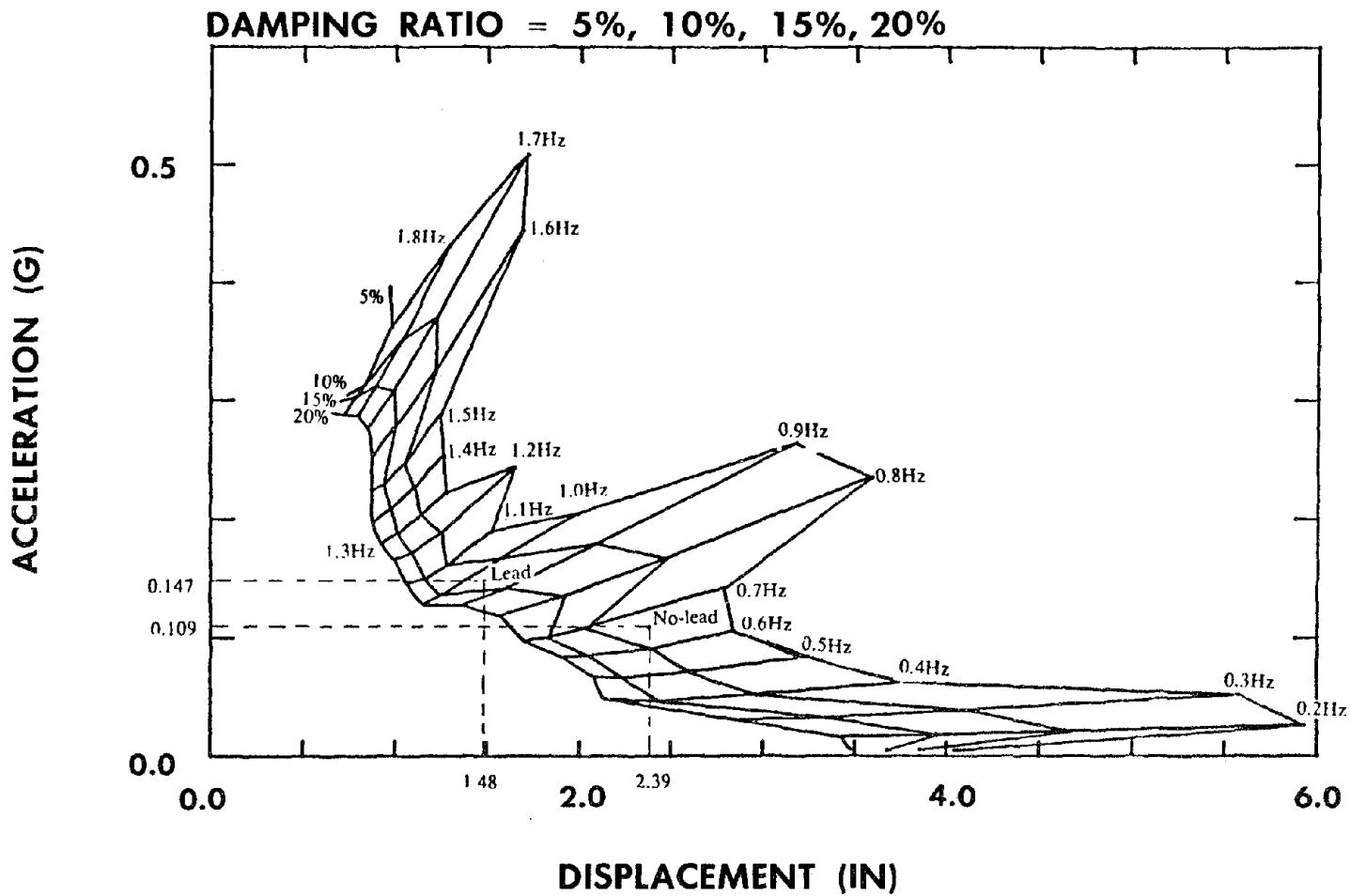


Figure 42 Response Network of Taft Time-Scaled Record at Span 750

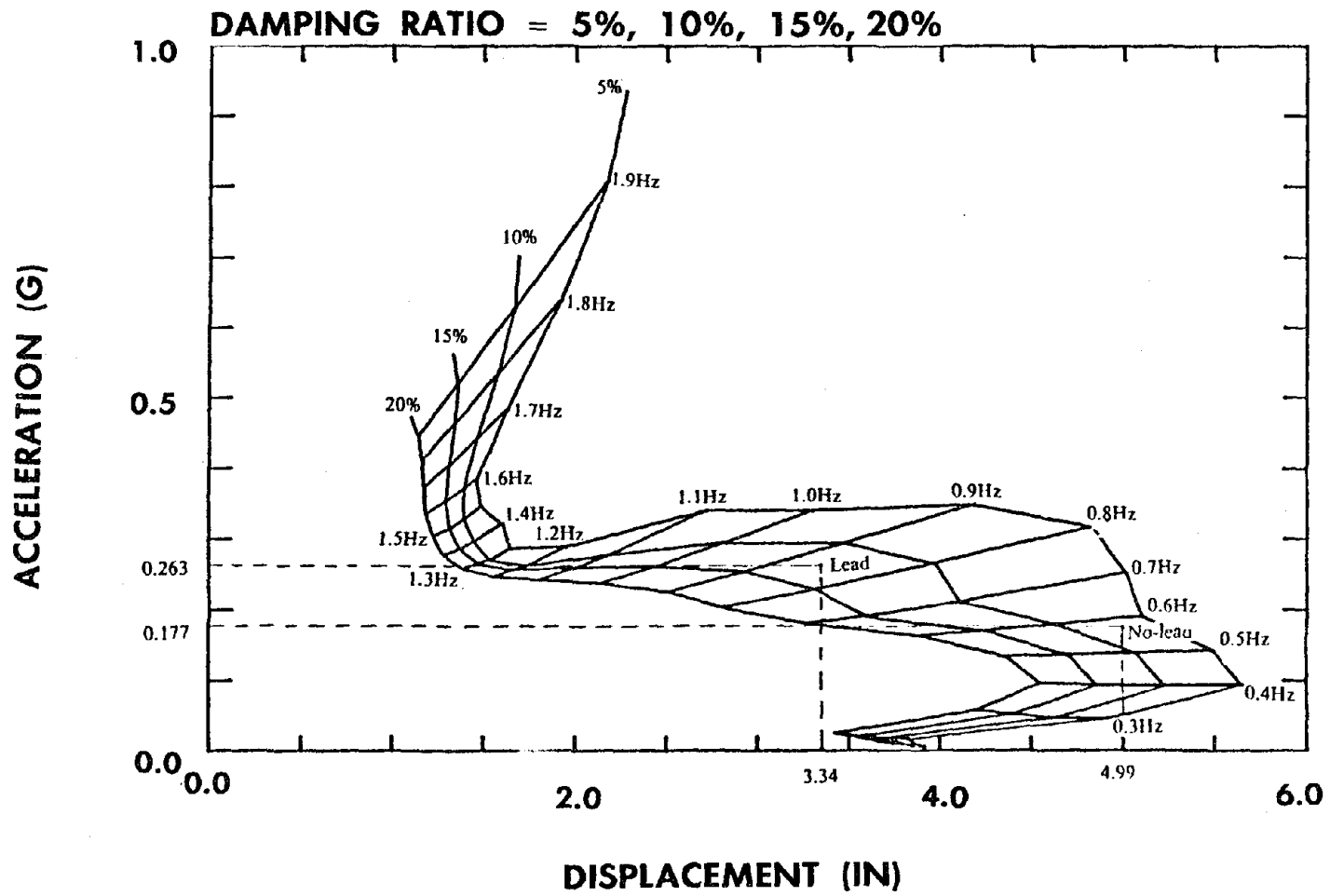


Figure 43 Response Network of Parkfield Time-Scaled Record at Span 750

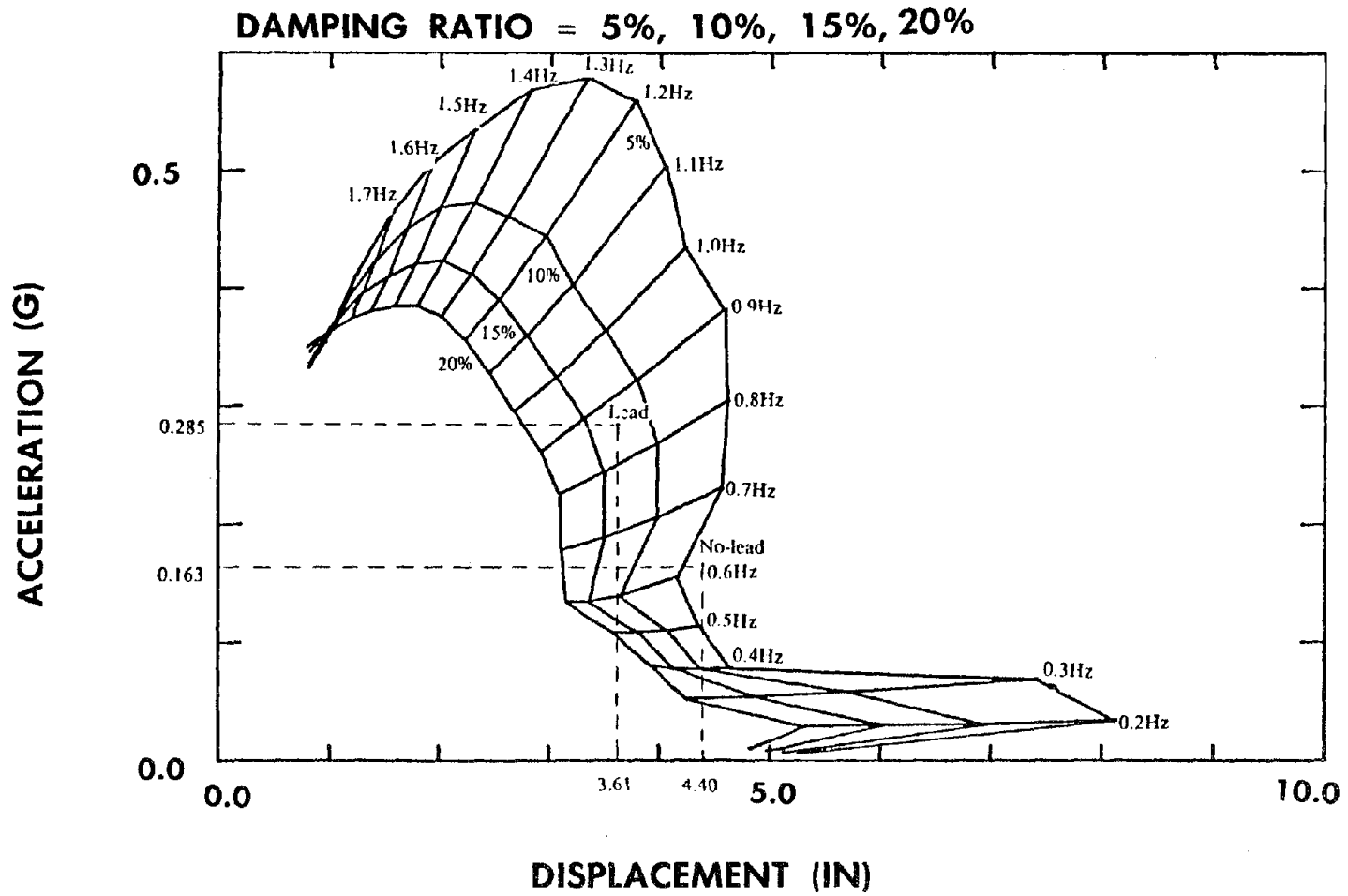


Figure 44 Response Network of Pacoima Dam Time-Scaled Record at Span 750

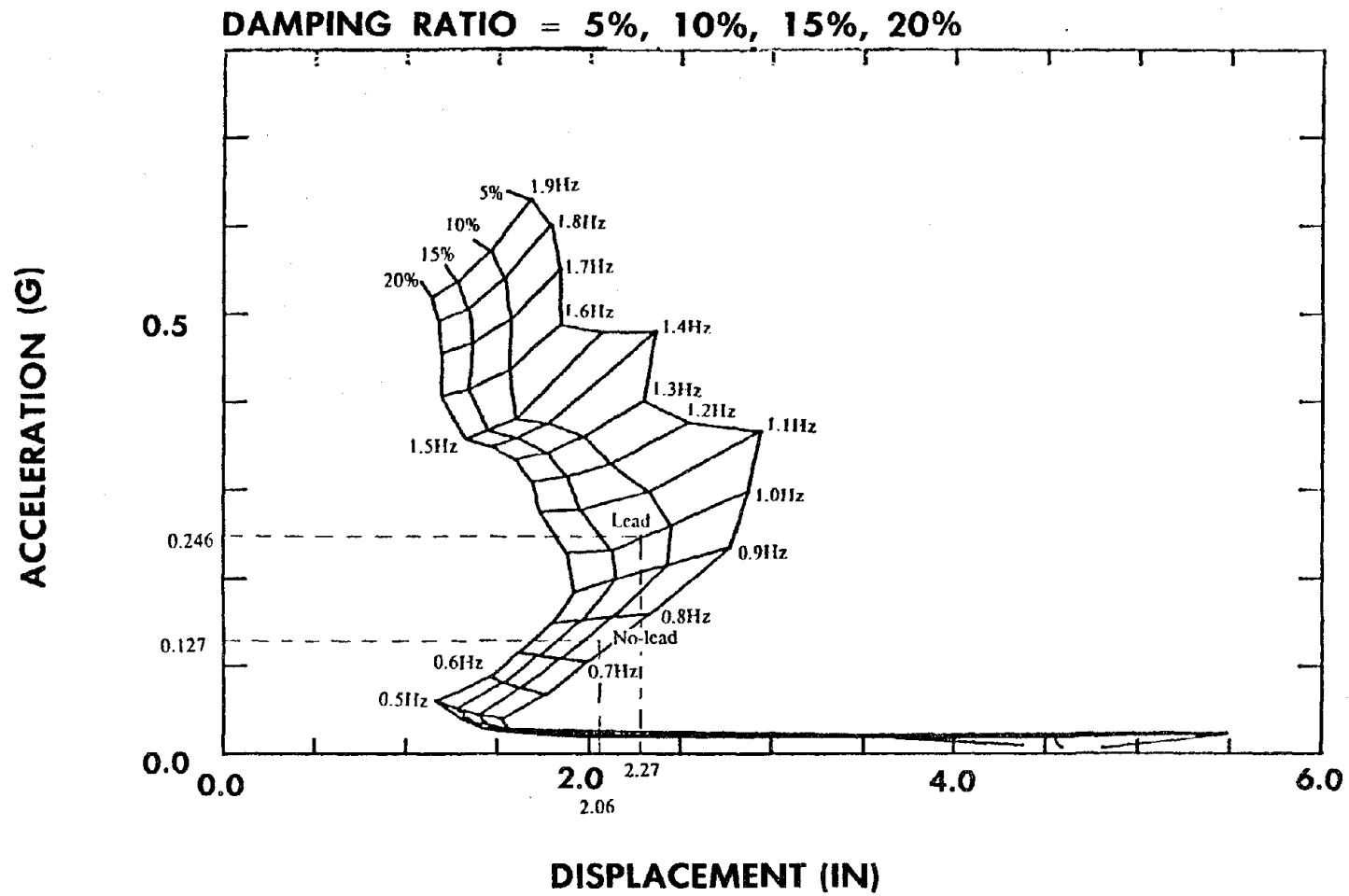


Figure 45 Response Network of San Francisco Time-Scaled Record at Span 750

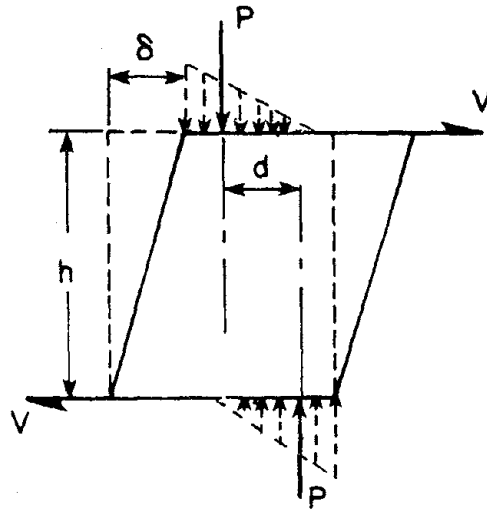


Figure 46 Forces Acting on Deformed Bearing

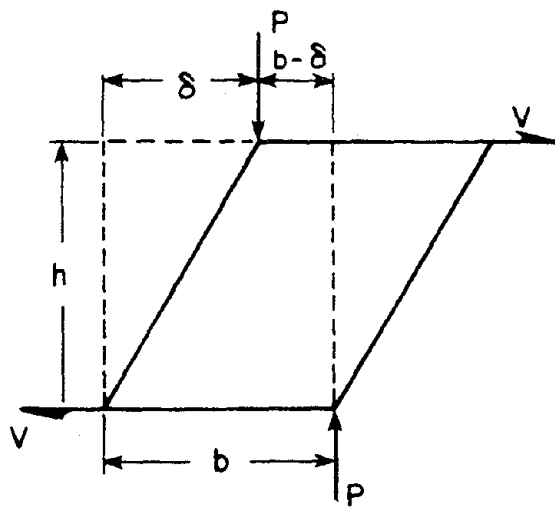


Figure 47 Forces Acting on Bearing in Limit State

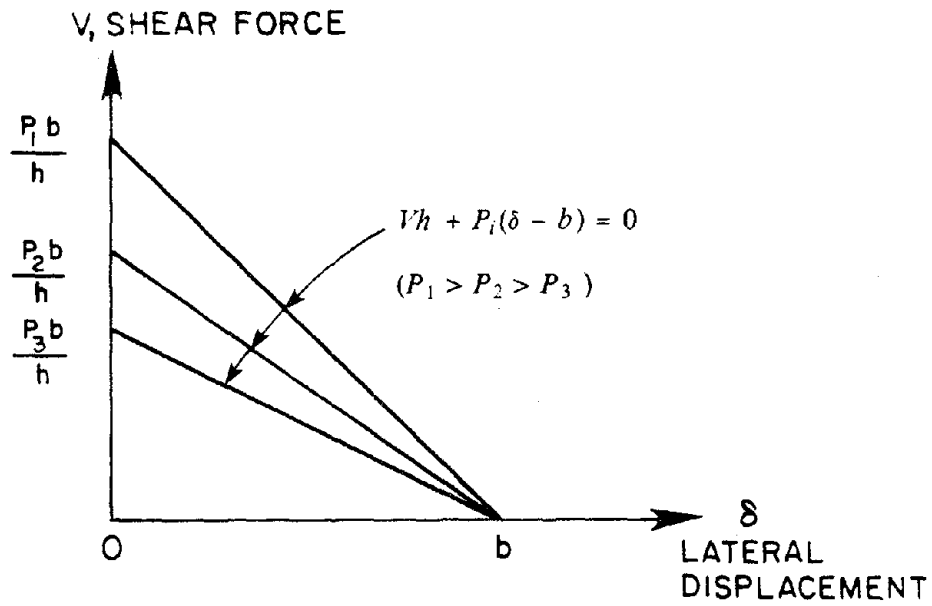


Figure 48 Relation between Shear Force and Lateral Displacement in Limit State

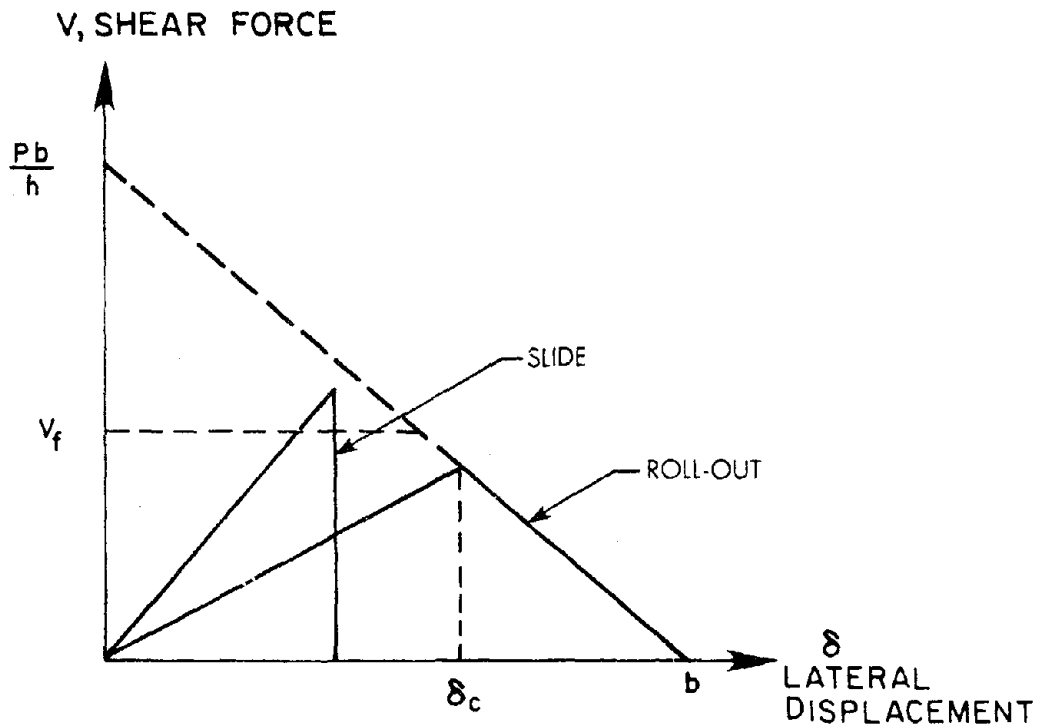


Figure 49 Force-Displacement Curves for Roll-out and Slide Failure Modes

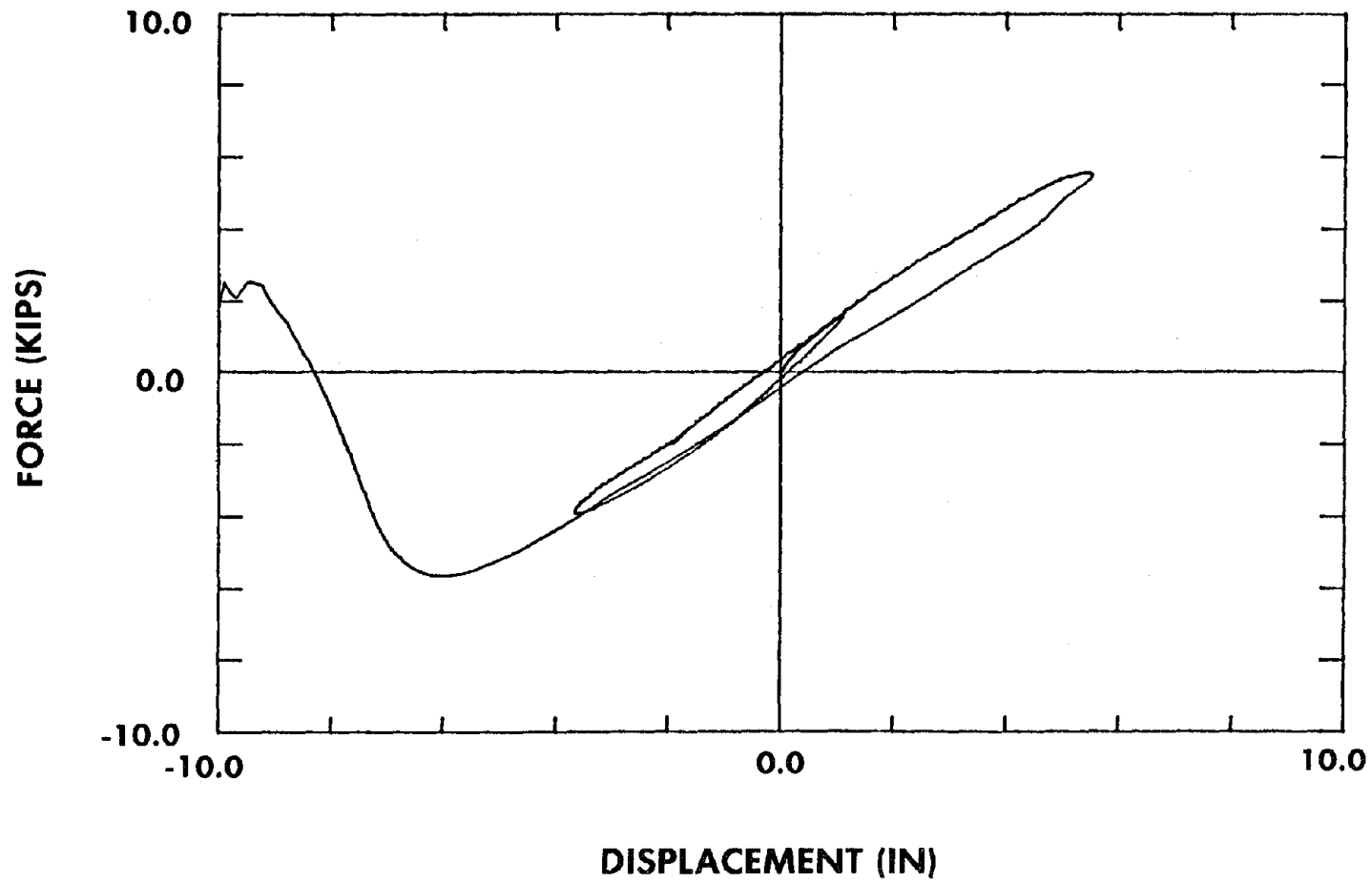


Figure 50 Force-displacement Curve in Roll-out Test of Plain Bearing System

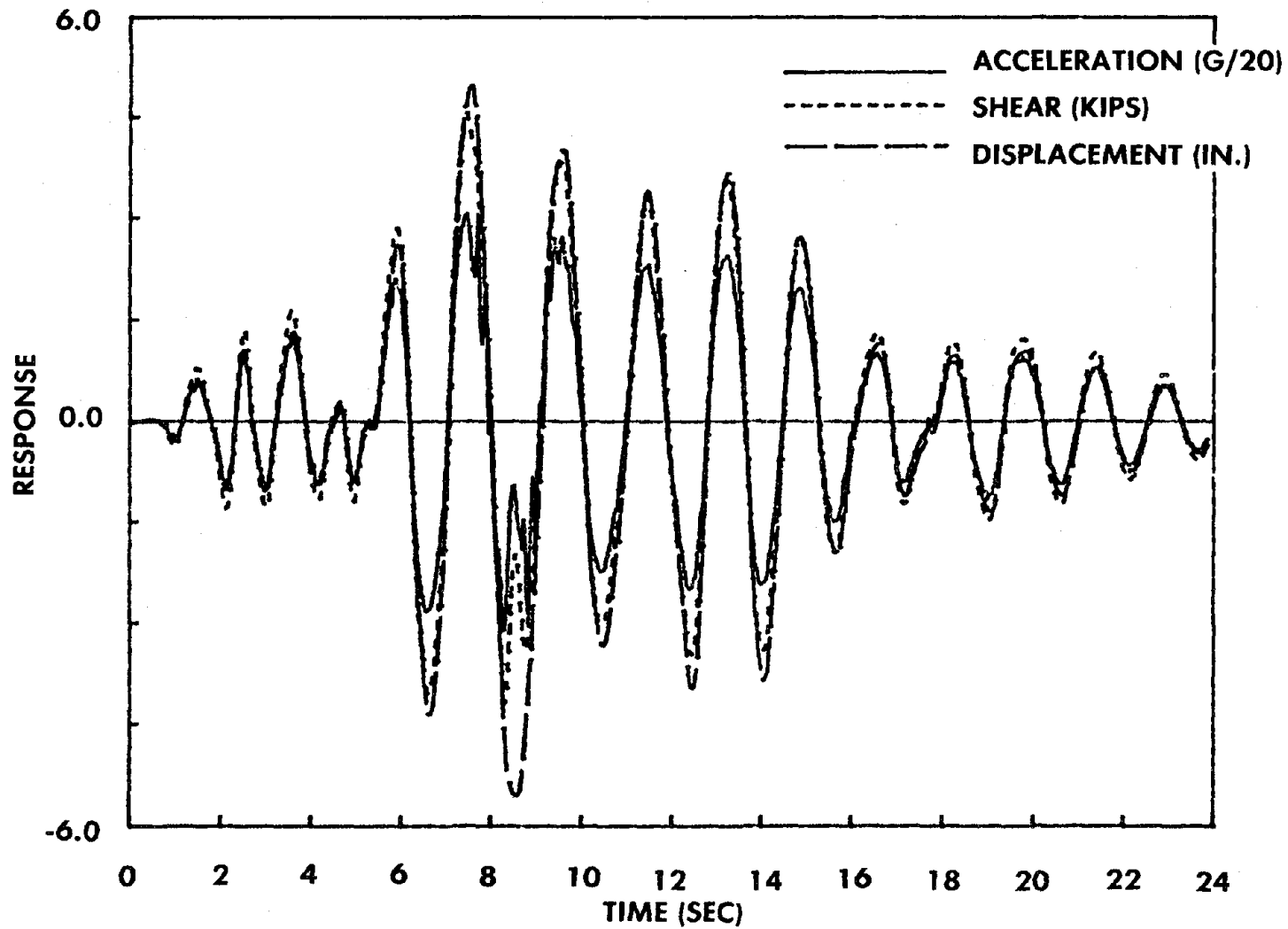


Figure 51 Response Time Histories in Plain Bearing System
under Real-Time ATC-3 Input at Span 400

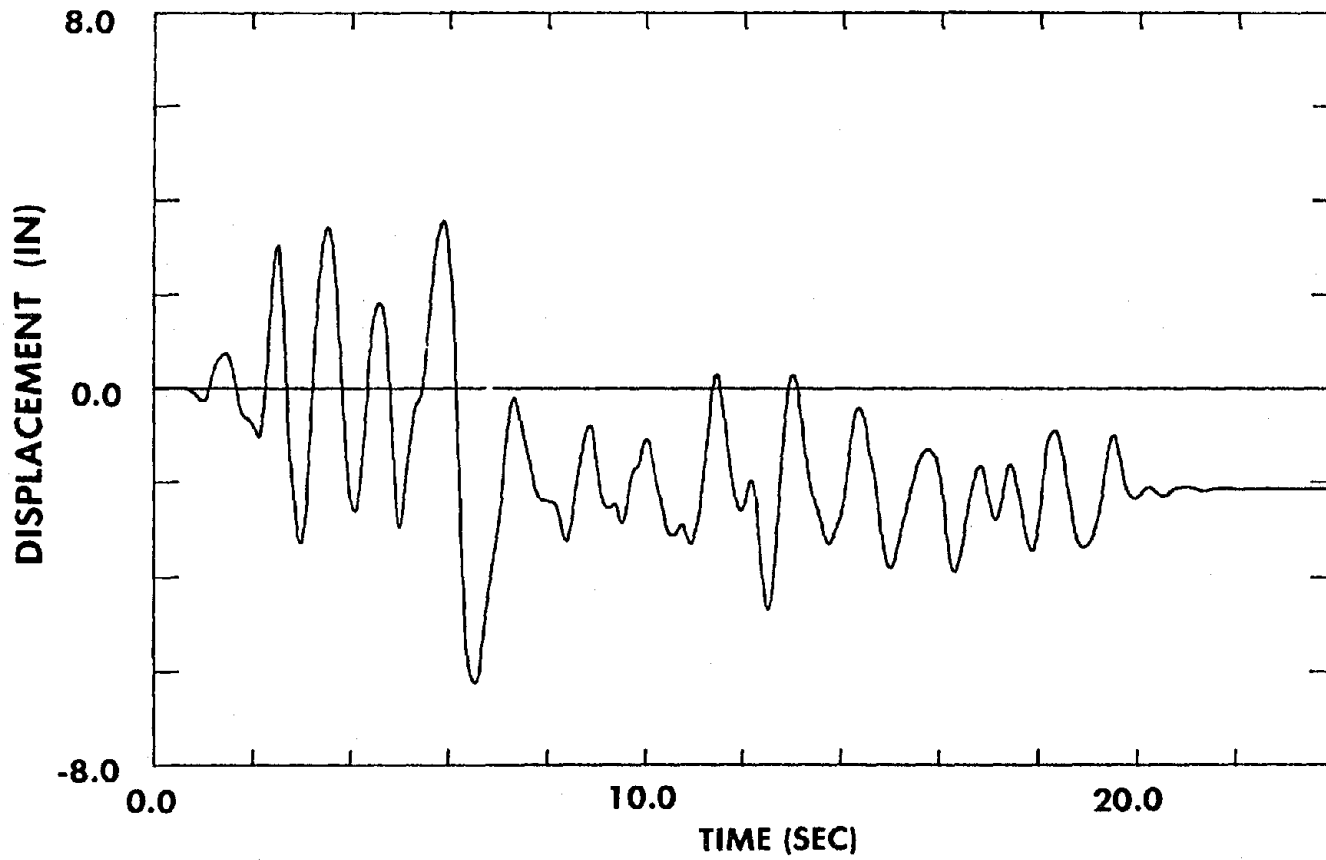


Figure 52 Deck Displacement Time History in Slide Test of Lead-Filled Bearing System

Reproduced from
best available copy.

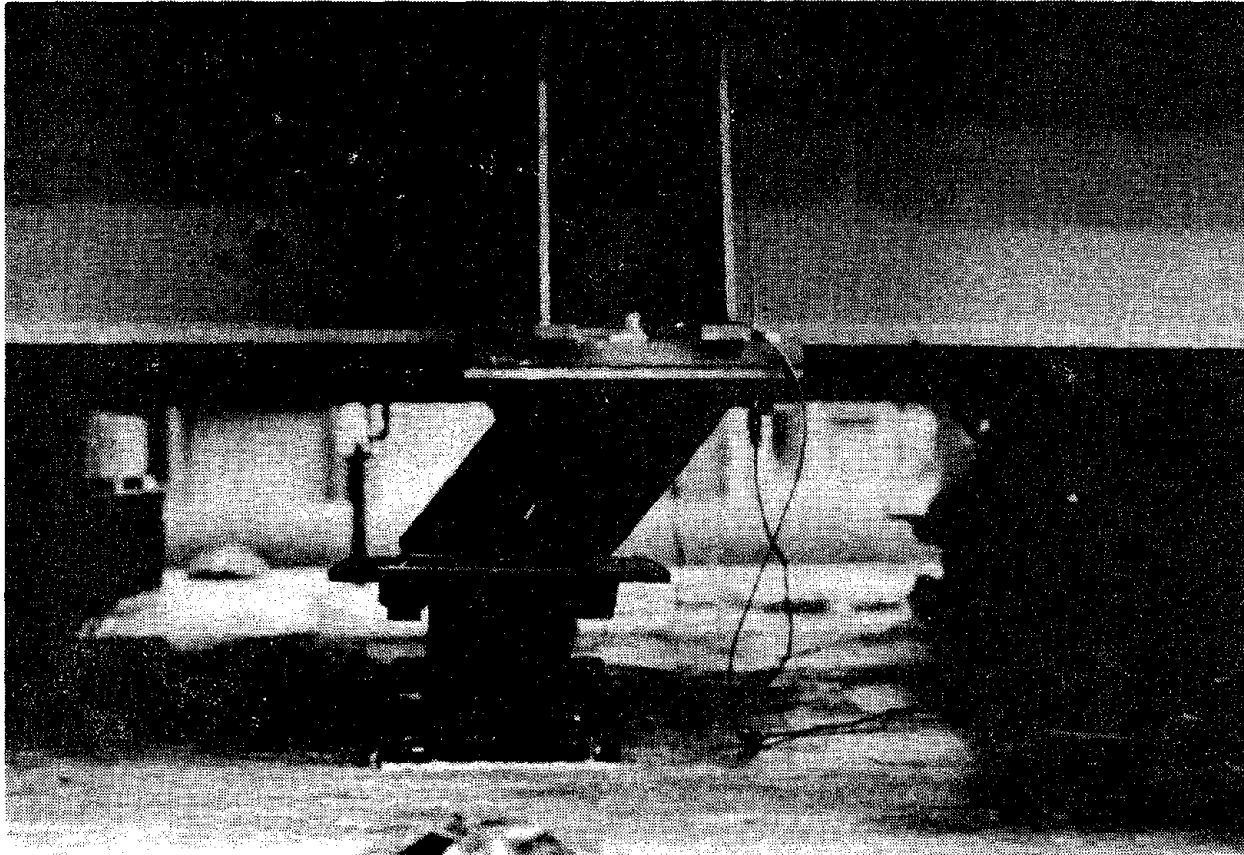


Figure 53 Lead-Filled Rubber Bearing after Slide

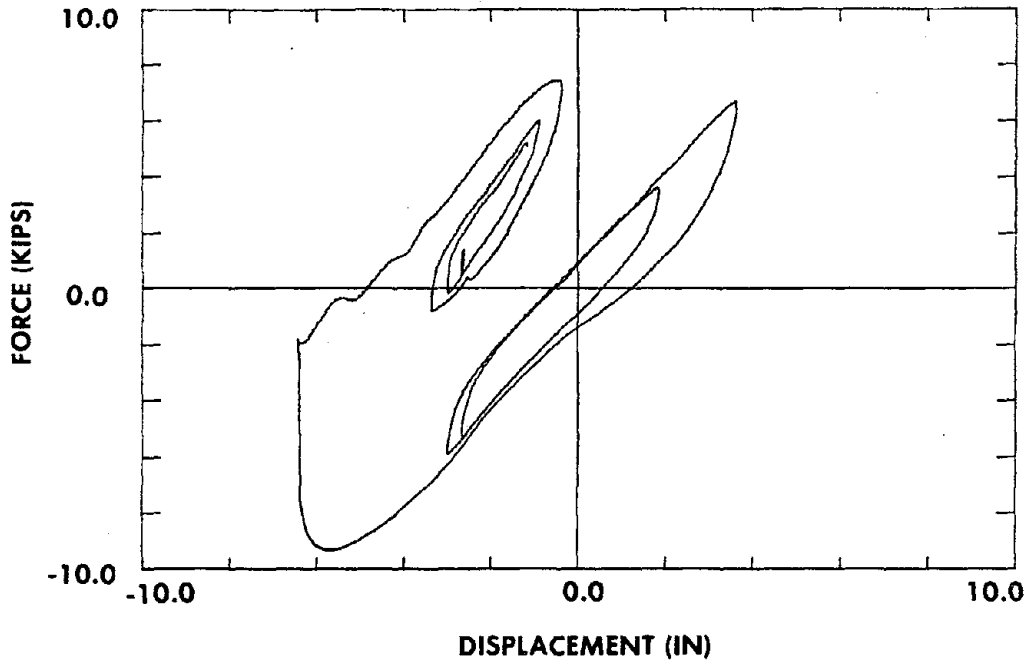


Figure 54 Force-Displacement Curve for Slidged Lead-Filled Bearing

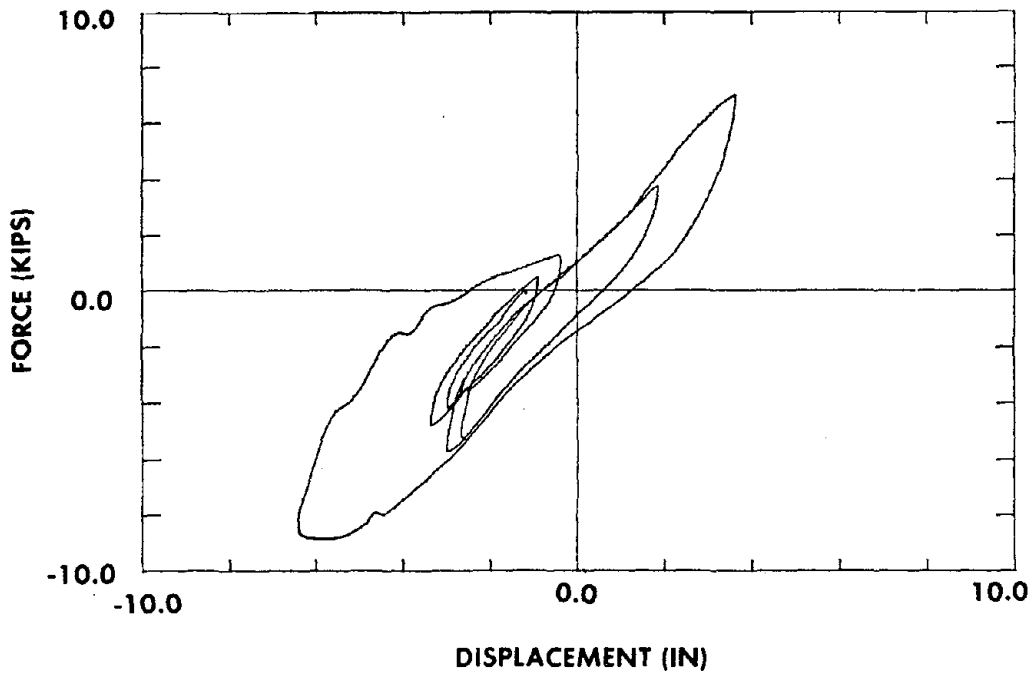


Figure 55 Force-Displacement Curve for Unslidged Lead-Filled Bearing

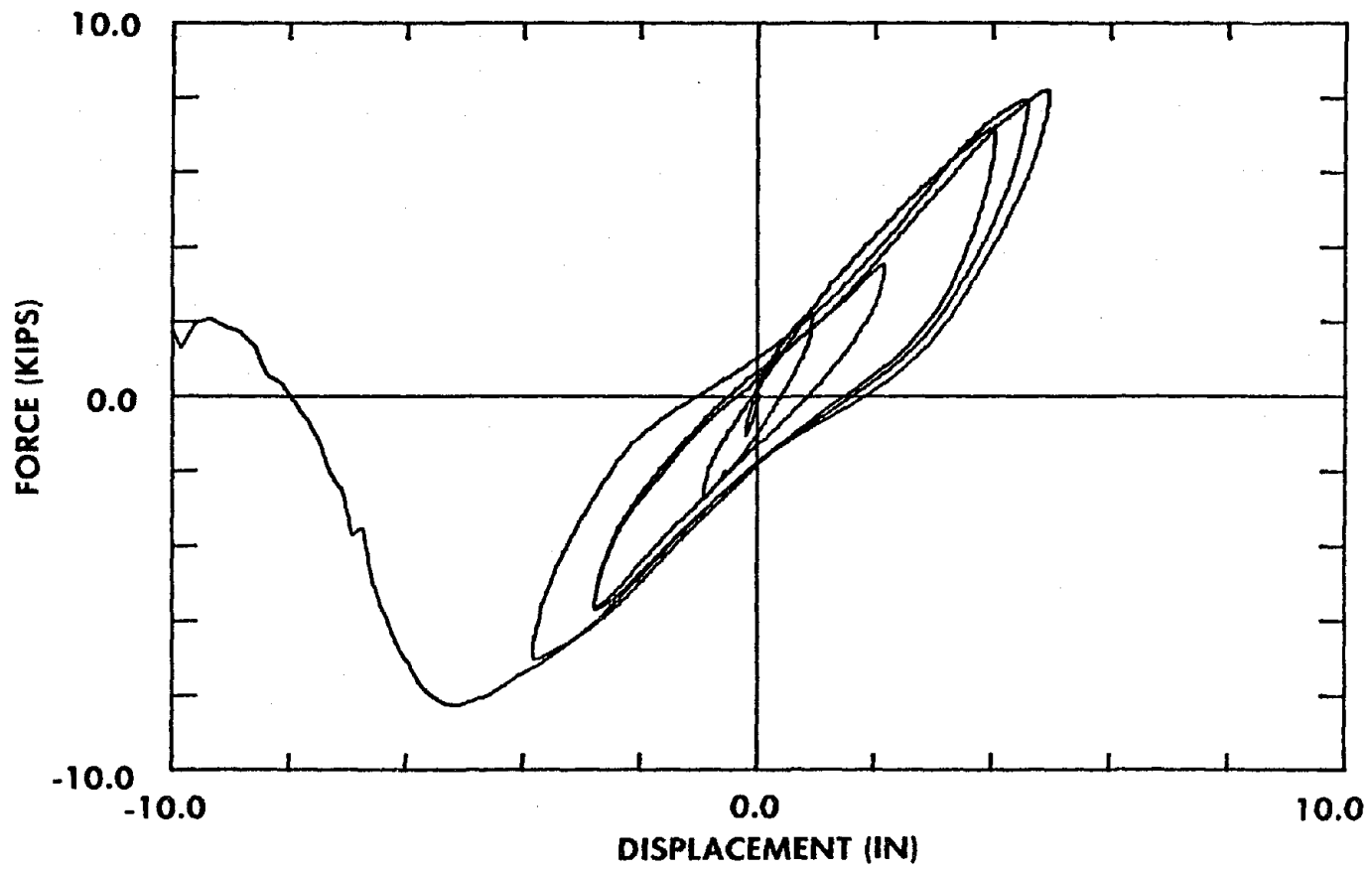


Figure 56 Force-Displacement Curve in Roll-out Test of Lead-Filled Bearing System

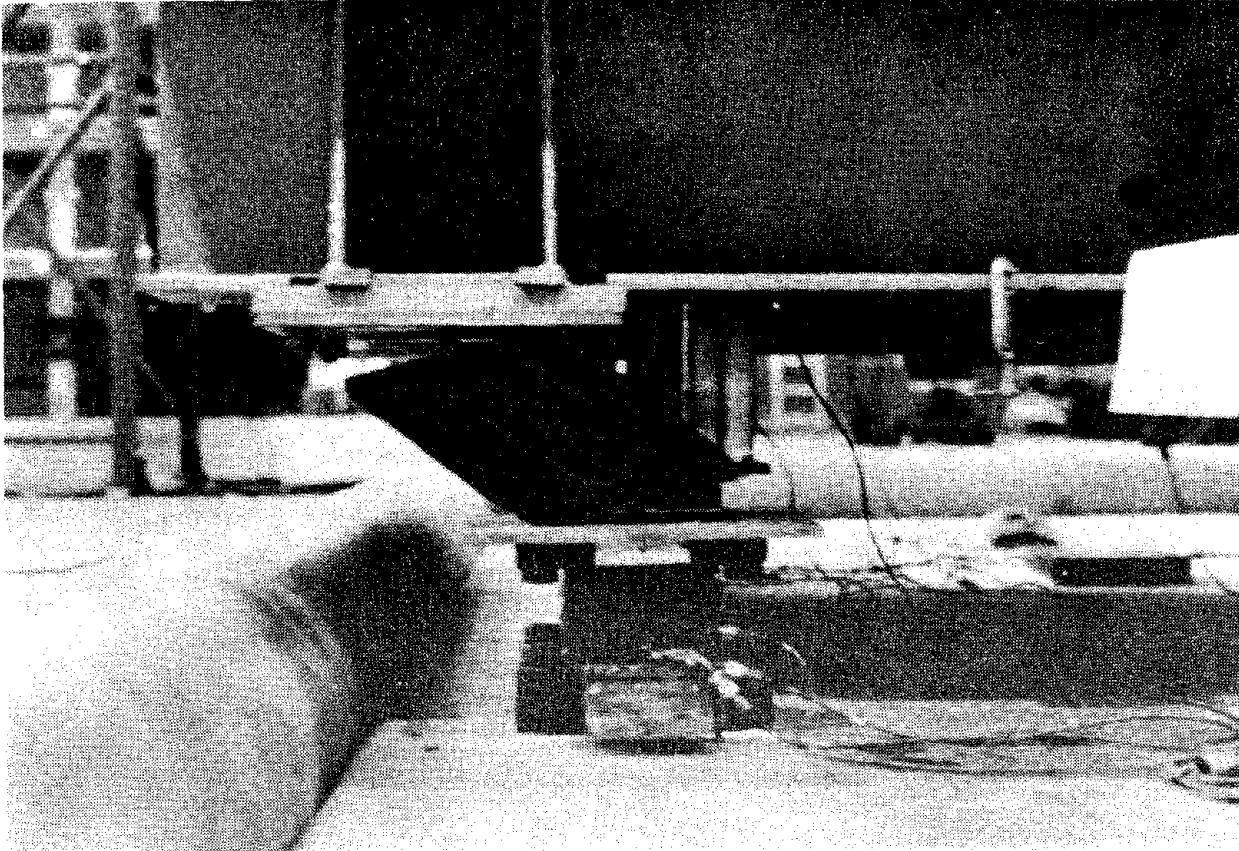


Figure 57 Lead-Filled Rubber Bearing before Roll-out



EARTHQUAKE ENGINEERING RESEARCH CENTER REPORTS

NOTE: Numbers in parentheses are Accession Numbers assigned by the National Technical Information Service; these are followed by a price code. Copies of the reports may be ordered from the National Technical Information Service, 5285 Port Royal Road, Springfield, Virginia, 22161. Accession Numbers should be quoted on orders for reports (PB --- ---) and remittance must accompany each order. Reports without this information were not available at time of printing. The complete list of EERC reports (from EERC 67-1) is available upon request from the Earthquake Engineering Research Center, University of California, Berkeley, 47th Street and Hoffman Boulevard, Richmond, California 94804.

- UCB/EERC-79/01 "Hysteretic Behavior of Lightweight Reinforced Concrete Beam-Column Subassemblages," by B. Forzani, E.P. Popov and V.V. Bertero - April 1979(PB 298 267)A06
- UCB/EERC-79/02 "The Development of a Mathematical Model to Predict the Flexural Response of Reinforced Concrete Beams to Cyclic Loads, Using System Identification," by J. Stanton & H. McNiven - Jan. 1979(PB 295 875)A10
- UCB/EERC-79/03 "Linear and Nonlinear Earthquake Response of Simple Torsionally Coupled Systems," by C.L. Kan and A.K. Chopra - Feb. 1979(PB 298 262)A06
- UCB/EERC-79/04 "A Mathematical Model of Masonry for Predicting its Linear Seismic Response Characteristics," by Y. Mengi and H.D. McNiven - Feb. 1979(PB 298 266)A06
- UCB/EERC-79/05 "Mechanical Behavior of Lightweight Concrete Confined by Different Types of Lateral Reinforcement," by M.A. Manrique, V.V. Bertero and E.P. Popov - May 1979(PB 301 114)A06
- UCB/EERC-79/06 "Static Tilt Tests of a Tall Cylindrical Liquid Storage Tank," by R.W. Clough and A. Niwa - Feb. 1979 (PB 301 167)A06
- UCB/EERC-79/07 "The Design of Steel Energy Absorbing Restrainers and Their Incorporation into Nuclear Power Plants for Enhanced Safety: Volume 1 - Summary Report," by P.N. Spencer, V.F. Zackay, and E.R. Parker - Feb. 1979(UCB/EERC-79/07)A09
- UCB/EERC-79/08 "The Design of Steel Energy Absorbing Restrainers and Their Incorporation into Nuclear Power Plants for Enhanced Safety: Volume 2 - The Development of Analyses for Reactor System Piping," "Simple Systems" by M.C. Lee, J. Penzien, A.K. Chopra and K. Suzuki "Complex Systems" by G.H. Powell, E.L. Wilson, R.W. Clough and D.G. Row - Feb. 1979(UCB/EERC-79/08)A10
- UCB/EERC-79/09 "The Design of Steel Energy Absorbing Restrainers and Their Incorporation into Nuclear Power Plants for Enhanced Safety: Volume 3 - Evaluation of Commercial Steels," by W.S. Owen, R.M.N. Pelloux, R.O. Ritchie, M. Faral, T. Ohhashi, J. Toplosky, S.J. Hartman, V.F. Zackay and E.R. Parker - Feb. 1979(UCB/EERC-79/09)A04
- UCB/EERC-79/10 "The Design of Steel Energy Absorbing Restrainers and Their Incorporation into Nuclear Power Plants for Enhanced Safety: Volume 4 - A Review of Energy-Absorbing Devices," by J.M. Kelly and M.S. Skinner - Feb. 1979(UCB/EERC-79/10)A04
- UCB/EERC-79/11 "Conservatism in Summation Rules for Closely Spaced Modes," by J.M. Kelly and J.L. Sackman - May 1979(PB 301 328)A03
- UCB/EERC-79/12 "Cyclic Loading Tests of Masonry Single Piers; Volume 3 - Height to Width Ratio of 0.5," by P.A. Hidalgo, R.L. Mayes, H.D. McNiven and R.W. Clough - May 1979(PB 301 321)A08
- UCB/EERC-79/13 "Cyclic Behavior of Dense Course-Grained Materials in Relation to the Seismic Stability of Dams," by N.G. Banerjee, H.B. Seed and C.K. Chan - June 1979(PB 301 373)A13
- UCB/EERC-79/14 "Seismic Behavior of Reinforced Concrete Interior Beam-Column Subassemblages," by S. Viathanatepa, E.P. Popov and V.V. Bertero - June 1979(PB 301 326)A10
- UCB/EERC-79/15 "Optimal Design of Localized Nonlinear Systems with Dual Performance Criteria Under Earthquake Excitations," by M.A. Bhatti - July 1979(PB 80 167 109)A06
- UCB/EERC-79/16 "OPTDYN - A General Purpose Optimization Program for Problems with or without Dynamic Constraints," by M.A. Bhatti, E. Polak and K.S. Pister - July 1979(PB 80 167 091)A05
- UCB/EERC-79/17 "ANSR-II, Analysis of Nonlinear Structural Response, Users Manual," by D.P. Mondkar and G.H. Powell July 1979(PB 80 113 301)A05
- UCB/EERC-79/18 "Soil Structure Interaction in Different Seismic Environments," A. Gomez-Masso, J. Lysmer, J.-C. Chen and H.B. Seed - August 1979(PB 80 101 520)A04
- UCB/EERC-79/19 "ARMA Models for Earthquake Ground Motions," by M.K. Chang, J.W. Kwiatkowski, R.F. Nau, R.M. Oliver and K.S. Pister - July 1979(PB 301 166)A05
- UCB/EERC-79/20 "Hysteretic Behavior of Reinforced Concrete Structural Walls," by J.M. Vallenat, V.V. Bertero and E.P. Popov - August 1979(PB 80 165 905)A12
- UCB/EERC-79/21 "Studies on High-Frequency Vibrations of Buildings - 1: The Column Effect," by J. Lubliner - August 1979 (PB 80 158 553)A03
- UCB/EERC-79/22 "Effects of Generalized Loadings on Bond Reinforcing Bars Embedded in Confined Concrete Blocks," by S. Viathanatepa, E.P. Popov and V.V. Bertero - August 1979(PB 81 124 018)A14
- UCB/EERC-79/23 "Shaking Table Study of Single-Story Masonry Houses, Volume 1: Test Structures 1 and 2," by P. Gülkan, R.L. Mayes and R.W. Clough - Sept. 1979 (HUD-000 1763)A12
- UCB/EERC-79/24 "Shaking Table Study of Single-Story Masonry Houses, Volume 2: Test Structures 3 and 4," by P. Gülkan, R.L. Mayes and R.W. Clough - Sept. 1979 (HUD-000 1836)A12
- UCB/EERC-79/25 "Shaking Table Study of Single-Story Masonry Houses, Volume 3: Summary, Conclusions and Recommendations," by R.W. Clough, R.L. Mayes and P. Gülkan - Sept. 1979 (HUD-000 1837)A06

Preceding page blank

- UCB/EERC-79/26 "Recommendations for a U.S.-Japan Cooperative Research Program Utilizing Large-Scale Testing Facilities," by U.S.-Japan Planning Group - Sept. 1979(PB 301 407)A06
- UCB/EERC-79/27 "Earthquake-Induced Liquefaction Near Lake Amatitlan, Guatemala," by H.B. Seed, I. Arango, C.K. Chan, A. Gomez-Masso and R. Grant de Ascoli - Sept. 1979(NUREG-CRI341)A03
- UCB/EERC-79/28 "Infill Panels: Their Influence on Seismic Response of Buildings," by J.W. Axley and V.V. Bertero Sept. 1979(PB 80 163 371)A10
- UCB/EERC-79/29 "3D Truss Bar Element (Type 1) for the ANSR-II Program," by D.P. Mondkar and G.H. Powell - Nov. 1979 (PB 80 169 709)A02
- UCB/EERC-79/30 "2D Beam-Column Element (Type 5 - Parallel Element Theory) for the ANSR-II Program," by D.G. Row, G.H. Powell and D.P. Mondkar - Dec. 1979(PB 80 167 224)A03
- UCB/EERC-79/31 "3D Beam-Column Element (Type 2 - Parallel Element Theory) for the ANSR-II Program," by A. Riahi, G.H. Powell and D.P. Mondkar - Dec. 1979(PB 80 167 216)A03
- UCB/EERC-79/32 "On Response of Structures to Stationary Excitation," by A. Der Kiureghian - Dec. 1979(PB 80 166 929)A03
- UCB/EERC-79/33 "Undisturbed Sampling and Cyclic Load Testing of Sands," by S. Singh, H.B. Seed and C.K. Chan Dec. 1979(ADA 087 298)A07
- UCB/EERC-79/34 "Interaction Effects of Simultaneous Torsional and Compressional Cyclic Loading of Sand," by P.M. Griffin and W.N. Houston - Dec. 1979(ADA 092 352)A15
- UCB/EERC-80/01 "Earthquake Response of Concrete Gravity Dams Including Hydrodynamic and Foundation Interaction Effects," by A.K. Chopra, P. Chakrabarti and S. Gupta - Jan. 1980(AD-A087297)A10
- UCB/EERC-80/02 "Rocking Response of Rigid Blocks to Earthquakes," by C.S. Yim, A.K. Chopra and J. Penzien - Jan. 1980 (PB80 166 002)A04
- UCB/EERC-80/03 "Optimum Inelastic Design of Seismic-Resistant Reinforced Concrete Frame Structures," by S.W. Zagajeski and V.V. Bertero - Jan. 1980(PB80 164 635)A06
- UCB/EERC-80/04 "Effects of Amount and Arrangement of Wall-Panel Reinforcement on Hysteretic Behavior of Reinforced Concrete Walls," by R. Iliya and V.V. Bertero - Feb. 1980(PB81 122 525)A09
- UCB/EERC-80/05 "Shaking Table Research on Concrete Dam Models," by A. Niwa and R.W. Clough - Sept. 1980(PB81 122 368)A06
- UCB/EERC-80/06 "The Design of Steel Energy-Absorbing Restrainers and their Incorporation into Nuclear Power Plants for Enhanced Safety (Vol 1A): Piping with Energy Absorbing Restrainers: Parameter Study on Small Systems," by G.H. Powell, C. Oughourlian and J. Simons - June 1980
- UCB/EERC-80/07 "Inelastic Torsional Response of Structures Subjected to Earthquake Ground Motions," by Y. Yamazaki April 1980(PB81 122 327)A08
- UCB/EERC-80/08 "Study of X-Braced Steel Frame Structures Under Earthquake Simulation," by Y. Ghanaat - April 1980 (PB81 122 335)A11
- UCB/EERC-80/09 "Hybrid Modelling of Soil-Structure Interaction," by S. Gupta, T.W. Lin, J. Penzien and C.S. Yeh May 1980(PB81 122 319)A07
- UCB/EERC-80/10 "General Applicability of a Nonlinear Model of a One Story Steel Frame," by B.I. Sveinsson and H.D. McNiven - May 1980(PB81 124 877)A06
- UCB/EERC-80/11 "A Green-Function Method for Wave Interaction with a Submerged Body," by W. Kioka - April 1980 (PB81 122 269)A07
- UCB/EERC-80/12 "Hydrodynamic Pressure and Added Mass for Axisymmetric Bodies," by F. Nilrat - May 1980(PB81 122 343)A08
- UCB/EERC-80/13 "Treatment of Non-Linear Drag Forces Acting on Offshore Platforms," by B.V. Dao and J. Penzien May 1980(PB81 153 413)A07
- UCB/EERC-80/14 "2D Plane/Axissymmetric Solid Element (Type 3 - Elastic or Elastic-Perfectly Plastic) for the ANSR-II Program," by D.P. Mondkar and G.H. Powell - July 1980(PB81 122 350)A03
- UCB/EERC-80/15 "A Response Spectrum Method for Random Vibrations," by A. Der Kiureghian - June 1980(PB81 122 301)A03
- UCB/EERC-80/16 "Cyclic Inelastic Buckling of Tubular Steel Braces," by V.A. Zayas, E.P. Popov and S.A. Mahin June 1980(PB81 124 885)A10
- UCB/EERC-80/17 "Dynamic Response of Simple Arch Dams Including Hydrodynamic Interaction," by C.S. Porter and A.K. Chopra - July 1980(PB81 124 000)A13
- UCB/EERC-80/18 "Experimental Testing of a Friction Damped Aseismic Base Isolation System with Fail-Safe Characteristics," by J.M. Kelly, K.E. Beucke and M.S. Skinner - July 1980(PB81 148 595)A04
- UCB/EERC-80/19 "The Design of Steel Energy-Absorbing Restrainers and their Incorporation into Nuclear Power Plants for Enhanced Safety (Vol 1B): Stochastic Seismic Analyses of Nuclear Power Plant Structures and Piping Systems Subjected to Multiple Support Excitations," by M.C. Lee and J. Penzien - June 1980
- UCB/EERC-80/20 "The Design of Steel Energy-Absorbing Restrainers and their Incorporation into Nuclear Power Plants for Enhanced Safety (Vol 1C): Numerical Method for Dynamic Substructure Analysis," by J.M. Dickens and E.L. Wilson - June 1980
- UCB/EERC-80/21 "The Design of Steel Energy-Absorbing Restrainers and their Incorporation into Nuclear Power Plants for Enhanced Safety (Vol 2): Development and Testing of Restraints for Nuclear Piping Systems," by J.M. Kelly and M.S. Skinner - June 1980
- UCB/EERC-80/22 "3D Solid Element (Type 4-Elastic or Elastic-Perfectly-Plastic) for the ANSR-II Program," by D.P. Mondkar and G.H. Powell - July 1980(PB81 123 242)A03
- UCB/EERC-80/23 "Gap-Friction Element (Type 5) for the ANSR-II Program," by D.P. Mondkar and G.H. Powell - July 1980 (PB81 122 285)A03

- UCB/EERC-80/24 "U-Bar Restraint Element (Type 11) for the ANSR-II Program," by C. Oughourlian and G.H. Powell July 1980(PB81 122 293)A03
- UCB/EERC-80/25 "Testing of a Natural Rubber Base Isolation System by an Explosively Simulated Earthquake," by J.M. Kelly - August 1980(PB81 201 360)A04
- UCB/EERC-80/26 "Input Identification from Structural Vibrational Response," by Y. Hu - August 1980(PB81 152 308)A05
- UCB/EERC-80/27 "Cyclic Inelastic Behavior of Steel Offshore Structures," by V.A. Zayas, S.A. Mahin and E.P. Popov August 1980(PB81 196 180)A15
- UCB/EERC-80/28 "Shaking Table Testing of a Reinforced Concrete Frame with Biaxial Response," by M.G. Oliva October 1980(PB81 154 304)A10
- UCB/EERC-80/29 "Dynamic Properties of a Twelve-Story Prefabricated Panel Building," by J.G. Bouwkamp, J.P. Kollegger and R.M. Stephen - October 1980(PB82 117 128)A06
- UCB/EERC-80/30 "Dynamic Properties of an Eight-Story Prefabricated Panel Building," by J.G. Bouwkamp, J.P. Kollegger and R.M. Stephen - October 1980(PB81 200 313)A05
- UCB/EERC-80/31 "Predictive Dynamic Response of Panel Type Structures Under Earthquakes," by J.P. Kollegger and J.G. Bouwkamp - October 1980(PB81 152 316)A04
- UCB/EERC-80/32 "The Design of Steel Energy-Absorbing Restrainers and their Incorporation into Nuclear Power Plants for Enhanced Safety (Vol 3): Testing of Commercial Steels in Low-Cycle Torsional Fatigue," by P. Spencer, E.R. Parker, E. Jongewaard and M. Drory
- UCB/EERC-80/33 "The Design of Steel Energy-Absorbing Restrainers and their Incorporation into Nuclear Power Plants for Enhanced Safety (Vol 4): Shaking Table Tests of Piping Systems with Energy-Absorbing Restrainers," by S.F. Stiemer and W.G. Godden - Sept. 1980
- UCB/EERC-80/34 "The Design of Steel Energy-Absorbing Restrainers and their Incorporation into Nuclear Power Plants for Enhanced Safety (Vol 5): Summary Report," by P. Spencer
- UCB/EERC-80/35 "Experimental Testing of an Energy-Absorbing Base Isolation System," by J.M. Kelly, M.S. Skinner and K.E. Beucke - October 1980(PB81 154 072)A04
- UCB/EERC-80/36 "Simulating and Analyzing Artificial Non-Stationary Earthquake Ground Motions," by R.F. Nau, R.M. Oliver and K.S. Pister - October 1980(PB81 153 397)A04
- UCB/EERC-80/37 "Earthquake Engineering at Berkeley - 1980," - Sept. 1980(PB81 205 874)A09
- UCB/EERC-80/38 "Inelastic Seismic Analysis of Large Panel Buildings," by V. Schricker and G.H. Powell - Sept. 1980 (PB81 154 338)A13
- UCB/EERC-80/39 "Dynamic Response of Embankment, Concrete-Gravity and Arch Dams Including Hydrodynamic Interaction," by J.F. Hall and A.K. Chopra - October 1980(PB81 152 324)A11
- UCB/EERC-80/40 "Inelastic Buckling of Steel Struts Under Cyclic Load Reversal," by R.G. Black, W.A. Wenger and E.P. Popov - October 1980(PB81 154 312)A08
- UCB/EERC-80/41 "Influence of Site Characteristics on Building Damage During the October 3, 1974 Lima Earthquake," by P. Repetto, I. Arango and H.B. Seed - Sept. 1980(PB81 161 739)A05
- UCB/EERC-80/42 "Evaluation of a Shaking Table Test Program on Response Behavior of a Two Story Reinforced Concrete Frame," by J.M. Blondet, R.W. Clough and S.A. Mahin
- UCB/EERC-80/43 "Modelling of Soil-Structure Interaction by Finite and Infinite Elements," by F. Medina - December 1980(PB81 229 270)A04
- UCB/EERC-81/01 "Control of Seismic Response of Piping Systems and Other Structures by Base Isolation," edited by J.M. Kelly - January 1981 (PB81 200 735)A05
- UCB/EERC-81/02 "OPTNSR - An Interactive Software System for Optimal Design of Statically and Dynamically Loaded Structures with Nonlinear Response," by M.A. Bhatti, V. Ciampi and K.S. Pister - January 1981 (PB81 218 851)A09
- UCB/EERC-81/03 "Analysis of Local Variations in Free Field Seismic Ground Motions," by J.-C. Chen, J. Lysmer and H.B. Seed - January 1981 (AD-A099508)A13
- UCB/EERC-81/04 "Inelastic Structural Modeling of Braced Offshore Platforms for Seismic Loading," by V.A. Zayas, P.-S.B. Shing, S.A. Mahin and E.P. Popov - January 1981(PB82 138 777)A07
- UCB/EERC-81/05 "Dynamic Response of Light Equipment in Structures," by A. Der Kiureghian, J.L. Sackman and B. Nour-Omid - April 1981 (PB81 218 497)A04
- UCB/EERC-81/06 "Preliminary Experimental Investigation of a Broad Base Liquid Storage Tank," by J.G. Bouwkamp, J.P. Kollegger and R.M. Stephen - May 1981(PB82 140 385)A03
- UCB/EERC-81/07 "The Seismic Resistant Design of Reinforced Concrete Coupled Structural Walls," by A.E. Aktan and V.V. Bertero - June 1981(PB82 113 358)A11
- UCB/EERC-81/08 "The Undrained Shearing Resistance of Cohesive Soils at Large Deformations," by M.R. Pyles and H.B. Seed - August 1981
- UCB/EERC-81/09 "Experimental Behavior of a Spatial Piping System with Steel Energy Absorbers Subjected to a Simulated Differential Seismic Input," by S.F. Stiemer, W.G. Godden and J.M. Kelly - July 1981

- UCB/EERC-81/10 "Evaluation of Seismic Design Provisions for Masonry in the United States," by B.I. Sveinsson, R.L. Mayes and H.D. McNiven - August 1981 (PB82 166 075)A08
- UCB/EERC-81/11 "Two-Dimensional Hybrid Modelling of Soil-Structure Interaction," by T.-J. Tzong, S. Gupta and J. Penzien - August 1981 (PB82 142 118)A04
- UCB/EERC-81/12 "Studies on Effects of Infills in Seismic Resistant R/C Construction," by S. Brokken and V.V. Bertero - September 1981 (PB82 166 190)A09
- UCB/EERC-81/13 "Linear Models to Predict the Nonlinear Seismic Behavior of a One-Story Steel Frame," by H. Valdimarsson, A.H. Shah and H.D. McNiven - September 1981 (PB82 138 793)A07
- UCB/EERC-81/14 "TLUSH: A Computer Program for the Three-Dimensional Dynamic Analysis of Earth Dams," by T. Kagawa, L.H. Mejia, H.B. Seed and J. Lysmer - September 1981 (PB82 139 940)A06
- UCB/EERC-81/15 "Three Dimensional Dynamic Response Analysis of Earth Dams," by L.H. Mejia and H.B. Seed - September 1981 (PB82 137 274)A12
- UCB/EERC-81/16 "Experimental Study of Lead and Elastomeric Dampers for Base Isolation Systems," by J.M. Kelly and S.B. Hodder - October 1981 (PB82 166 182)A05
- UCB/EERC-81/17 "The Influence of Base Isolation on the Seismic Response of Light Secondary Equipment," by J.M. Kelly - April 1981 (PB82 255 266)A04
- UCB/EERC-81/18 "Studies on Evaluation of Shaking Table Response Analysis Procedures," by J. Marcial Blondet - November 1981 (PB82 197 278)A10
- UCB/EERC-81/19 "DELIGHT.STRUCT: A Computer-Aided Design Environment for Structural Engineering," by R.J. Balling, K.S. Pister and E. Polak - December 1981 (PB82 218 496)A07
- UCB/EERC-81/20 "Optimal Design of Seismic-Resistant Planar Steel Frames," by R.J. Balling, V. Ciampi, K.S. Pister and E. Polak - December 1981 (PB82 220 179)A07
- UCB/EERC-82/01 "Dynamic Behavior of Ground for Seismic Analysis of Lifeline Systems," by T. Sato and A. Der Kiureghian - January 1982 (PB82 218 926)A05
- UCB/EERC-82/02 "Shaking Table Tests of a Tubular Steel Frame Model," by Y. Ghanaat and R. W. Clough - January 1982 (PB82 220 161)A07
- UCB/EERC-82/03 "Behavior of a Piping System under Seismic Excitation: Experimental Investigations of a Spatial Piping System supported by Mechanical Shock Arrestors and Steel Energy Absorbing Devices under Seismic Excitation," by S. Schneider, H.-M. Lee and W. G. Godden - May 1982 (PB83 172 544)A09
- UCB/EERC-82/04 "New Approaches for the Dynamic Analysis of Large Structural Systems," by E. L. Wilson - June 1982 (PB83 148 080)A05
- UCB/EERC-82/05 "Model Study of Effects of Damage on the Vibration Properties of Steel Offshore Platforms," by F. Shahriver and J. G. Bouwkamp - June 1982 (PB83 148 742)A10
- UCB/EERC-82/06 "States of the Art and Practice in the Optimum Seismic Design and Analytical Response Prediction of R/C Frame-Wall Structures," by A. E. Aktan and V. V. Bertero - July 1982 (PB83 147 736)A05
- UCB/EERC-82/07 "Further Study of the Earthquake Response of a Broad Cylindrical Liquid-Storage Tank Model," by G. C. Manos and R. W. Clough - July 1982 (PB83 147 744)A11
- UCB/EERC-82/08 "An Evaluation of the Design and Analytical Seismic Response of a Seven Story Reinforced Concrete Frame - Wall Structure," by F. A. Charney and V. V. Bertero - July 1982 (PB83 157 628)A09
- UCB/EERC-82/09 "Fluid-Structure Interactions: Added Mass Computations for Incompressible Fluid," by J. S.-H. Kuo - August 1982 (PB83 156 281)A07
- UCB/EERC-82/10 "Joint-Opening Nonlinear Mechanism: Interface Smeared Crack Model," by J. S.-H. Kuo - August 1982 (PB83 149 195)A05
- UCB/EERC-82/11 "Dynamic Response Analysis of Techi Dam," by R. W. Clough, R. M. Stephen and J. S.-H. Kuo - August 1982 (PB83 147 496)A06
- UCB/EERC-82/12 "Prediction of the Seismic Responses of R/C Frame-Coupled Wall Structures," by A. E. Aktan, V. V. Bertero and M. Piazza - August 1982 (PB83 149 203)A09
- UCB/EERC-82/13 "Preliminary Report on the SMART 1 Strong Motion Array in Taiwan," by B. A. Bolt, C. H. Loh, J. Penzien, Y. B. Tsai and Y. T. Yeh - August 1982 (PB83 159 400)A10
- UCB/EERC-82/14 "Shaking-Table Studies of an Eccentrically X-Braced Steel Structure," by M. S. Yang - September 1982 (PB83 260 778)A12
- UCB/EERC-82/15 "The Performance of Stairways in Earthquakes," by C. Roha, J. W. Axley and V. V. Bertero - September 1982 (PB83 157 693)A07
- UCB/EERC-82/16 "The Behavior of Submerged Multiple Bodies in Earthquakes," by W.-G. Liao - Sept. 1982 (PB83 158 709)A07
- UCB/EERC-82/17 "Effects of Concrete Types and Loading Conditions on Local Bond-Slip Relationships," by A. D. Cowell, E. P. Popov and V. V. Bertero - September 1982 (PB83 153 577)A04

- UCB/EERC-82/18 "Mechanical Behavior of Shear Wall Vertical Boundary Members: An Experimental Investigation," by M. T. Wagner and V. V. Bertero - October 1982 (PB83 159 764)A05
- UCB/EERC-82/19 "Experimental Studies of Multi-support Seismic Loading on Piping Systems," by J. M. Kelly and A. D. Cowell - November 1982
- UCB/EERC-82/20 "Generalized Plastic Hinge Concepts for 3D Beam-Column Elements," by P. F.-S. Chen and G. H. Powell - November 1982 (PB83 247 981)A13
- UCB/EERC-82/21 "ANSR-III: General Purpose Computer Program for Nonlinear Structural Analysis," by C. V. Oughourlian and G. H. Powell - November 1982 (PB83 251 330)A12
- UCB/EERC-82/22 "Solution Strategies for Statically Loaded Nonlinear Structures," by J. W. Simons and G. H. Powell - November 1982 (PB83 197 970)A06
- UCB/EERC-82/23 "Analytical Model of Deformed Bar Anchorages under Generalized Excitations," by V. Ciampi, R. Eligehausen, V. V. Bertero and E. P. Popov - November 1982 (PB83 169 532)A06
- UCB/EERC-82/24 "A Mathematical Model for the Response of Masonry Walls to Dynamic Excitations," by H. Sucuoğlu, Y. Mengi and H. D. McNiven - November 1982 (PB83 169 011)A07
- UCB/EERC-82/25 "Earthquake Response Considerations of Broad Liquid Storage Tanks," by F. J. Cambra - November 1982 (PB83 251 215)A09
- UCB/EERC-82/26 "Computational Models for Cyclic Plasticity, Rate Dependence and Creep," by B. Hosaddad and G. H. Powell - November 1982 (PB83 245 829)A08
- UCB/EERC-82/27 "Inelastic Analysis of Piping and Tubular Structures," by M. Mahasuerachai and G. H. Powell - November 1982 (PB83 249 987)A07
- UCB/EERC-83/01 "The Economic Feasibility of Seismic Rehabilitation of Buildings by Base Isolation," by J. M. Kelly - January 1983 (PB83 197 988)A05
- UCB/EERC-83/02 "Seismic Moment Connections for Moment-Resisting Steel Frames," by E. P. Popov - January 1983 (PB83 195 412)A04
- UCB/EERC-83/03 "Design of Links and Beam-to-Column Connections for Eccentrically Braced Steel Frames," by E. P. Popov and J. O. Malley - January 1983 (PB83 194 811)A04
- UCB/EERC-83/04 "Numerical Techniques for the Evaluation of Soil-Structure Interaction Effects in the Time Domain," by E. Bayo and E. L. Wilson - February 1983 (PB83 245 605)A09
- UCB/EERC-83/05 "A Transducer for Measuring the Internal Forces in the Columns of a Frame-Wall Reinforced Concrete Structure," by R. Sause and V. V. Bertero - May 1983 (PB84 119 494)A06
- UCB/EERC-83/06 "Dynamic Interactions between Floating Ice and Offshore Structures," by P. Croteau - May 1983 (PB84 119 486)A16
- UCB/EERC-83/07 "Dynamic Analysis of Multiply Tuned and Arbitrarily Supported Secondary Systems," by T. Igusa and A. Der Kiureghian - June 1983 (PB84 118 272)A11
- UCB/EERC-83/08 "A Laboratory Study of Submerged Multi-body Systems in Earthquakes," by G. R. Ansari - June 1983 (PB83 261 842)A17
- UCB/EERC-83/09 "Effects of Transient Foundation Uplift on Earthquake Response of Structures," by C.-S. Yim and A. K. Chopra - June 1983 (PB83 261 396)A07
- UCB/EERC-83/10 "Optimal Design of Friction-Braced Frames under Seismic Loading," by M. A. Austin and K. S. Pister - June 1983 (PB84 119 288)A06
- UCB/EERC-83/11 "Shaking Table Study of Single-Story Masonry Houses: Dynamic Performance under Three Component Seismic Input and Recommendations," by G. C. Manos, R. W. Clough and R. L. Mayes - June 1983
- UCB/EERC-83/12 "Experimental Error Propagation in Pseudodynamic Testing," by P. B. Shing and S. A. Mahin - June 1983 (PB84 119 270)A09
- UCB/EERC-83/13 "Experimental and Analytical Predictions of the Mechanical Characteristics of a 1/5-scale Model of a 7-story R/C Frame-Wall Building Structure," by A. E. Aktan, V. V. Bertero, A. A. Chowdhury and T. Nagashima - August 1983 (PB84 119 213)A07
- UCB/EERC-83/14 "Shaking Table Tests of Large-Panel Precast Concrete Building System Assemblages," by M. G. Oliva and R. W. Clough - August 1983
- UCB/EERC-83/15 "Seismic Behavior of Active Beam Links in Eccentrically Braced Frames," by K. D. Hjelmstad and E. P. Popov - July 1983 (PB84 119 676)A09
- UCB/EERC-83/16 "System Identification of Structures with Joint Rotation," by J. S. Dimsdale and H. D. McNiven - July 1983
- UCB/EERC-83/17 "Construction of Inelastic Response Spectra for Single-Degree-of-Freedom Systems," by S. Mahin and J. Lin - July 1983

- UCB/EERC-83/18 "Interactive Computer Analysis Methods for Predicting the Inelastic Cyclic Behaviour of Structural Sections," by S. Kaba and S. Mahin - July 1983 (PB84 192 012) A06
- UCB/EERC-83/19 "Effects of Bond Deterioration on Hysteretic Behavior of Reinforced Concrete Joints," by F.C. Filippou, E.P. Popov and V.V. Bertero - August 1983 (PB84 192 020) A10
- UCB/EERC-83/20 "Analytical and Experimental Correlation of Large-Panel Precast Building System Performance," by M.G. Oliva, R.W. Clough, M. Velkov, P. Gavrilovic and J. Petrovski - November 1983
- UCB/EERC-83/21 "Mechanical Characteristics of Materials Used in a 1/5 Scale Model of a 7-Story Reinforced Concrete Test Structure," by V.V. Bertero, A.E. Aktan, H.G. Harris and A.A. Chowdhury - September 1983 (PB84 193 697) A05
- UCB/EERC-83/22 "Hybrid Modelling of Soil-Structure Interaction in Layered Media," by T.-J. Tzong and J. Penzien - October 1983 (PB84 192 178) A08
- UCB/EERC-83/23 "Local Bond Stress-Slip Relationships of Deformed Bars under Generalized Excitations," by R. Eligehausen, E.P. Popov and V.V. Bertero - October 1983 (PB84 192 848) A09
- UCB/EERC-83/24 "Design Considerations for Shear Links in Eccentrically Braced Frames," by J.O. Malley and E.P. Popov - November 1983 (PB84 192 186) A07
- UCB/EERC-84/01 "Pseudodynamic Test Method for Seismic Performance Evaluation: Theory and Implementation," by P.-S. B. Shing and S. A. Mahin - January 1984 (PB84 190 644) A08
- UCB/EERC-84/02 "Dynamic Response Behavior of Xiang Hong Dian Dam," by R.W. Clough, K.-T. Chang, H.-Q. Chen, R.M. Stephen, G.-L. Wang, and Y. Ghanaat - April 1984
- UCB/EERC-84/03 "Refined Modelling of Reinforced Concrete Columns for Seismic Analysis," by S.A. Kaba and S.A. Mahin - April, 1984
- UCB/EERC-84/04 "A New Floor Response Spectrum Method for Seismic Analysis of Multiply Supported Secondary Systems," by A. Asfura and A. Der Kiureghian - June 1984
- UCB/EERC-84/05 "Earthquake Simulation Tests and Associated Studies of a 1/5th-scale Model of a 7-Story R/C Frame-Wall Test Structure," by V.V. Bertero, A.E. Aktan, F.A. Charney and R. Sause - June 1984
- UCB/EERC-84/06 "R/C Structural Walls: Seismic Design for Shear," by A.E. Aktan and V.V. Bertero
- UCB/EERC-84/07 "Behavior of Interior and Exterior Flat-Plate Connections subjected to Inelastic Load Reversals," by H.L. Zee and J.P. Moehle
- UCB/EERC-84/08 "Experimental Study of the Seismic Behavior of a two-story Flat-Plate Structure," by J.W. Diebold and J.P. Moehle
- UCB/EERC-84/09 "Phenomenological Modeling of Steel Braces under Cyclic Loading," by K. Ikeda, S.A. Mahin and S.N. Dermitzakis - May 1984
- UCB/EERC-84/10 "Earthquake Analysis and Response of Concrete Gravity Dams," by G. Fenves and A.K. Chopra - August 1984
- UCB/EERC-84/11 "EAGD-84: A Computer Program for Earthquake Analysis of Concrete Gravity Dams," by G. Fenves and A.K. Chopra - August 1984
- UCB/EERC-84/12 "A Refined Physical Theory Model for Predicting the Seismic Behavior of Braced Steel Frames," by K. Ikeda and S.A. Mahin - July 1984
- UCB/EERC-84/13 "Earthquake Engineering Research at Berkeley - 1984" - August 1984
- UCB/EERC-84/14 "Moduli and Damping Factors for Dynamic Analyses of Cohesionless Soils," by H.B. Seed, R.T. Wong, I.M. Idriss and K. Tokimatsu - September 1984
- UCB/EERC-84/15 "The Influence of SPT Procedures in Soil Liquefaction Resistance Evaluations," by H. B. Seed, K. Tokimatsu, L. F. Harder and R. M. Chung - October 1984
- UCB/EERC-84/16 "Simplified Procedures for the Evaluation of Settlements in Sands Due to Earthquake Shaking," by K. Tokimatsu and H. B. Seed - October 1984
- UCB/EERC-84/17 "Evaluation and Improvement of Energy Absorption Characteristics of Bridges under Seismic Conditions," by R. A. Imbsen and J. Penzien - November 1984
- UCB/EERC-84/18 "Structure-Foundation Interactions under Dynamic Loads," by W. D. Liu and J. Penzien - November 1984
- UCB/EERC-84/19 "Seismic Modelling of Deep Foundations," by C.-H. Chen and J. Penzien - November 1984
- UCB/EERC-84/20 "Dynamic Response Behavior of Quan Shui Dam," by R. W. Clough, K.-T. Chang, H.-Q. Chen, R. M. Stephen, Y. Ghanaat and J.-H. Qi - November 1984

- UCB/EERC-85/01 "Simplified Methods of Analysis for Earthquake Resistant Design of Buildings," by E.F. Cruz and A.K. Chopra - Feb. 1985 (PB86 112299/AS) A12
- UCB/EERC-85/02 "Estimation of Seismic Wave Coherency and Rupture Velocity using the SMART 1 Strong-Motion Array Recordings," by N.A. Abrahamson - March 1985
- UCB/EERC-85/03 "Dynamic Properties of a Thirty Story Condominium Tower Building," by R.M. Stephen, E.L. Wilson and N. Stander - April 1985 (PB86 118965/AS) A06
- UCB/EERC-85/04 "Development of Substructuring Techniques for On-Line Computer Controlled Seismic Performance Testing," by S. Dermitzakis and S. Mahin - February 1985 (PB86 132941/AS) A08
- UCB/EERC-85/05 "A Simple Model for Reinforcing Bar Anchorages under Cyclic Excitations," by F.C. Filippou - March 1985 (PB86 112919/AS) A05
- UCB/EERC-85/06 "Racking Behavior of Wood-Framed Gypsum Panels under Dynamic Load," by M.G. Oliva - June 1985
- UCB/EERC-85/07 "Earthquake Analysis and Response of Concrete Arch Dams," by K.-L. Fok and A.K. Chopra - June 1985 (PB86 139672/AS) A10
- UCB/EERC-85/08 "Effect of Inelastic Behavior on the Analysis and Design of Earthquake Resistant Structures," by J.P. Lin and S.A. Mahin - June 1985 (PB86 135340/AS) A08
- UCB/EERC-85/09 "Earthquake Simulator Testing of a Base-Isolated Bridge Deck." by J.M. Kelly and I.G. Buckle - January 1986

